

A *Spitzer* MIPS Study of 2.5-2.0 M_{\odot} Stars in Scorpius-Centaurus

Christine H. Chen¹, Mark Pecaut², Eric E. Mamajek^{2,3}, Kate Y. L. Su⁴, Martin Bitner

ABSTRACT

We have obtained *Spitzer Space Telescope* Multiband Imaging Photometer for *Spitzer* (MIPS) 24 μm and 70 μm observations of 215 nearby, *Hipparcos* B- and A-type common proper motion single and binary systems in the nearest OB association, Scorpius-Centaurus. Combining our MIPS observations with those of other ScoCen stars in the literature, we estimate 24 μm B+A-type disk fractions of 17/67 ($25^{+6\%}_{-5\%}$), 36/131 ($27^{+4\%}_{-4\%}$), and 23/95 ($24^{+5\%}_{-4\%}$) for Upper Scorpius (\sim 11 Myr), Upper Centaurus Lupus (\sim 15 Myr), and Lower Centaurus Crux (\sim 17 Myr), respectively, somewhat smaller disk fractions than previously obtained for F- and G-type members. We confirm previous *IRAS* excess detections and present new discoveries of 51 protoplanetary and debris disk systems, with fractional infrared luminosities ranging from $L_{IR}/L_{*} = 10^{-6}$ to 10^{-2} and grain temperatures ranging from $T_{gr} = 40 - 300$ K. In addition, we confirm that the 24 μm and 70 μm excesses (or fractional infrared luminosities) around B+A type stars are smaller than those measured toward F+G type stars and hypothesize that the observed disk property dependence on stellar mass may be the result of a higher stellar companion fraction around B- and A-type stars at 10 - 200 AU and/or the presence of Jupiter-mass companions in the disks around F- and G-type stars. Finally, we note that the majority of the ScoCen 24 μm excess sources also possess 12 μm excess, indicating that Earth-like planets may be forming via collisions in the terrestrial planet zone at \sim 10 - 100 Myr.

Subject headings: open clusters and associations: individual (Upper Scorpius, Lower Centaurus-Crux, Upper Centaurus-Lupus)—stars: circumstellar matter—planetary systems: formation

¹Space Telescope Science Institute, 3700 San Martin Dr., Baltimore, MD 21218; cchen@stsci.edu

²Department of Physics and Astronomy, University of Rochester, Rochester, NY 14627

³Cerro Tololo Inter-American Observatory, Casilla 603, La Serena, Chile

⁴Steward Observatory, University of Arizona, 933 North Cherry Avenue, Tucson, AZ 85721

1. Introduction

Radial velocity studies of solar-like stars and "retired" intermediate-mass stars have discovered hundreds of Jovian-like planets and revealed correlations between host star properties and planet frequency. Measurements of [Fe/H] suggest that stars with super-solar metal abundance (>0.3 dex) are almost $10\times$ more likely to possess gas giant companions than those with subsolar abundance ($-0.5 < [\text{Fe}/\text{H}] < 0.0$) (Fischer & Valenti 2005). Studies of host star mass suggest that the fraction of stars with Jovian planet companions increases as a function of stellar mass with intermediate mass stars ($2 M_{\odot}$) possessing twice as many companions on average compared to solar-like stars (Johnson et al. 2010). Since planets are believed to form in circumstellar disks around young stars, planetary demographics in conjunction with disk observations, are expected to place constraints on the processes by which planets form. We have conducted a search for dusty disks around young stars in ScoCen to determine whether disk properties (e.g. frequency, fractional infrared luminosity, grain temperature) are consistent with oligarchic growth models and dependent on stellar host properties.

The Scorpius-Centaurus OB association (ScoCen), with typical stellar distances of ~ 100 - 200 pc, is the closest OB association to the Sun and contains three subgroups: Upper Scorpius (US), Upper Centaurus Lupus (UCL), and Lower Centaurus Crux (LCC), with estimated ages of ~ 11 Myr (Pecaut et al. 2012), ~ 15 Myr, and ~ 17 Myr (Mamajek et al. 2002), respectively. The close proximity of ScoCen and the age of its constituent stars make this association an excellent laboratory for studying the formation and evolution of planetary systems. Several hundred candidate members have been identified to date; although, the association probably contains thousands of low-mass members. Member stars with spectral type F and earlier have been identified using moving group analysis of *Hipparcos* positions, parallaxes, and proper motions (de Zeeuw et al. 1999), while later type members have been identified using youth indicators (i.e., high coronal X-ray activity and large lithium abundance; Preibisch & Mamajek (2008); Slesnick et al. (2006)).

Infrared surveys of ~ 10 - 20 Myr old moving groups and clusters indicate that young stars possess disks with a wide variety of properties. A *Spitzer* IRAC and IRS peak-up survey of 204 B- through M-type (0.1 - $20 M_{\odot}$) stars in Upper Sco found that the disks around late-type K- and M-type members are optically thick and accreting while those around B- and A-type members are optically thin and gas-poor, consistent with the expectation that disks evolve faster around higher mass stars (Carpenter et al. 2006). High-resolution imaging studies of TW Hya and HR 4796A in the ~ 10 Myr old TW Hya Association suggest that 10 - 20 Myr old disks may be sculpted by planets regardless of the mass of the central star or the evolutionary state of the disk. VLA thermal emission mapping has revealed the presence of

a \sim 4 AU inner hole in the TW Hya disk that may be dynamically cleared by a forming giant planet (Hughes et al. 2007). *HST* STIS scattered light imaging has revealed the presence of a steep inner truncation at \sim 65 AU in the ring-like debris disk around HR 4796A that is consistent with the presence of one or more planetary-mass companions (Schneider et al. 2009).

Kenyon & Bromley (2004, 2008) have developed "self-stirred" disk models to describe the formation of oligarchs and their impact on disk evolution around solar to intermediate mass stars with ages $>$ few million years. They assume that disks are initially gas-rich and possess planetesimals with radii 1 m - 1 km at 30 - 150 AU from the central star. Since the disks are initially gas rich, the relative velocities between planetesimals are small, leading to constructive collisions between planetesimals that continue to grow until they have formed oligarchs (1000 km-sized bodies) that have depleted their feeding zone. The oligarchs are then massive enough to gravitationally perturb remnant planetesimals into eccentric orbits where they collide at high relative velocities, generating micron-size sized grains that may be detected via thermal emission. Kenyon & Bromley (2004, 2008) predict that the number of micron-sized debris particles and therefore the infrared excess emission rises rapidly at 5 Myr and peaks at 10-15 Myr. Their models assume that the total planetesimal mass is proportional to the stellar mass, suggesting that the disks around intermediate-mass stars are dustier and brighter than those around solar-like stars. Their models also indicate that evolutionary timescale for disks around intermediate-mass stars is faster than that around solar-like stars because the dynamical timescale around higher mass stars is shorter.

Several groups have used *Spitzer* MIPS at 24 μ m to search for infrared excess trends expected from self-stirred disks around intermediate mass stars at 5 - 100 Myr. The first such study was carried out by Hernández et al. (2006) who compared measurements of 26 early-type (F5 or earlier) stars in the \sim 5 Myr Orion OB1a and 34 early-type stars in the \sim 10 Myr Orion OB1b at \sim 400 pc with observations of intermediate-mass stars in young clusters. Based on a modest sample of stars, they concluded that 24 μ m excess peaks at 10 Myr, consistent with the onset of oligarchic growth at 30-150 AU. Currie et al. (2008) carried out a larger survey of \sim 600 intermediate and high-mass stars in h and χ Persei at \sim 2.5 kpc. Their statistical analysis also indicated a peak in 24 μ m excess emission at 10-15 Myr, followed by a decline up to 1 Gyr. More recently, Carpenter et al. (2009) observed 62 B- and A-type members of the \sim 11 Myr Upper Sco. They found that an increase in 24 μ m excess emission for stars with ages between 5 and 17 Myr was statistically insignificant ($<2\sigma$).

We report the results of a *Spitzer* MIPS 24 μ m and 70 μ m survey of 215 B- and A-type *Hipparcos* common proper motion members of ScoCen stars, expanding on our survey of 182

F- and G-type members (Chen et al. 2011). We list the targets for the full sample, along with their spectral types, distances, and subgroup memberships in Table 1. We compare our data with (1) Kenyon & Bromley (2004, 2008) self-stirred disk models to determine whether models of 10-20 Myr disks are consistent with our data and (2) MIPS 24 μm and 70 μm photometry of F- and G-type members (Chen et al. 2011) to search for evidence of stellar mass dependent disk evolution, expected based on results from radial velocity surveys. A recent cursory analysis of the preliminary WISE ScoCen data indicates that the disks around intermediate type members are less massive than those around solar-like members (Rizzuto et al. 2012).

2. Observations

The *Hipparcos* satellite enabled high-precision measurements of stellar position, parallax, and proper motion for stars with V-band magnitudes, $m_V < 9$, providing the ability to efficiently identify candidate members of OB associations kinematically with spectral types later than B for the first time. de Zeeuw et al. (1999) (hereafter dZ99) analyzed the *Hipparcos* measurements of OB associations using the de Bruijne (1999) refurbished convergent point method and the Hoogerwerf & Aguilar (1999) "Spaghetti method" to determine the average position and space motions of each association, including the US, UCL, and LCC subgroups of ScoCen. By cross correlating the *Hipparcos* measurements of individual stars with mean subgroup properties, dZ99 carried out a detailed census of high- and intermediate-mass stars in ScoCen. In particular, they identified more than 300 probable new intermediate-mass members of US (49 B-type and 34 A-type stars), UCL (66 B-type and 68 A-type stars), and LCC (42 B-type and 55 A-type stars). However, they cautioned that up to $\sim 30\%$ of their candidate members may be interlopers because the stellar radial velocities were not measured. Recently, Rizzuto et al. (2011) re-examined the membership of high mass stars in the ScoCen region ($285^\circ \leq l \leq 360^\circ$, $-10^\circ \leq b \leq 60^\circ$), estimating membership probabilities based on stellar distances, Galactic velocities, latitudes, and longitudes inferred from *Hipparcos* positions, proper motions, and parallaxes and 2nd Catalog of Radial Velocities with Astrometric Data (CRVAS-2) radial velocities, where available.

Since our survey was defined prior to the Rizzuto et al. (2011) analysis, we sought to obtain MIPS 24 μm and 70 μm photometry of all of the intermediate-mass ScoCen members identified by dZ99. Prior to our study, several groups had already begun to explore US in detail. Oudmaijer et al. (1992) had discovered *IRAS* excesses associated with 2 B-type (HIP 80569/HD 148184 and HIP 81474/HD 149914) and 2 A-type (HIP 79476/HD 145718 and HIP 81624/HD 150193) binary and single star systems in US. Using *Spitzer* MIPS,

Carpenter et al. (2009) had observed and 37 B-type and 25 A-type binary and single star systems in US using MIPS and Su et al. (2006) had observed 3 B-type stars in US and 10 B-type and 6 A-type stars in UCL. We have obtained *Spitzer* MIPS observations of 1 A-type star in US, and 56 B-type and 62 A-type stars in UCL, completing the dZ99 sample of B- and A-type stars in UCL. We have also obtained observations of 42 B-type and 54 A-type members of LCC, all dZ99 B- and A-type members of LCC except one A-type star (HIP 78541/HD 143488).

2.1. MIPS Observations

We obtained *Spitzer* (Werner et al. 2004) MIPS (Rieke et al. 2004) observations of 215 candidate ScoCen single and binary systems in photometry mode at 24 μm and 70 μm (default scale). Each system was observed once between 2007 August and 2008 September 2008, using 1 cycle of 3 s integrations at 24 μm and 1 - 6 cycle(s) of 10 s integrations at 70 μm , corresponding to on-source integration times of 24.1 s and 125.8 s - 754.8 s at 24 μm and 70 μm respectively. All the data were processed using the MIPS instrument team Data Analysis Tool (Gordon et al. 2005) for basic reduction (dark subtraction, flat-fielding/illumination correction). A series of additional steps designed to provide homogeneous reduction for MIPS data was applied as part of a *Spitzer* legacy catalog (Su et al. 2010). In short, a second flat field constructed from the 24 μm data itself was applied to all of the 24 μm data to remove scattered-light gradient and dark latency to improve sensitivity (e.g., Engelbracht et al. (2007)) except for observations that possess complex background. The known transient behaviors associated with the MIPS 70 μm array were removed by masking out bright sources in the field of view and time filtering the data (for details see Gordon et al. (2007)). The processed data were then combined using the World Coordinate System information to produce final mosaics with pixels half the size of the physical pixel scale. For 70 μm data, an additional outlier rejection was performed using the spatial redundancy of each processed data frame to further remove hot pixels in the data. This extra process can improve the data quality, especially for observations where sources are not detected (K. Y. L. Su et al., in preparation).

Since the majority of the sources in the sample are not resolved, we extract the photometry using point-spread function (PSF) fitting. The input PSF's were constructed using observed calibration stars and smoothed STinyTim model PSFs, and have been tested to ensure that photometric results are consistent with the MIPS calibration (Engelbracht et al. 2007; Gordon et al. 2007). The systematic errors were estimated based on the pixel-to-pixel variation on the source-free (PSF-subtracted) images. We also performed aperture pho-

tometry (using the multiple aperture setting in Su et al. (2006). The aperture photometry measurements were used as a reference to screen targets that might be contaminated by nearby sources, background nebulosity, or source extension. We list our measurements in Table 2; stars with 24 μm contamination are noted with a dagger. All of the targets were detected at 24 μm . Accurate 24 μm photometry could not be measured for the heavily saturated Herbig Ae/Be star HIP 56379 (HD 100546). Each target position was refined using two-dimensional Gaussian fitting and then compared to the SIMBAD stellar position to ensure the correct source extraction. For the sources that were not detected at 70 μm , the PSF was fixed at the position of the 24 μm source position to extract PSF fitting photometry using the minimum χ^2 technique. We quote 3σ upper limits for systems that were not detected. The total photometric uncertainty is the sum in quadrature of (1) the source photon counting uncertainty, (2) the detector repeatability uncertainty (0.4% and 4.5% of the total flux at 24 and 70 μm , respectively), and (3) the absolute calibration uncertainty (2% and 5% of the total flux at 24 and 70 μm , respectively).

3. Disk Fractions

We estimate the stellar photospheric fluxes for our sample based on 2MASS (Cutri et al. 2003) K_s-band magnitudes and intrinsic main sequence colors calculated by E. Mamajek¹. First, we assembled the *Hipparcos* B- and V-band photometry, Cousins I-band photometry (where available), and 2MASS J-, H-, and K_s-band photometry and constructed measured $B - V$, $V - I_c$, $V - J$, $V - H$, and $V - K_s$ colors. Second, we calculated the extinction for each star. For B-type stars with Stromgren photometry (Hauck & Mermilliod 1998), we estimated the extinction using the prescription of Shobbrook (1983); for B-type stars without Stromgren photometry but with UBV photometry (Mermilliod & Mermilliod 1994), we estimated the extinction using the reddening-free Q parameter, $Q = (U-B) - 0.72*(B-V)$. For all remaining B-type stars and all the A-type stars, we calculated the extinction in each color assuming that the stars possess intrinsic main sequence colors, an average visual extinction, A_V , and its uncertainty based on the standard deviation of the extinction measurements. Fourth, we extrapolated the average A_V to the K_s -band assuming that $A_K = 0.116 A_V$, consistent with $R_V = 3.1$ and a Cardelli, Clayton, & Mathis (1989) extinction law. Fifth, we corrected the measured 2MASS K_s -band magnitudes for extinction. Finally, we used Kurucz models to estimate the predicted 24 μm and 70 μm fluxes based on the extinction-corrected K_s band magnitudes and stellar spectral types, assuming the Kenyon & Hartmann (1995) conversion between spectral type and effective temperature. For example, a star with $T_{\text{eff}} =$

¹http://www.pas.rochester.edu/~emamajek/EEM_dwarf_UBVIJHK_colors_Teff.html

10,000 K, is expected to possess $F_\nu(K_s)/F_\nu(24 \mu\text{m}) = 96.7$ and $F_\nu(K_s)/F_\nu(70 \mu\text{m}) = 890.0$.

For comparison with our measured (but not color-corrected) fluxes, we list the predicted photospheric 24 and 70 μm fluxes integrated over the MIPS bandpasses, F_ν , in Table 2. We calculate the excess significance of each detected source, $\chi = (\text{Measured Flux} - \text{Predicted Flux})/\text{Uncertainty}$, where the Uncertainty includes absolute calibration uncertainty (2%), repeatability uncertainty (0.4%), the photospheric model uncertainty ($\sim 3\%$), and statistical uncertainty of the 24 μm photometry summed in quadrature. We list excess objects with $\chi \geq 6$ at 24 and/or 70 μm in Table 3. We verify our stellar atmosphere model fits by examining the $K_s - [24]$ colors of our sources. All of our excess sources possess $K_s - [24] > 0.2$ mag. We plot the $K_s - [24]$ color as a function of $J - H$ color (as a proxy for spectral type) for all of the sources in our study in Figure 1. We show the distribution of significance of the 24 μm excesses ($\chi_{24} = (\text{Measured } F_\nu(24 \mu\text{m}) - \text{Predicted } F_\nu(24 \mu\text{m}))/\text{Measured } \sigma_{F_{24}}$) in Figure 2. Our $K_s - [24]$ selection criteria robustly identified sources with large excesses but may not identify sources with weaker excesses. Follow-up IRS spectroscopy for three of our excess sources indicates that they possess hydrogen emission lines, consistent with Be stars (HIP 63005, HIP 67472, and HIP 69618); the infrared excess associated with these disks is generated by excretion disks rather than debris disks.

Thirty-four sources, including twenty-seven 24 μm excess sources (not excluding Be stars), are detected at 70 μm . Since our 70 μm integration times were short, the majority of the objects detected at 70 μm possess strong 70 μm excesses; however, a handful of photospheres around bright B-type stars are also detected. We plot the $K_s - [70]$ color as a function of $J - H$ color for all of the sources in our study in Figure 3. For each 24 μm plus 70 μm excess source, we fit the MIPS 24 μm and 70 μm excess fluxes with a single-temperature blackbody, T_{gr} (see Table 3), and infer color temperatures $T_{gr} = 40 - 300$ K and fractional infrared luminosities $L_{IR}/L_* = 1 \times 10^{-5}$ to 4×10^{-2} . For each 24 μm excess only source, we cannot constrain the color temperatures without additional infrared excess detections at other wavelengths; however, we estimate grain temperature lower limits. Our 70 μm flux upper limits suggest that the color temperatures for these sources are consistent with those typically measured toward debris disks. For these sources, we infer infrared dust luminosities assuming that $F_{IR} \sim \nu F_\nu(24 \mu\text{m})$.

We measure B+A type 24 μm disk fractions for the two older ScoCen subgroups using data from our sample, excluding 3 Be stars in UCL and 1 Be star in LCC: 27/115 ($23^{+4}_{-3}\%$) for UCL (~ 15 Myr) and 23/95 ($24^{+5}_{-4}\%$) for LCC (~ 17 Myr), respectively. Since our census of LCC B+A stars is complete (except for one unobserved star), our estimated LCC B+A disk fraction accurately reflects the known demographics of the subgroup. We combine our dZ99 UCL B+A sample with that of Su et al. (2006) to determine a complete dZ99 UCL B+A

disk fraction. We discovered 24 μm excess around 8/53 B- and 19/62 A-type dZ99 UCL stars, excluding Be stars; Su et al. (2006) discovered 24 μm excesses around 6/10 B- and 3/6 A-type dZ99 UCL stars, suggesting a combined dZ99 UCL B+A 24 μm excess fraction: 36/131 ($27^{+4}_{-4}\%$). Finally, we combine the Oudmaijer et al. (1992), Carpenter et al. (2009), and Su et al. (2006) dZ99 US B+A samples to determine the most complete dZ99 US B+A disk fraction. Oudmaijer et al. (1992) discovered *IRAS* 25 μm excesses around 1/1 B-type and 2/2 A-type dZ99 US stars, excluding 1 Be star (HIP 80569); Carpenter et al. (2009) discovered MIPS 24 μm excesses around 6/35 B- and 7/25 A-type dZ99 US stars, excluding 2 Be stars (HIP 77859 and HIP 78207); Su et al. (2006) discovered MIPS 24 μm excesses around 0/3 B-type dZ99 US stars; we measured a MIPS 24 μm excess around 1 A-type dZ99 US star, suggesting a combined dZ99 US B+A 24 μm excess fraction: 17/67 ($25^{+6}_{-5}\%$). Since the dZ99 sample was selected on the basis of *Hipparcos* position, parallax, and common proper motion, it is expected to be contaminated by interlopers. dZ99 estimate that (1-5)/49 B-type and (2-6)/34 A-type stars in US, (5-12)/66 B-type and (10-15)/68 A-type stars in UCL, and (4-7)/42 B-type and (8-11)/55 A-type stars in LCC are interlopers, respectively.

The evolution of disks around stars with masses 1-3 M_{\odot} has been modeled by Kenyon & Bromley (2004, 2008). Approximately half (120/215) of the B- and A-type ScoCen members in our sample correspond to stars in this mass range (2.0-2.5 M_{\odot}). We searched for trends in the disk fraction around 2.0-2.5 M_{\odot} as a function of time. By comparing the infrared excess emission of stars with different ages, we can quantify disk evolution. We expect that 2.5 M_{\odot} stars will appear as B9.5 through B9 members of US, UCL, and LCC and that 2.0 M_{\odot} stars will appear as A9 through A0 members of US and as A7 through A0 members of UCL and LCC (Table 4). For US, we infer a disk fraction of 6/16 ($38^{+13}_{-10}\%$) for 2.5 M_{\odot} stars and 7/20 ($35^{+12}_{-9}\%$) for 2.0 M_{\odot} stars from the Oudmaijer et al. (1992) *IRAS* 25 μm survey and the Carpenter et al. (2009) MIPS 24 μm survey. We note that 2 of the excess systems around A-type stars, discovered by Oudmaijer et al. (1992), are "primordial" based on the presence of H α emission: HIP 79476/HD 145718 and HIP 81624/HD 150193 (Vieira et al. 2003). We measured 2.5 M_{\odot} disk fractions of 6/20 ($30^{+12}_{-8}\%$) and 4/10 ($40^{+16}_{-12}\%$) in UCL and LCC from this survey and the Oudmaijer et al. (1992) *IRAS* 25 μm survey, respectively, including one accreting, "primordial disk" in LCC (HIP 56379/HD 100546). We measured 2.0 M_{\odot} disk fractions of 16/50 ($32^{+7}_{-6}\%$) and 15/49 ($31^{+7}_{-6}\%$) in UCL and LCC, respectively. Since the US disk fractions are similar to the UCL and LCC disk fractions (both including and excluding primordial systems), we do not believe that there is strong evidence for a change in the disk fractions between ages \sim 11 Myr and \sim 15-20 Myr for 2.0-2.5 M_{\odot} stars.

The MIPS 24 μm observations in our survey can be combined with those from other surveys (Chen et al. 2011; Carpenter et al. 2009; Su et al. 2006; Oudmaijer et al. 1992) to determine whether ScoCen disks exhibit mass dependent evolution. We find that the disk

fractions for 2.0-2.5 M_{\odot} stars are somewhat smaller than those measured for 1.0-1.5 M_{\odot} stars ($\sim 33\%$) and that the disk fraction for higher mass stars ($> 3 M_{\odot}$) is substantially smaller, 4/57 ($7\%^{+5\%}_{-2\%}$) with Be stars forming the majority of high mass systems with 24 μm and/or 70 μm excess. We plot the ratio of the observed and expected photospheric 24 μm and 70 μm fluxes for all of the stars observed in ScoCen as a function of stellar mass in Figure 4 and Figure 5. Only HIP 81972 of the four high mass stars ($> 3 M_{\odot}$) with 24 μm excess is not a Be star. High-resolution, ground-based, near-infrared imaging suggests that HIP 81972 is a multiple system with at least one confirmed companion with an estimated mass 0.35 M_{\odot} , located at an angular separation of 5.0'' (Kouwenhoven et al. 2007). Since the angular resolution of *Spitzer* at 24 μm is $\sim 6''$, we can not determine whether the primary star, HIP 81972A, or its confirmed late-type companion is the source of the detected infrared excess.

4. Disk Evolution

Kenyon & Bromley (2004, 2008, 2010) model the infrared excess emission from self-stirred disks around stars with masses 1-3 M_{\odot} as a function of time, assuming that the disk is initially composed of planetesimals ranging in size from ~ 1 -1000 m at 30 - 150 AU. In these simulations, 1000 km planetary embryos first form at small radii where the surface density of solids is highest and then at subsequently greater distances with time. Once planetary embryos form, they trigger collisional cascades between nearby leftover planetesimals that grind remnant planetesimals into micron-sized dust grains that can be detected via thermal emission. Since the Kenyon & Bromley (2004, 2008, 2010) models initially include no primordial, micron-sized grains, they initially predict that the disks possess no infrared excess. As planetary embryo formation sweeps through the disk, the 24 μm flux ratio, $F_{\nu}(\text{observed})/F_{\nu}(\text{predicted})$, increases until it reaches a peak around 5-20 Myr and then decreases as planetary embryo formation propagates into the outer regions of the disk where dust debris possesses thermal equilibrium temperatures, $T_{gr} < 40$ K, too cold to emit strongly at 24 μm . Since 70 μm excess emission is diagnostic of cooler dust, the models predict that the 70 μm excess declines more slowly with time.

We plot the MIPS 24 μm and 70 μm flux ratios, $F_{\nu}(\text{observed})/F_{\nu}(\text{predicted})$, for nearby, intermediate-mass stars ($2.0 \pm 0.2 M_{\odot}$ and $2.5 \pm 0.2 M_{\odot}$ stars within 200 pc of the Sun), including our Sco Cen data and other data from the literature (Table 4) in Figures 6 and 7, consistent with our analysis of solar-like systems (Chen et al. 2011). Stars with accreting, primordial disks are shown with asterisks while those with debris disks are shown with solid circles. We list the disk type and accretion properties of 2.5 and 2.0 M_{\odot} ScoCen stars in Tables 5 and 7. Our current sample of intermediate-mass ScoCen stars only includes a

handful of primordial disks, unlike our previously-studied sample of ScoCen solar-like stars; therefore, inclusions or exclusion of primordial systems has a smaller effect on our current analysis. In general, we find that the 24 μm excess ratio associated with 2.0-2.5 M_\odot stars is consistent with Kenyon & Bromley (2004, 2008, 2010) expectations; however, the observed 24 μm excess around 2.5 M_\odot stars is somewhat lower than predicted. In Chen et al. (2011), we hypothesized that 1.0 M_\odot stars possessed larger than expected 24 μm excesses because the inner radii of the disks may have been smaller than 30 AU. We quantify trends in disk properties as a function of stellar mass and describe possible scenarios explaining the observations in the Section 6.

Since the subgroups of ScoCen possess slightly different ages, we searched for differences in the disk demographics between subgroups. We plot the cumulative disk fractions for 2.0 and 2.5 M_\odot stars in US, UCL, and LCC as a function of $F_\nu(24 \mu\text{m})/F_*(24 \mu\text{m})$ (Figure 8). Currie et al. (2008) searched for statistical trends in similar measurements of B-, A-, and F-type stars in Orion OB1b (\sim 5 Myr), Orion OB1a (\sim 10 Myr), and ScoCen (\sim 10-20 Myr). They performed a Wilcoxon rank sum analysis on measurements of [24] - [24]_{*} in Orion OB1a and ScoCen compared to Orion OB1b. For two samples, the Wilcoxon rank sum test determines the equality or inequality of two distributions by computing the mean rank of one distribution in a combined sample of both distributions. Currie et al. (2008) compute negative Z parameters and small probabilities, indicating that the mean 24 μm excess for stars measured in Orion OB1a and ScoCen were statistically smaller than that of Orion OB1b. We performed the Wilcoxon rank sum test on our sample of ScoCen intermediate mass star $F_\nu(24 \mu\text{m})/F_*(24 \mu\text{m})$ measurements, comparing each subgroup with US and UCL for 1.0 and 1.5 M_\odot stars both including and excluding primordial disks (see Table 8). For both 2.0 and 2.5 M_\odot stars, we find that the Wilcoxon rank sum test yields large probabilities ($>4\%$) when comparing US to UCL and LCC, indicating that the excesses around UCL and LCC are not statistically indistinguishable from those around US.

To better understand the $F_\nu(24 \mu\text{m})/F_*(24 \mu\text{m})$ distributions, we calculated the first quartile, median, and third quartile $F_\nu(24 \mu\text{m})/F_*(24 \mu\text{m})$ for 2.5 and 2.0 M_\odot stars in US, UCL, and LCC (see Table 8). Typical measurement uncertainties for $F_\nu(24 \mu\text{m})/F_*(24 \mu\text{m})$ in US, UCL, and LCC are 0.07, 0.05, and 0.05, respectively, suggesting that the median $F_\nu(24 \mu\text{m})/F_*(24 \mu\text{m})$ for each subgroup is consistent with a bare photosphere. We calculate the mean and standard deviation of $F_\nu(24 \mu\text{m})/F_*(24 \mu\text{m})$ (see Table 8) and overlay these values in our diagram showing excess trends as a function of age (Figure 6). For both 2.5 and 2.0 M_\odot stars, the $F_\nu(24 \mu\text{m})/F_*(24 \mu\text{m})$ standard deviation is very large, making it difficult to determine whether any robust evolutionary trend exists from the mean or the median alone. However, the first quartile values probe the strength of the 24 μm excess systems and indicate increased 24 μm excess for 2.0 and 2.5 M_\odot stars, regardless of whether

all disks are included or primordial disks are excluded from the analysis. Unfortunately, we detect only $\sim 10\%$ of our objects at $70 \mu\text{m}$. The detected objects possess excesses that are consistent with the expectations from KB08; however, the majority of the systems possess 3σ flux upper limits that are consistent with the models.

5. Dust Grain Properties

We compare the grain properties for detected ScoCen debris disks with those measured for debris disks in mature planetary systems. We estimate typical measured fractional infrared luminosities ($2 \times 10^{-6} < L_{IR}/L_* < 4 \times 10^{-2}$ and MIPS 24 and $70 \mu\text{m}$ blackbody color temperatures ($40 \text{ K} < T_{gr} < 300 \text{ K}$) around B- and A-type stars at $\sim 10\text{-}20 \text{ Myr}$. Su et al. (2006) estimate typical fractional infrared luminosities ($3 \times 10^{-6} < L_{IR}/L_* < 1 \times 10^{-3}$) and color temperatures ($60 \text{ K} < T_{gr} < 250 \text{ K}$) for debris disks around 1 Myr to 1 Gyr B6-A7-type stars. Our sample contains nine disks with somewhat higher fractional infrared luminosities ($L_{IR}/L_* > 1 \times 10^{-3}$) and warm terrestrial temperature debris ($T_{gr} > 200 \text{ K}$), consistent with the younger ages of these systems.

We estimate the minimum dust grain size, a_{min} , assuming that radiation pressure removes the smallest grains if $\beta (=F_{rad}/F_{grav}) > 0.5$.

$$a_{min} > \frac{6L_* < Q_{pr}(a) >}{16\pi GM_* c \rho_s} \quad (1)$$

(Artymowicz 1988) where L_* and M_* are the stellar luminosity and mass, $< Q_{pr}(a) > (= (\int F_\lambda d\lambda)^{-1} \int Q_{pr}(a, \lambda) F_\lambda d\lambda)$ is the radiation pressure coupling coefficient, and ρ_s is the density of an individual dust grain. We estimate stellar masses for UCL/LCC members using our estimated stellar effective temperatures and a 15 Myr isochrone (Bertelli et al. 1994; Dotter et al. 2008). Infrared spectroscopy of T Tauri disks suggest that the bulk of the dust in these systems is probably amorphous olivine (Watson et al. 2009); therefore, we use optical constants measured for amorphous olivine ($\rho_s = 3.71 \text{ g cm}^{-3}$; Dorschner et al. (1995)) to estimate the radiation pressure coupling coefficient; for simplicity, we assume that the grains are spherical. In general, the estimated minimum grain sizes are too small for the grains to behave as simple blackbodies ($Q_{abs} \propto \text{constant}$) and too large for the grains to behave in the small grain approximation ($2\pi a \ll \lambda$).

We estimate the grain distance of the dust from the grain temperature, T_{gr} , assuming that the dust particles are in radiative equilibrium, and possess an average grain size, $< a > = 5/3 a_{min}$, expected if the grains are in collisional equilibrium. Dust grains, D , in

radiative equilibrium with a star are located at a distance, D

$$\left(\frac{R_*}{D}\right)^2 \int_0^\infty Q_{abs}(\nu) B_\nu(T_*) d\nu = 4 \int_0^\infty Q_{abs} B_\nu(T_{gr}) d\nu \quad (2)$$

where Q_{abs} is the absorption coefficient for the dust grains. We estimate dust distances using optical constants measured for amorphous olivine and calculate absorption coefficients assuming that the grains are spherical, with radius, $\langle a \rangle$. Our data are consistent with the presence of dust located in rings at Kuiper-Belt-like distances, suggesting that the average ScoCen debris disk is a massive analog to our Kuiper Belt at an age <20 Myr.

We estimate the minimum mass of infrared-emitting dust grains, assuming that the grains have a radius, $\langle a \rangle$; if the grains are larger, then our estimate is a lower bound. If we assume a thin shell of dust at distance, D , from the central star, and if the grains are spheres of radius, $\langle a \rangle$, and if the cross section of the grains is equal to their geometric cross section, then the mass of dust is

$$M_d \geq \frac{16}{3} \pi \frac{L_{IR}}{L_*} \rho_s D^2 \langle a \rangle \quad (3)$$

where L_{IR} is the luminosity of the dust. The bulk of the dust mass is expected to be located in larger grains.

We estimate the minimum mass in parent bodies assuming that the disk is Poynting–Robertson (PR) drag dominated and in steady state. We hypothesize that each system possesses at least as much mass in parent bodies today as that which would have been destroyed if the system were in steady state during the lifetime of the star. If MPB denotes the mass in parent bodies, then we may write

$$M_{PB} \geq \frac{4L_{IR}t_{age}}{c^2} \quad (4)$$

(Chen & Jura 2001). If the disk is dominated by collisions, as is probably the case, then this estimate will be a lower bound.

6. Stellar Mass Dependence

We combine the data from our survey of 215 ScoCen B- and A-type stars with that from the survey of Chen et al. (2011) of 181 ScoCen F- and G-type stars to search for trends in disk properties as a function of stellar mass. We find that (1) few stars with masses $>3 M_\odot$ possess 24 μm and/or 70 μm excess and (2) stars with masses 1.0–1.75 M_\odot possess larger first quartile and median $F_\nu(24 \mu\text{m})/F_*(24 \mu\text{m})$ and $F_\nu(70 \mu\text{m})/F_*(70 \mu\text{m})$ than stars with

masses 1.75-3.0 M_{\odot} (see Figures 4 and 5). The first quartile $F_{\nu}(24 \mu\text{m})/F_{*}(24 \mu\text{m})$ values for 1.0-1.75 M_{\odot} and 1.75-3.0 M_{\odot} stars are 1.59 and 1.32, respectively. Comparing the 24 μm flux ratio measurements of the low mass stars with those of the high mass stars, the Wilcoxon-Rank Sum test yields a Z-parameter of 2.96 and a probability of 0.2%, indicating that the 1.0-1.75 M_{\odot} stars possess a higher median $F_{\nu}(24 \mu\text{m})/F_{*}(24 \mu\text{m})$ value than the 1.75-3.0 M_{\odot} stars. The first quartile $F_{\nu}(70 \mu\text{m})/F_{*}(70 \mu\text{m})$ values for 1.0-1.75 M_{\odot} and 1.75-3.0 M_{\odot} stars are 520 and 175, respectively. Comparing the 70 μm flux ratio measurements of the low mass stars with those of the high mass stars, the Wilcoxon-Rank Sum test yields a Z-parameter of 3.62 and a probability of 0.01%, indicating that the 1.0-1.75 M_{\odot} stars possess a higher median $F_{\nu}(70 \mu\text{m})/F_{*}(70 \mu\text{m})$ value than the 1.75-3.0 M_{\odot} stars. While our shallow MIPS observations are sensitive to stellar photospheres at 24 μm , they are not sensitive to stellar photospheres at 70 μm . Since our $F_{\nu}(70 \mu\text{m})/F_{*}(70 \mu\text{m})$ measurements are more sensitive for higher mass stars, our $F_{\nu}(70 \mu\text{m})/F_{*}(70 \mu\text{m})$ statistics may be biased.

Since debris disks are typically characterized by their the fractional infrared luminosities and dust grain temperatures, we also searched for trends in these quantities as a function of stellar mass. We find that L_{IR}/L_{*} is mass dependent with 1.0-1.75 M_{\odot} stars possessing higher L_{IR}/L_{*} than 1.75-3.0 M_{\odot} stars (see Figure 9). The first quartile L_{IR}/L_{*} values for 1.0-1.75 M_{\odot} and 1.75-3.0 M_{\odot} stars are 0.003 and 0.0002, respectively. Comparing the fractional infrared luminosity measurements of the low mass stars with those of the high mass stars, the Wilcoxon-Rank Sum test yields a Z-parameter of 3.71 and a probability of 0.01%, indicating that the 1.0-1.75 M_{\odot} stars possess a higher median $F_{\nu}(24 \mu\text{m})/F_{*}(24 \mu\text{m})$ value than the 1.75-3.0 M_{\odot} stars. If the dust grains are optically thin, then our results may indicate that the dust mass in micron-sized grains decreases as a function of stellar mass. Measurements of the thermal continuum at submillimeter and/or millimeter wavelengths, where the dust is more likely to be optically thin, are needed to determine definitively whether dust mass declines with stellar mass. We do not find any dependence of T_{gr} on stellar mass (see Figure 10); however, we note that our temperatures are only estimated from our MIPS 24 μm and 70 μm photometry. Measurements of the infrared excess at other wavelengths are needed to better characterize the dust temperature in detail. For a more direct comparison with planet formation models, we also plot our estimated dust masses, M_d , and estimated dust distances, D , as a function of stellar mass (see Figure 11 and Figure 12). We note that (1) the estimated dust distance depends sensitively on assumed grain properties and that observations of resolved disks indicate that similarly estimated distances may be inconsistent with observations by as much as a factor of two and (2) the estimated dust mass only represents the estimated mass in micron-sized grains observed at mid- to far-infrared wavelengths. Our estimated dust distances indicate that the cold planetesimal belts in ScoCen are too distant to be influenced by giant planets on circular orbits that are

predicted to have formed via traditional core-accretion models. Studies of the location of the snow-line in giant planet forming disks indicate that giant planets form at \sim 6-10 AU and \sim 8-20 AU around 1 and 3 M_{\odot} stars, respectively (Kennedy & Kenyon 2008).

In the Kenyon & Bromley (2004, 2008, 2010) models, the mass of the central star plays a critical role in determining the evolution of the disk. Since the models assume that the mass in initial parent bodies is proportional to stellar mass, the number of small grains generated via collisional cascade is expected to be larger around higher mass stars. The dust in debris disks around higher mass stars is also expected to be warmer than that around lower mass stars because all of the disks are assumed to possess the same inner and outer radii and the higher mass stars are more luminous and therefore more effectively heat circumstellar dust. In Figures 4 and 5, we overplot the Kenyon & Bromley (2008) $F_{\nu}(24 \mu\text{m})/F_{*}(24 \mu\text{m})$ and $F_{\nu}(70 \mu\text{m})/F_{*}(70 \mu\text{m})$ predictions as a function of stellar mass for 11, 15, and 17 Myr old stars with initial disk masses similar to the MMSN and disks with masses 1/3 lower and 3 times higher and Kenyon & Bromley (2010) predictions for disks with weak planetesimals or a surface density profile, $\Sigma \propto r^{-1}$ rather than $r^{-3/2}$. We estimate the fraction of stars with excesses above the Kenyon & Bromley (2008) model predictions, consistent with the Kenyon & Bromley (2008) model predictions, and below the Kenyon & Bromley (2008) model predictions for 1.0-1.75 and 1.75-3.0 M_{\odot} stars. For 1.00-1.75 M_{\odot} stars, we estimate that 23/190 ($12^{+3}_{-2}\%$), 82/190 ($43^{+4}_{-3}\%$), and 85/190 ($45^{+4}_{-4}\%$) of systems possess 24 μm excesses above, consistent with, and below the models. For 1.75-3.00 M_{\odot} stars, we estimate that 5/171 ($3^{+2}_{-1}\%$), 22/171 ($13^{+3}_{-2}\%$), and 144/171 ($84^{+2}_{-3}\%$) of systems possess 24 μm excesses above, consistent with, and below the models, suggesting that the infrared excesses associated with 1.75-3.0 M_{\odot} is disproportionately low compared with the models. Our estimates for the dust grain temperature around ScoCen stars is significantly higher than that predicted for 10-20 Myr old stars by (Kenyon & Bromley 2008). The discrepancy between the observed and Kenyon & Bromley (2008) predicted dust grain temperature is probably the result of the artificial 30-150 AU boundary conditions assumed by the models. A similar discrepancy has been noted for debris disks around older, A-type stars and has been used to argue for the presence of narrow debris belts (Kennedy & Wyatt 2010).

6.1. Parent Body Mass

Current models for debris disks assume that the radiation pressure blow-out limit sets the minimum grain size, suggesting that the minimum grain size around higher mass stars is larger than that around lower mass stars. One possible explanation for the smaller infrared excesses around B- and A-type stars is that all systems possess the same parent body mass;

however, the higher radiation pressure of higher mass stars disproportionately removes the smallest grains which radiate the bulk of the infrared excess. To determine whether blow-out size effects can account for the discrepancies in our observations, we estimate the increased surface area in small grains generated by lowering the minimum grain size. For dust particles in collisional equilibrium, the surface area in particles, $\sigma_{tot} \propto a_{min}^{-0.5}$ (Kennedy & Wyatt 2010). Therefore lowering the blowout size from $\sim 10 \mu\text{m}$ around a $25 L_\odot$, $2.1 M_\odot$ star to $\sim 1 \mu\text{m}$ around a $1 L_\odot$, $1 M_\odot$ star is expected to decrease the dust surface area and therefore the fractional infrared luminosity by a factor ~ 3 . Since the ratio of the 1st quartile fractional infrared excesses for $1.0\text{-}1.75 M_\odot$ and $1.75\text{-}3 M_\odot$ stars is $0.003/0.0002 (\sim 15)$, significantly larger than based on minimum grain size effects alone, we conclude that radiation pressure blowout is probably not responsible for the observed fractional infrared luminosity dependence on stellar mass.

6.2. Stellar Companions

A large fraction of ScoCen members may be members of binary or multiple systems. Forty B- and A-type and thirty-three F- and G-type ScoCen stars are listed as binary or multiple systems in the Catalog of the Components of Double and Multiple stars (CCDM, Domanget & Nys (2002)). More recently, Kouwenhoven et al. (2005) have carried out a near-infrared adaptive optics search (using VLT ADONIS) for companions around 199 B- and A-type members of ScoCen; they discovered 41 new candidate companions with angular separations $0.22'' - 12.4''$, corresponding to projected separations of 28.6 AU - 1600 AU. A follow-up demographic study of ScoCen multiplicity, taking into account all available observations of ScoCen intermediate-mass, visual, spectroscopic, and astrometric binaries suggests that the ScoCen intermediate-mass binary fraction may be as large as $>70\%$ (Kouwenhoven et al. 2007). For each multiple system in our sample, we list the estimated angular separation(s) between the primary and its known and/or candidate companion(s) in Table 1.

Binary systems have been observed to possess both circumbinary disks that surround both stars and circumstellar disk(s) that surround the primary and/or secondary star(s). Detailed SPH modeling of binary systems suggest that the inner edge of the circumbinary disk is typically located at $1.8a$ to $3a$ and that the outer edges of the circumstellar disks are located at $<0.5a$, where a is the binary semi-major axis (Lubow & Artymowicz 2000). Therefore, companions may truncate the inner and/or outer edges of planetesimals distributions, modifying the expected properties of collisionally-generated, micron-sized grains (e.g. distance, temperature). To determine whether companions may truncate the outer edges of ScoCen disks, we plotted a histogram showing the percentage of the sample with binary

separations 10 - 200 AU for intermediate-mass and solar-mass stars (see Figure 13). We estimate that \sim 20% of the B- and A-type stars in our ScoCen sample and \sim 10% of the F- and G-type stars in the Chen et al. (2011) sample possess companions within 200 AU. We hypothesize that the lower excesses associated with intermediate-mass stars may be due to disk truncation; however, we note that the ScoCen F- and G-type members have not been systematically searched for companions. Indeed, we described two new companions to two solar-like ScoCen stars (HIP 72033B and HIP 77520B) for the first time in Chen et al. (2011). In Figure 13, we overlaid the distribution of binary systems with 24 μm excesses; we additionally found that most binary systems do not possess 24 μm excess.

Two A-type stars (HIP 77150 and HIP 77315) and two F-type stars (HIP 56673/HD 101088, and HIP 63975/HD 113766) apparently possess 24 μm excesses despite the presence of companions at 10 - 200 AU. For HIP 77315 and HIP 63975, the excesses are detected at 24 and 70 μm , consistent with the presence of dust at 12.2 AU and 3 AU, respectively, significantly closer to the star than the observed companions at 100 AU and 150 AU, respectively, and consistent with either circumprimary and/or circumsecondary disks. For HIP 77150 and HIP 56673, the excesses are only detected at 24 μm ; therefore, the estimates of grain temperature are lower limits and those of dust distance are upper limits. For HIP 77150, the dust is expected be located at a distance $<$ 82 AU, consistent with the presence of circumbinary dust around the 25 AU separation binary. For HIP 56673 with a binary separation of 19 AU, the data are more challenging to interpret. Follow-up IRS spectra indicate that the shape of the 5-35 μm spectrum is photospheric, suggesting that this system does not possess thermal emission from circumstellar dust; however, multi-epoch, high-resolution visual spectra indicate the presence of time-variable H α emission consistent with the presence of an accretion disk around one of the components in this binary system (Bitner et al. 2010).

7. Discussion

The *Wide-field Infrared Survey Explorer* (WISE, Wright et al. (2010)) recently completed its mission to map the sky at 3.4, 4.6, 12, and 22 μm with an angular resolution of 6.1'', 6.4'', 6.5'', and 12.0'', and 5 σ point source sensitivities \sim 0.08, 0.11, 1, and 6 mJy. In March 2012, the mission released an all-sky photometric catalog. Since ScoCen members are \sim 10 - 20 Myr old, their SEDS are expected to be photospheric at 3.4 and 4.6 μm with possible excesses at 12 and 22 μm . In 2MASS K_s , the B- through G-type members possess measured K_s -band magnitudes typically between 4th and 9th magnitude, suggesting that while the WISE 3.4 and 4.6 μm photometry is typically saturated, the 2MASS J, H, and K_s -band photometry is not. Therefore, we prefer to estimate photospheric fluxes at mid-

infrared wavelengths from 2MASS data rather than WISE data even though the WISE data are observed at longer wavelengths and would provide more accurate photospheric estimates if the data were not saturated. In addition, we prefer to compare the WISE 12 and 22 μm brightnesses directly with 2MASS J, H, K_s brightnesses to determine whether sources possess long wavelength excesses.

Similarly, we expect that our *Spitzer* MIPS 24 μm photometry observations should supercede the WISE 22 μm observations because (a) the MIPS 24 μm beam has an angular size $\sim 6''$, half the size of WISE 22 μm beam, and is therefore less subject to source confusion and (b) our MIPS 24 μm measurements are more sensitive than the WISE 22 μm measurements and therefore possess higher signal-to-noise ratios. We compare the WISE 22 μm and MIPS 24 μm photometry for all of the ScoCen members that were observed using MIPS (see Figure 14). In general, we find that the 22 and 24 μm fluxes are well-correlated with a modest dispersion; the UCL and LCC mean [22]-[24] colors are -0.06 mag and -0.04 mag, respectively, with standard deviations of 0.29 mag and 0.30 mag, respectively, suggesting that the WISE 22 μm data are consistent with the MIPS 24 μm data to $\sim 30\%$. Two stars, HIP 67472 (a Be star in UCL) and PDS 66 (a protoplanetary disk in LCC), possess [22]-[24] > 1 mag; since these objects possess 24 and 70 μm excesses, the [22]-[24] colors are probably a measurement of the local SED slope. Three stars in UCL (HIP 80663, HIP 80897, and HIP 81380) and four stars stars in LCC (HIP 53701, HIP 59716, HIP 62677, and HIP 67230) possess [22]-[24] < -1 mag. The majority of the outliers (HIP 53701, HIP 62677, HIP 67230, HIP 80897, HIP 80897, and HIP 81380) are located in regions with bright cirrus; therefore, both MIPS and WISE photometry measurements are probably confused. The MIPS 24 μm image of HIP 59716 reveals a bright infrared companion at $2.6''$ that probably confuses the WISE 22 μm photometry.

The WISE 12 μm band does provide a new opportunity to survey all of the ScoCen members at an additional wavelength. The 12 μm photometry can be used to probe warm terrestrial temperature dust (~ 240 K) at closer distances than the cooler dust detected at 24 μm (~ 120 K). The 12 μm excess associated with ScoCen members is significantly smaller than the 24 μm excess (see Figure 15), indicating that the inner regions of the disks possess less dust than the outer disk but that the terrestrial planet zone has not been completely cleared of parent bodies. We plotted K_s -[24] color as a function of K_s -[24] color (see Figure 16) to determine whether any trends exist in the infrared properties. We find that (1) stars without infrared excess appear to fall on a line that passes through the origin in K_s -[24] versus K_s -[12] space; (2) the majority of stars with K_s -[24] > 0.5 excess typically also possess weak K_s -[12] > 0.1 excess; and (3) UCL possesses more stars with weak 12 and 24 μm excess. Follow-up *Spitzer* IRS spectra are required to characterize in detail the temperature distribution of the dust and therefore the spatial distribution of dust in these systems. We

also plotted the time evolution of the normalized 12 μm fluxes, $F_\nu(12 \mu\text{m})/F_*(12 \mu\text{m})$, (see Figure 17) for young (<300 Myr), nearby ($\lesssim 200$ pc) stars using the same sample as described in Table 4) for 2.0-2.5 M_\odot stars and the same sample as described by Chen et al. (2011) for 1.0-1.5 M_\odot stars. Our analysis indicates that the production of warm terrestrial dust has subsided by an age of ~ 30 Myr and ~ 100 Myr for intermediate- and solar-mass stars, respectively, approximately the same timescale as observed for colder dust. The similarity in warm and cold dust dissipation timescales may indicate the presence of not only inner and outer disks of planetesimals but also giant planets at Jupiter- Saturn distances that are in stable or weakly unstable systems (Raymond et al. 2011).

8. Conclusions

We have obtained *Spitzer* MIPS 24 and 70 μm photometry of 215 candidate B- and A-type members of Scorpius-Centaurus. We conclude the following:

1. The ScoCen subgroups US, UCL, and LCC possess statistically indistinguishable B+A 24 μm excess fractions of $25^{+6}_{-5}\%$, $27^{+4}_{-4}\%$, and $24^{+5}_{-4}\%$, somewhat lower than the disk fractions observed by Chen et al. (2011) for F+G stars.
2. The $F_\nu(24 \mu\text{m})/F_*(24 \mu\text{m})$ and $F_\nu(70 \mu\text{m})/F_*(70 \mu\text{m})$ excesses of B+A stars is systematically smaller than that measured toward F+G stars, consistent with recent WISE observations (Rizzuto et al. 2012). Estimates of fractional infrared luminosity and grain temperature suggest that L_{IR}/L_* decreases with increasing stellar mass and T_{gr} is not dependent on stellar mass.
3. For 2.5 M_\odot stars, the debris disk fraction does not appear to change statistically between 10 Myr and 15-20 Myr; however the 1st quartile of the MIPS $F_\nu(24 \mu\text{m})/F_*(24 \mu\text{m})$ increases as expected from collisions between oligarchs at 30-150 AU in self-stirred disks. For 2.0 M_\odot stars, the disk fraction does not appear to change statistically between 10 Myr and 15-20 Myr and the 1st quartile of the MIPS $F_\nu(24 \mu\text{m})/F_*(24 \mu\text{m})$ increases only if primordial disks are retained in the sample.
4. The known fraction of stellar companions at 10 - 200 AU around B+A stars is approximately a factor of two higher than that around F+G stars; therefore, the lower disk fraction and the lower fractional infrared excesses associated with detected disks may be the result of disk truncation.
5. ScoCen B- through G-type members with MIPS 24 μm excess also possess weak WISE 12 μm excess, indicating the presence of additional warm dust in the terrestrial planet

forming zone, suggesting that terrestrial planets may still be forming around ScoCen stars at 10 - 100 Myr.

We would like to thank D. Hines, G. Kennedy, S. Kenyon, S. Lubow, and M. Wyatt for their helpful comments and suggestions. This work is based on observations made with the *Spitzer Space Telescope*, which is operated by JPL/Caltech under a contract with NASA. Support for this work was provided by NASA through an award issued by JPL/Caltech. This research made use of the SIMBAD database, operated at CDS, Strasbourg, France, and data products from the 2MASS, which is a joint project of the U. Massachusetts and the Infrared Processing and Analysis Center/Caltech, funded by NASA and the NSF.

REFERENCES

- Artymowicz, P. 1988, ApJ, 335, L79
- Bertelli, G., Bressan, A., Chiosi, C., Fagotto, F., & Nasi, E. 1994, A&AS, 106, 275
- Bitner, M. A., Chen, C. H., Muzeirole, J., Weinberger, A. J., Pecaut, M., Mamajek, E. E., & McClure, M. K. 2010, ApJ, 714, 1542
- Buscombe, W., & Kennedy, P. M. 1965, MNRAS, 130, 281
- Carpenter, J. M., Bouwman, J., Silverstone, M. D., Kim, J. S., Stauffer, J., Cohen, M., Hines, D. C., Meyer, M. R., & Crockett, N. 2008, ApJS, 179, 423
- Carpenter, J. M., Mamajek, E. E., Hillenbrand, L. A., & Meyer, M. R. 2006, ApJ, 651, L49
—. 2009, ApJ, 705, 1646
- Chen, C. H., & Jura, M. 2001, ApJ, 560, L171
- Chen, C. H., Mamajek, E. E., Bitner, M. A., Pecaut, M., Su, K. Y. L., & Weinberger, A. J. 2011, ApJ, 738, 122
- Corbally, C. J. 1984, ApJS, 55, 657
- Currie, T., Kenyon, S. J., Balog, Z., Rieke, G., Bragg, A., & Bromley, B. 2008, ApJ, 672, 558
- Cutri, R. M., Skrutskie, M. F., van Dyk, S., Beichman, C. A., Carpenter, J. M., Chester, T., Cambresy, L., Evans, T., Fowler, J., Gizis, J., Howard, E., Huchra, J., Jarrett, T., Kopan, E. L., Kirkpatrick, J. D., Light, R. M., Marsh, K. A., McCallon, H.,

- Schneider, S., Stiening, R., Sykes, M., Weinberg, M., Wheaton, W. A., Wheelock, S., & Zacarias, N. 2003, VizieR Online Data Catalog, 2246, 0
- de Bruijne, J. H. J. 1999, MNRAS, 306, 381
- de Zeeuw, P. T., Hoogerwerf, R., de Bruijne, J. H. J., Brown, A. G. A., & Blaauw, A. 1999, AJ, 117, 354
- Dommangé, J., & Nys, O. 2002, VizieR Online Data Catalog, 1274, 0
- Dorschner, J., Begemann, B., Henning, T., Jaeger, C., & Mutschke, H. 1995, A&A, 300, 503
- Dotter, A., Chaboyer, B., Jevremović, D., Kostov, V., Baron, E., & Ferguson, J. W. 2008, ApJS, 178, 89
- Engelbracht, C. W., Blaylock, M., Su, K. Y. L., Rho, J., Rieke, G. H., Muzerolle, J., Padgett, D. L., Hines, D. C., Gordon, K. D., Fadda, D., Noriega-Crespo, A., Kelly, D. M., Latter, W. B., Hinz, J. L., Misselt, K. A., Morrison, J. E., Stansberry, J. A., Shupe, D. L., Stolovy, S., Wheaton, W. A., Young, E. T., Neugebauer, G., Wachter, S., Pérez-González, P. G., Frayer, D. T., & Marleau, F. R. 2007, PASP, 119, 994
- Fischer, D. A., & Valenti, J. 2005, ApJ, 622, 1102
- Gahm, G. F., Ahlin, P., & Lindroos, K. P. 1983, A&AS, 51, 143
- Garrison, R. F. 1967, ApJ, 147, 1003
- Garrison, R. F., & Gray, R. O. 1994, AJ, 107, 1556
- Gordon, K. D., Engelbracht, C. W., Fadda, D., Stansberry, J., Wachter, S., Frayer, D. T., Rieke, G., Noriega-Crespo, A., Latter, W. B., Young, E., Neugebauer, G., Balog, Z., Beeman, J. W., Dole, H., Egami, E., Haller, E. E., Hines, D., Kelly, D., Marleau, F., Misselt, K., Morrison, J., Pérez-González, P., Rho, J., & Wheaton, W. A. 2007, PASP, 119, 1019
- Gordon, K. D., Rieke, G. H., Engelbracht, C. W., Muzerolle, J., Stansberry, J. A., Misselt, K. A., Morrison, J. E., Cadien, J., Young, E. T., Dole, H., Kelly, D. M., Alonso-Herrero, A., Egami, E., Su, K. Y. L., Papovich, C., Smith, P. S., Hines, D. C., Rieke, M. J., Blaylock, M., Pérez-González, P. G., Le Floc'h, E., Hinz, J. L., Latter, W. B., Hesselroth, T., Frayer, D. T., Noriega-Crespo, A., Masci, F. J., Padgett, D. L., Smylie, M. P., & Haegel, N. M. 2005, PASP, 117, 503

- Gorlova, N., Rieke, G. H., Muzerolle, J., Stauffer, J. R., Siegler, N., Young, E. T., & Stansberry, J. H. 2006, ApJ, 649, 1028
- Gray, R. O., & Garrison, R. F. 1987, ApJS, 65, 581
- . 1989, ApJS, 70, 623
- Hauck, B., & Mermilliod, M. 1998, A&AS, 129, 431
- Hernández, J., Briceño, C., Calvet, N., Hartmann, L., Muzerolle, J., & Quintero, A. 2006, ApJ, 652, 472
- Hiltner, W. A., Garrison, R. F., & Schild, R. E. 1969, ApJ, 157, 313
- Hoogerwerf, R., & Aguilar, L. A. 1999, MNRAS, 306, 394
- Houk, N. 1978, Michigan catalogue of two-dimensional spectral types for the HD stars, ed. Houk, N.
- . 1982, Michigan Catalogue of Two-dimensional Spectral Types for the HD stars. Volume -3. Declinations -40 to -26, ed. Houk, N.
- Houk, N., & Cowley, A. P. 1975, University of Michigan Catalogue of two-dimensional spectral types for the HD stars. Volume I. Declinations -90 to -53, ed. Houk, N. & Cowley, A. P.
- Hube, D. P. 1970, MmRAS, 72, 233
- Hughes, A. M., Wilner, D. J., Calvet, N., D'Alessio, P., Claussen, M. J., & Hogerheijde, M. R. 2007, ApJ, 664, 536
- Jaschek, C., Jaschek, M., Morgan, W. W., & Slettebak, A. 1968, ApJ, 153, L87
- Johnson, J. A., Aller, K. M., Howard, A. W., & Crepp, J. R. 2010, PASP, 122, 905
- Jordi, C., Ribas, I., Torra, J., & Gimenez, A. 1997, A&A, 326, 1044
- Kennedy, G. M., & Kenyon, S. J. 2008, ApJ, 673, 502
- Kennedy, G. M., & Wyatt, M. C. 2010, MNRAS, 405, 1253
- Kenyon, S. J., & Bromley, B. C. 2004, AJ, 127, 513
- . 2008, ApJS, 179, 451

- . 2010, ApJS, 188, 242
- Kouwenhoven, M. B. N., Brown, A. G. A., Portegies Zwart, S. F., & Kaper, L. 2007, A&A, 474, 77
- Kouwenhoven, M. B. N., Brown, A. G. A., Zinnecker, H., Kaper, L., & Portegies Zwart, S. F. 2005, A&A, 430, 137
- Levato, H., Malaroda, S., Morrell, N., & Solivella, G. 1987, ApJS, 64, 487
- Levato, H., Malaroda, S., Morrell, N., Solivella, G., & Grossi, M. 1996, A&AS, 118, 231
- Lubow, S. H., & Artymowicz, P. 2000, Protostars and Planets IV, 731
- Mamajek, E. E., Meyer, M. R., & Liebert, J. 2002, AJ, 124, 1670
- Mermilliod, J.-C., & Mermilliod, M. 1994, Catalogue of Mean UBV Data on Stars, ed. Mermilliod, J.-C. & Mermilliod, M.
- Morgan, W. W., Abt, H. A., & Tapscott, J. W. 1978, Revised MK Spectral Atlas for stars earlier than the sun, ed. Morgan, W. W., Abt, H. A., & Tapscott, J. W.
- Morris, P. M. 1961, MNRAS, 122, 325
- Osawa, K. 1965, Annals of the Tokyo Astronomical Observatory, 9, 121
- Oudmaijer, R. D., van der Veen, W. E. C. J., Waters, L. B. F. M., Trams, N. R., Waelkens, C., & Engelsman, E. 1992, A&AS, 96, 625
- Paunzen, E., Duffee, B., Heiter, U., Kuschnig, R., & Weiss, W. W. 2001, A&A, 373, 625
- Pecaut, M. J., Mamajek, E. E., & Bubar, E. J. 2012, ApJ, 746, 154
- Plavchan, P., Werner, M. W., Chen, C. H., Stapelfeldt, K. R., Su, K. Y. L., Stauffer, J. R., & Song, I. 2009, ApJ, 698, 1068
- Preibisch, T., & Mamajek, E. 2008, The Nearest OB Association: Scorpius-Centaurus (Sco OB2), ed. Reipurth, B., 235
- Raymond, S. N., Armitage, P. J., Moro-Martín, A., Booth, M., Wyatt, M. C., Armstrong, J. C., Mandell, A. M., Selsis, F., & West, A. A. 2011, A&A, 530, A62
- Rebull, L. M., Stapelfeldt, K. R., Werner, M. W., Mannings, V. G., Chen, C., Stauffer, J. R., Smith, P. S., Song, I., Hines, D., & Low, F. J. 2008, ApJ, 681, 1484

- Rieke, G. H., Young, E. T., Engelbracht, C. W., Kelly, D. M., Low, F. J., Haller, E. E., Beeman, J. W., Gordon, K. D., Stansberry, J. A., Misselt, K. A., Cadien, J., Morrison, J. E., Rivlis, G., Latter, W. B., Noriega-Crespo, A., Padgett, D. L., Stapelfeldt, K. R., Hines, D. C., Egami, E., Muzerolle, J., Alonso-Herrero, A., Blaylock, M., Dole, H., Hinz, J. L., Le Floc'h, E., Papovich, C., Pérez-González, P. G., Smith, P. S., Su, K. Y. L., Bennett, L., Frayer, D. T., Henderson, D., Lu, N., Masci, F., Pesenson, M., Rebull, L., Rho, J., Keene, J., Stolovy, S., Wachter, S., Wheaton, W., Werner, M. W., & Richards, P. L. 2004, ApJS, 154, 25
- Rizzuto, A. C., Ireland, M. J., & Robertson, J. G. 2011, MNRAS, 416, 3108
- Rizzuto, A. C., Ireland, M. J., & Zucker, D. B. 2012, MNRAS, L406
- Schild, R. E., Neugebauer, G., & Westphal, J. A. 1971, AJ, 76, 237
- Schneider, G., Weinberger, A. J., Becklin, E. E., Debes, J. H., & Smith, B. A. 2009, AJ, 137, 53
- Shatsky, N., & Tokovinin, A. 2002, A&A, 382, 92
- Shobbrook, R. R. 1983, MNRAS, 205, 1215
- Siegler, N., Muzerolle, J., Young, E. T., Rieke, G. H., Mamajek, E. E., Trilling, D. E., Gorlova, N., & Su, K. Y. L. 2007, ApJ, 654, 580
- Slesnick, C. L., Carpenter, J. M., & Hillenbrand, L. A. 2006, AJ, 131, 3016
- Stauffer, J. R., Rebull, L. M., Carpenter, J., Hillenbrand, L., Backman, D., Meyer, M., Kim, J. S., Silverstone, M., Young, E., Hines, D. C., Soderblom, D. R., Mamajek, E., Morris, P., Bouwman, J., & Strom, S. E. 2005, AJ, 130, 1834
- Su, K. Y. L., Rieke, G., Stapelfeldt, K., Bryden, G., Werner, M., Plavchan, P., Trilling, D., Gaspar, A., & Morales, F. 2010, in Bulletin of the American Astronomical Society, Vol. 42, American Astronomical Society Meeting Abstracts 215, 428.26
- Su, K. Y. L., Rieke, G. H., Stansberry, J. A., Bryden, G., Stapelfeldt, K. R., Trilling, D. E., Muzerolle, J., Beichman, C. A., Moro-Martin, A., Hines, D. C., & Werner, M. W. 2006, ApJ, 653, 675
- Uppgren, A. R., Grossenbacher, R., Penhallow, W. S., MacConnell, D. J., & Frye, R. L. 1972, AJ, 77, 486

- Vieira, S. L. A., Corradi, W. J. B., Alencar, S. H. P., Mendes, L. T. S., Torres, C. A. O., Quast, G. R., Guimarães, M. M., & da Silva, L. 2003, AJ, 126, 2971
- Watson, D. M., Leisenring, J. M., Furlan, E., Bohac, C. J., Sargent, B., Forrest, W. J., Calvet, N., Hartmann, L., Nordhaus, J. T., Green, J. D., Kim, K. H., Sloan, G. C., Chen, C. H., Keller, L. D., d'Alessio, P., Najita, J., Uchida, K. I., & Houck, J. R. 2009, ApJS, 180, 84
- Werner, M. W., Roellig, T. L., Low, F. J., Rieke, G. H., Rieke, M., Hoffmann, W. F., Young, E., Houck, J. R., Brandl, B., Fazio, G. G., Hora, J. L., Gehrz, R. D., Helou, G., Soifer, B. T., Stauffer, J., Keene, J., Eisenhardt, P., Gallagher, D., Gautier, T. N., Irace, W., Lawrence, C. R., Simmons, L., Van Cleve, J. E., Jura, M., Wright, E. L., & Cruikshank, D. P. 2004, ApJS, 154, 1
- Wood, R. 1977, MmRAS, 84, 119
- Wright, E. L., Eisenhardt, P. R. M., Mainzer, A. K., Ressler, M. E., Cutri, R. M., Jarrett, T., Kirkpatrick, J. D., Padgett, D., McMillan, R. S., Skrutskie, M., Stanford, S. A., Cohen, M., Walker, R. G., Mather, J. C., Leisawitz, D., Gautier, III, T. N., McLean, I., Benford, D., Lonsdale, C. J., Blain, A., Mendez, B., Irace, W. R., Duval, V., Liu, F., Royer, D., Heinrichsen, I., Howard, J., Shannon, M., Kendall, M., Walsh, A. L., Larsen, M., Cardon, J. G., Schick, S., Schwalm, M., Abid, M., Fabinsky, B., Naes, L., & Tsai, C.-W. 2010, AJ, 140, 1868
- Zuckerman, B., Rhee, J. H., Song, I., & Bessell, M. S. 2011, ApJ, 732, 61

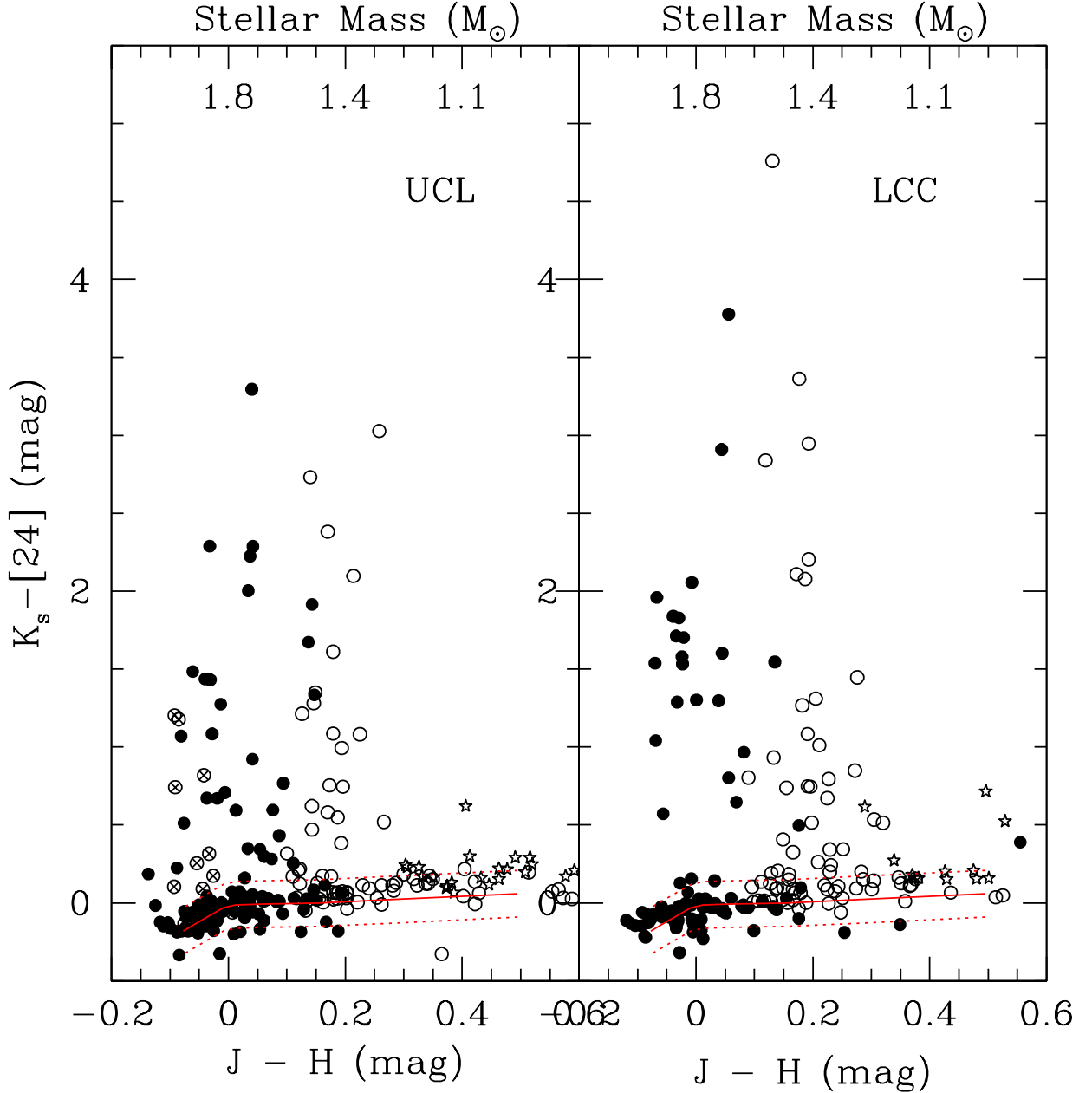


Fig. 1.— The K_s - [24] color plotted as a function of the J - H color for the Upper Centaurus Lupus (UCL) and Lower Centaurus Crux (LCC) subgroups of Sco Cen. Our sample of 209 B- and A-type stars is shown as filled circles; open circles with crosses represent A-type stars from Su et al. (2006); F- and G-type stars from Chen et al. (2011) are shown as open circles; and the Carpenter et al. (2008) sample of F- and G-type stars is shown as open stars. The solid line represents the colors for main sequence stars based on Kurucz models with $\log g = 4.0$ and solar metallicity. The dashed lines show the 3σ range in K_s - [24] color (0.15 mag) around the main sequence.

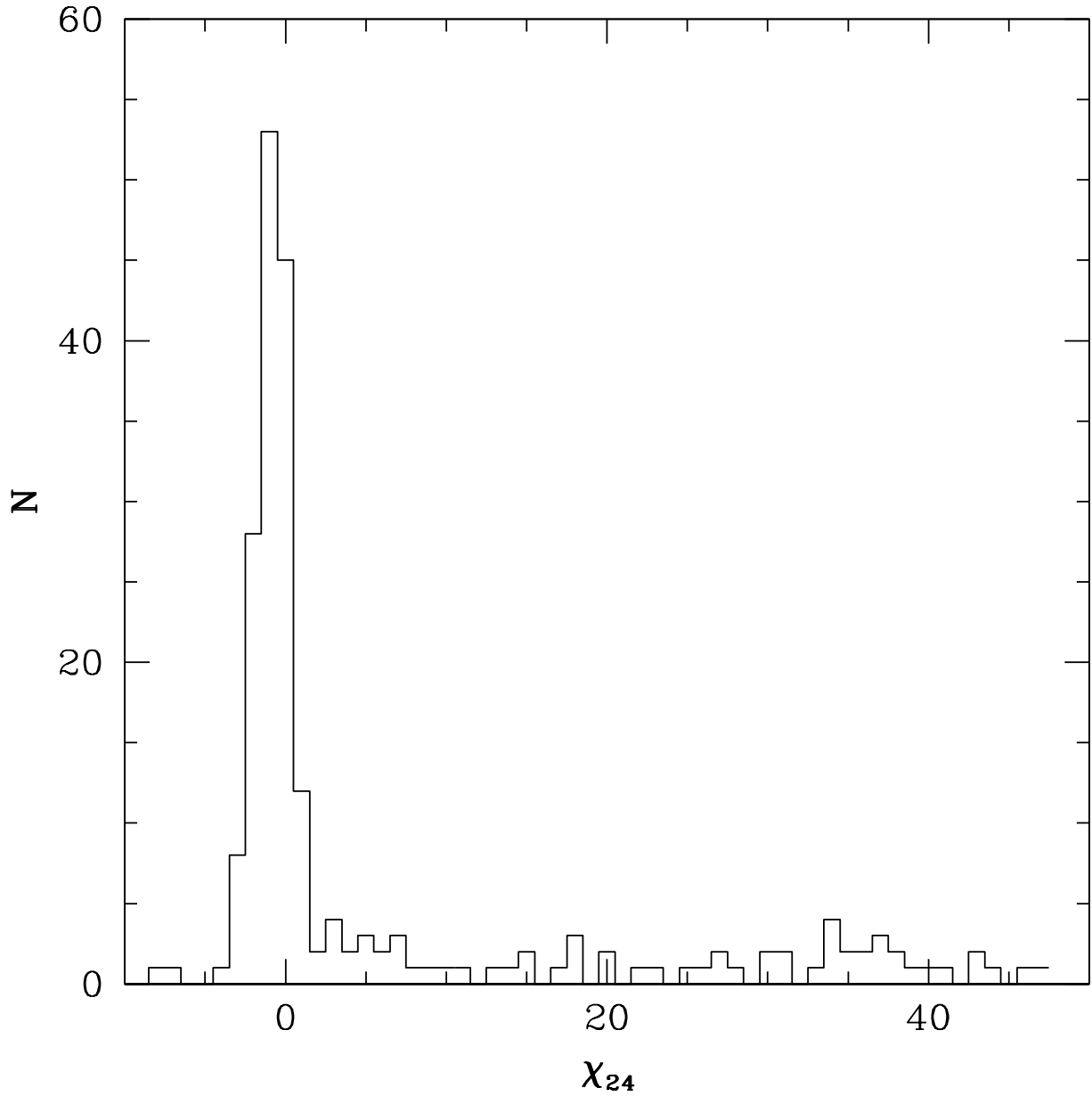


Fig. 2.— Histogram of the significances ($\chi = (F_\nu(24 \mu\text{m}) - F_*(24 \mu\text{m})) / \sigma_{F24}$) of observed 24 μm excesses. The histogram includes all sources in our study regardless of the membership in ScoCen. Sources with $\chi \geq 6$ also possess $K_s - [24] > 0.30$ mag and were identified as having significant excess.

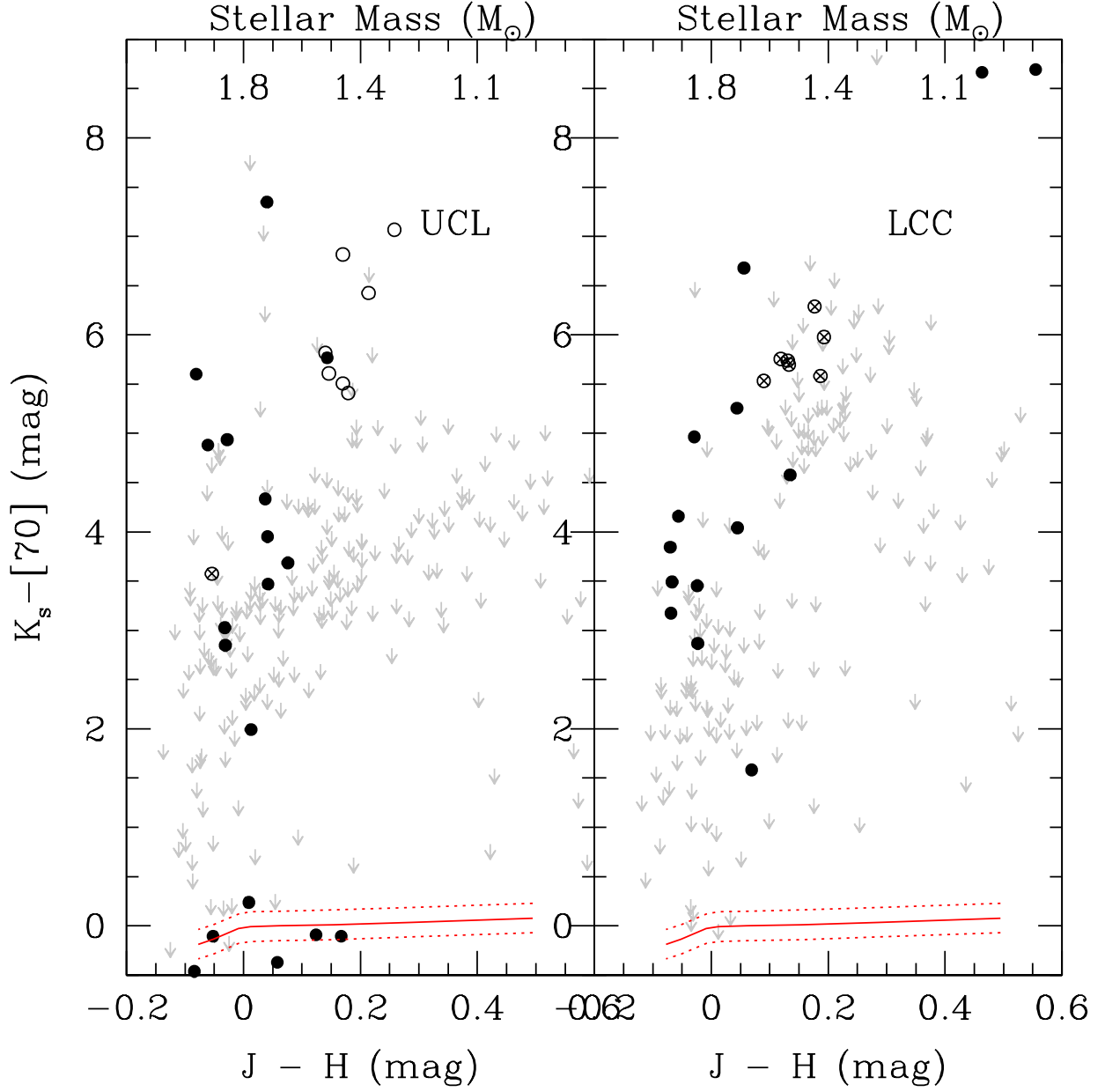


Fig. 3.— $K_s - [70]$ color plotted as a function of $J - H$ color for subgroups of Sco Cen. The symbols are as described in Figure 1. Non-detections are shown as gray upper limit symbols. The solid line represents the colors for main sequence stars based on Kurucz models with $\log g = 4.0$ and solar metallicity. The dashed lines show the 3σ range in $K_s - [70]$ color (0.23 mag) around the main sequence.

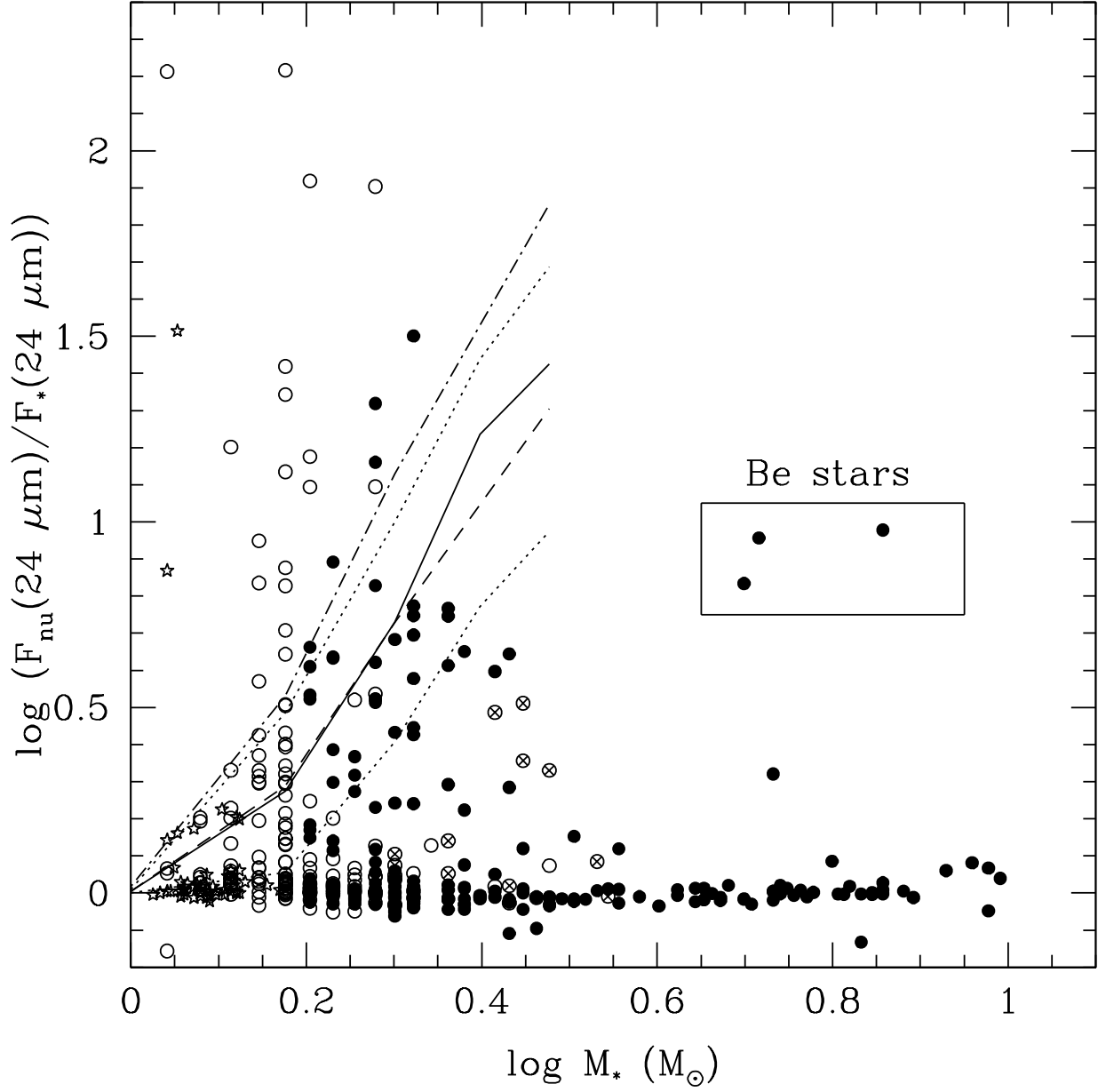


Fig. 4.— The $24 \mu\text{m}$ flux ratio ($F_\nu(24 \mu\text{m})/F_*(24 \mu\text{m})$) plotted as a function of stellar mass. B- and A-type stars in this survey are shown with solid circles while F- and G-type stars from Chen et al. (2011) are shown with open circles. The solid line shows the $24 \mu\text{m}$ flux ratios predicted in the Kenyon & Bromley (2008) model for typical disks with ages $\sim 10 - 20$ Myr. The dotted lines show models for disks with masses that are a factor of three higher and lower than typical disks. The dashed line and the dashed-dotted line show Kenyon & Bromley (2010) models for disks with weak planetesimals and an initial planetesimal surface density, $\Sigma \propto a^{-1}$ rather than $a^{-3/2}$. High mass stars with large infrared excess are Be stars.

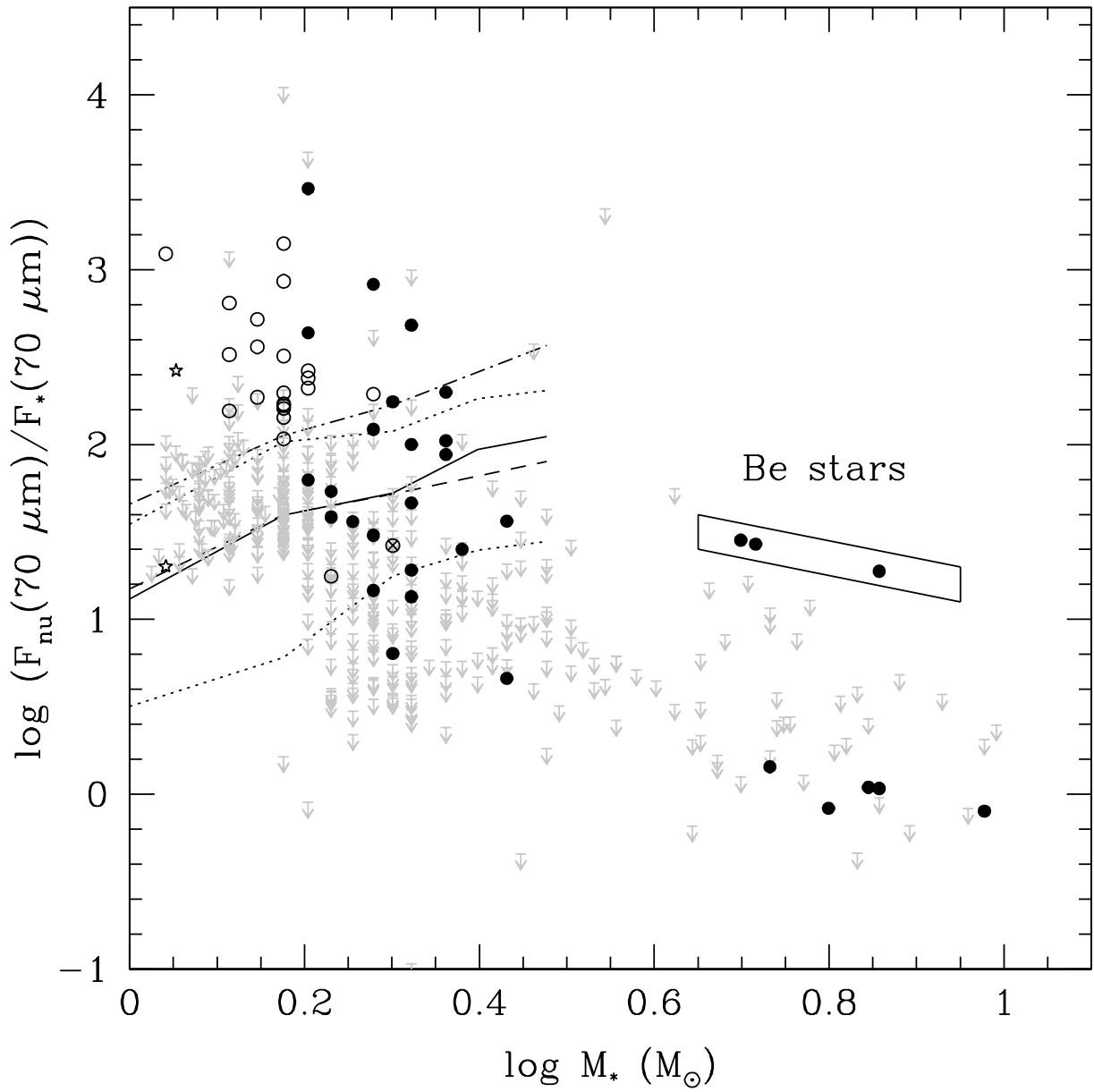


Fig. 5.— Same as Figure 4 for the 70 μm flux ratio, ($F_{\nu}(70 \mu\text{m})/F_{*}(70 \mu\text{m})$).

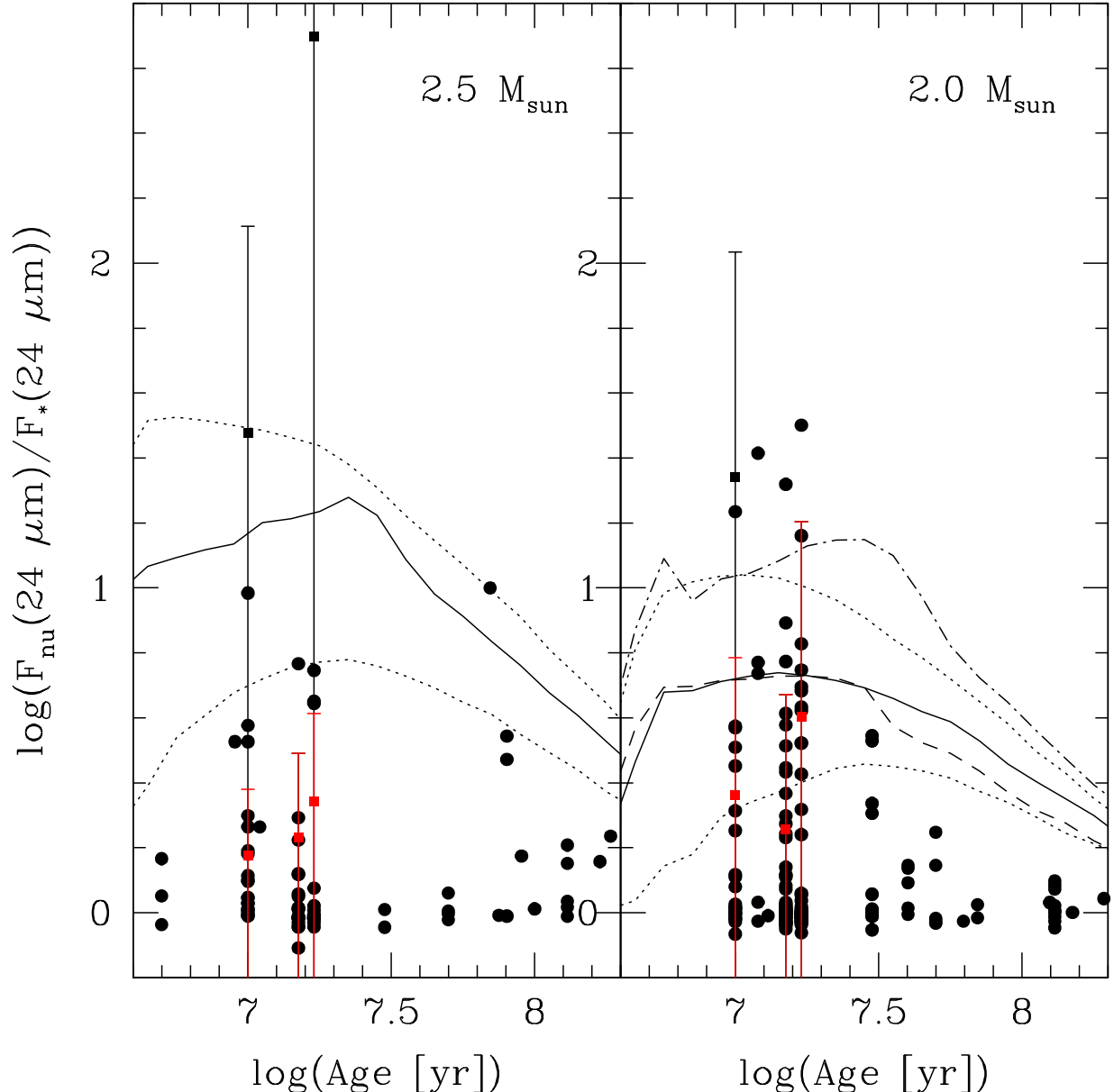


Fig. 6.— The $24 \mu\text{m}$ flux ratio ($F_\nu(24 \mu\text{m})/F_*(24 \mu\text{m})$) as a function of stellar age. Our observations of ScoCen are plotted along with data from several young clusters and moving groups in the published literature (See Table 4). Objects with near-infrared (e.g., IRAC) and MIPS $24 \mu\text{m}$ excesses are plotted using asterisks; objects with only MIPS $24 \mu\text{m}$ excesses are plotted using solid circles. The solid line shows the evolution of thermal emission from dust generated via collisional cascade at distances 30 - 150 AU from the central star ?kenyon08) from a typical disk; for $1 M_\odot$ stars, the model corresponds to a Minimum Mass Solar Nebula. The dotted lines show models for disks with masses that are a factor of three higher and lower. The dashed line and the dashed-dotted line show Kenyon & Bromley (2010) models for disks with weak planetesimals and an initial planetesimal surface density, $\Sigma \propto a^{-1}$ rather than $a^{-3/2}$. Objects with near- and mid-infrared excesses may be accreting, primordial disks (e.g., HD 100546). Black squares and error bars show mean and standard deviation of ScoCen sample while black red squares and error bars show mean and standard deviation if

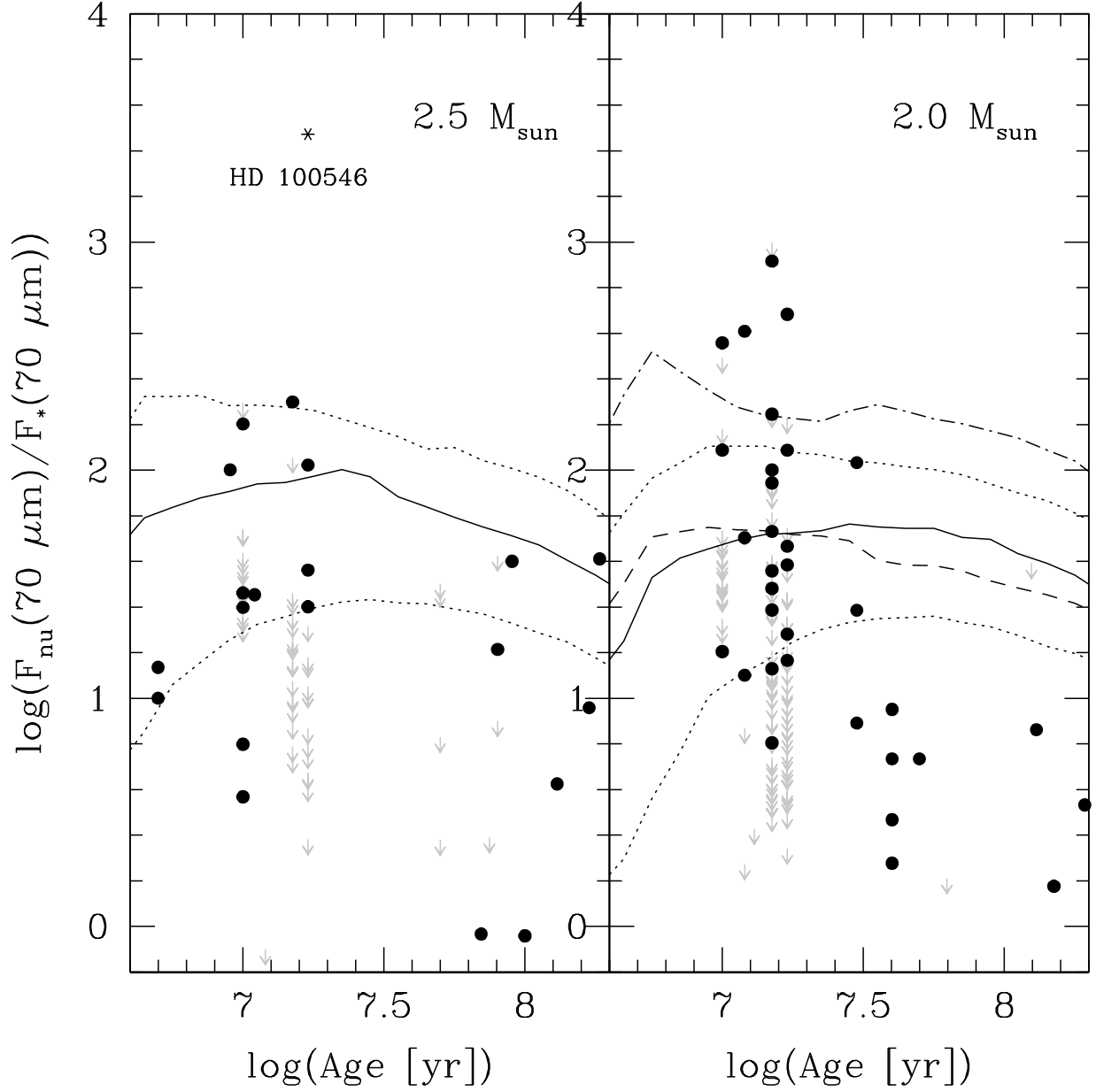


Fig. 7.— Same as Figure 6 for the 70 μm flux ratio, ($F_{\nu}(70 \mu\text{m})/F_*(70 \mu\text{m})$). Objects that are not detected with MIPS at 70 μm are plotted as gray upper limit symbols. The solid line shows the evolution of 70 μm emission from material generated via collisional cascade at distance 30 - 150 AU from the central star (Kenyon & Bromley 2008) from a typical disk; for 1 M_{\odot} stars, the model corresponds to a Minimum Mass Solar Nebula. The dotted lines show models for disks with masses that are a factor of three higher and lower. The dashed line and the dashed-dotted line show Kenyon & Bromley (2010) models for disks with weak planetesimals and an initial planetesimal surface density, $\Sigma \propto a^{-1}$ rather than $a^{-3/2}$.

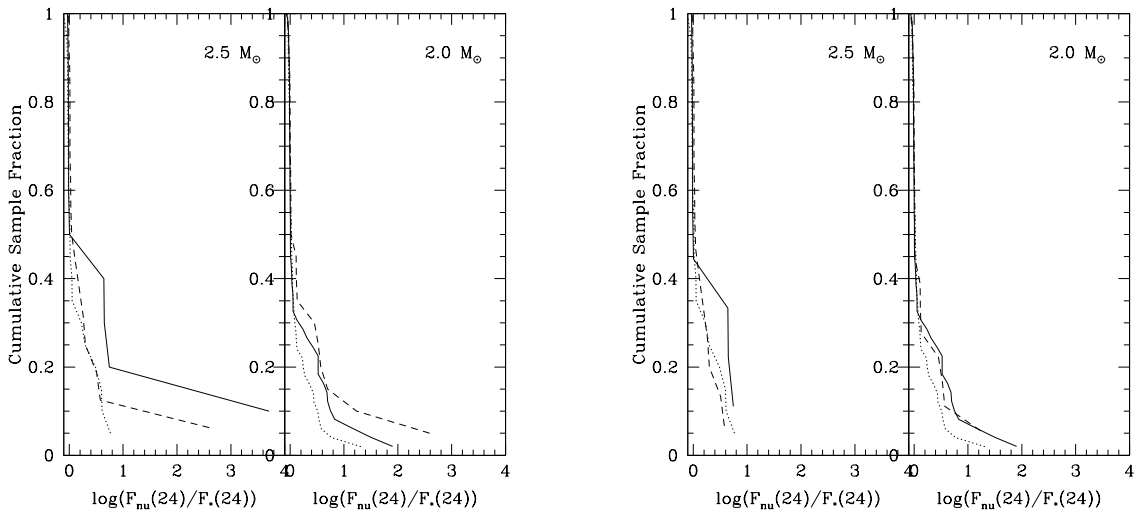


Fig. 8.— (a) The cumulative distribution functions of $F_{\nu}(24 \mu\text{m})/F_*(24 \mu\text{m})$ for 2.5 and $1.0 M_\odot$ stars in US (dashed line), UCL (dotted line), and LCC (solid line) including both "primordial" and "debris" disks. (b) Same as (a) with "primordial" disks removed.

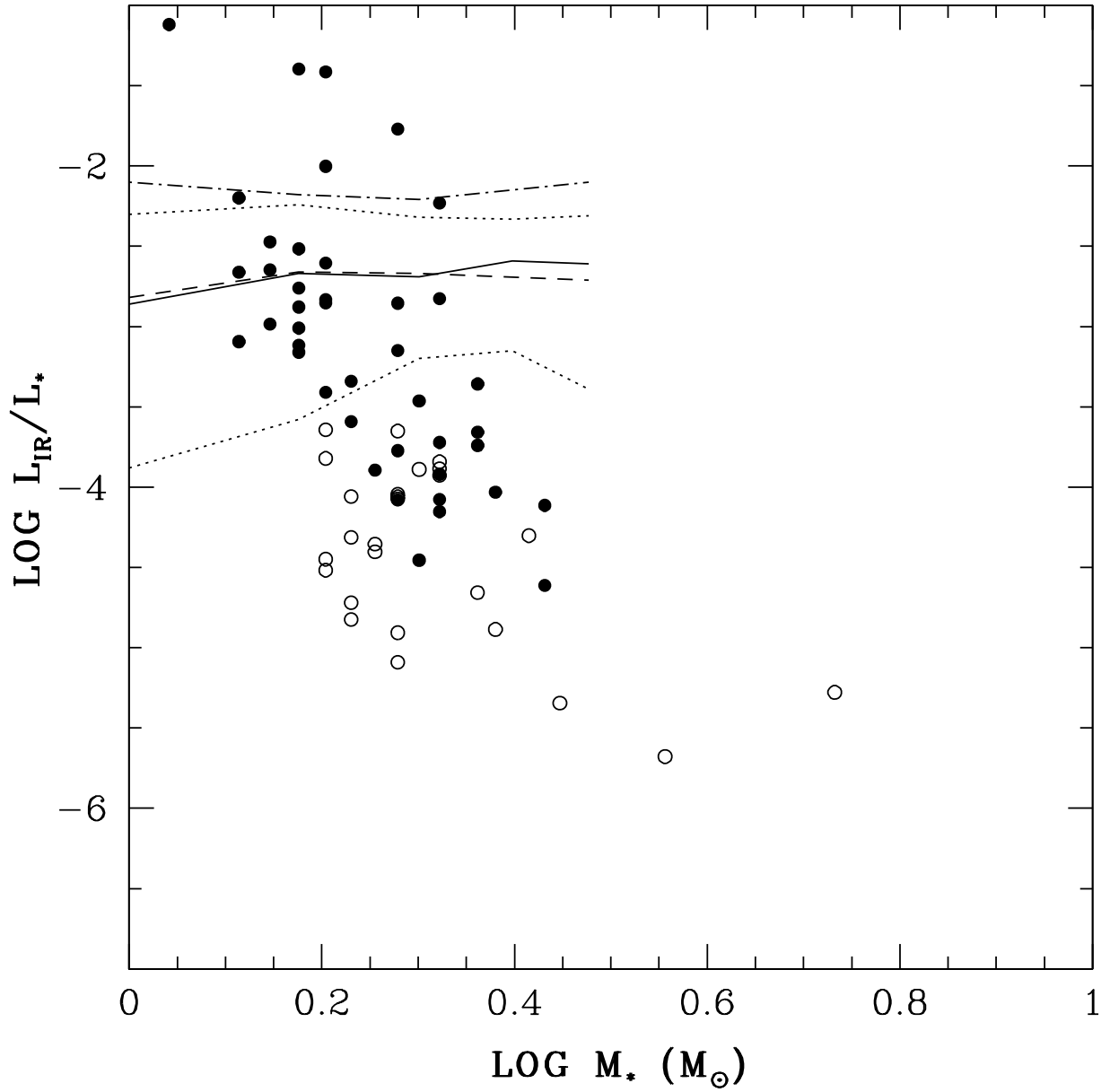


Fig. 9.— Fractional infrared luminosity (L_{IR}/L_*) of excess stars plotted as a function of stellar mass. Stars with infrared excess detected at both 24 and 70 μm are shown with solid circles while those that are only detected at 24 μm are shown with open circles. The solid line shows the fractional infrared luminosities predicted in the Kenyon & Bromley (2008) model for typical disks in which disk mass scales with stellar mass. The dotted lines show models for disks with masses that are a factor of three higher and lower. The dashed line and the dashed-dotted line show Kenyon & Bromley (2010) models for disks with weak planetesimals and an initial planetesimal surface density, $\Sigma \propto a^{-1}$ rather than $a^{-3/2}$. Be stars with infrared excesses have been removed from the sample.

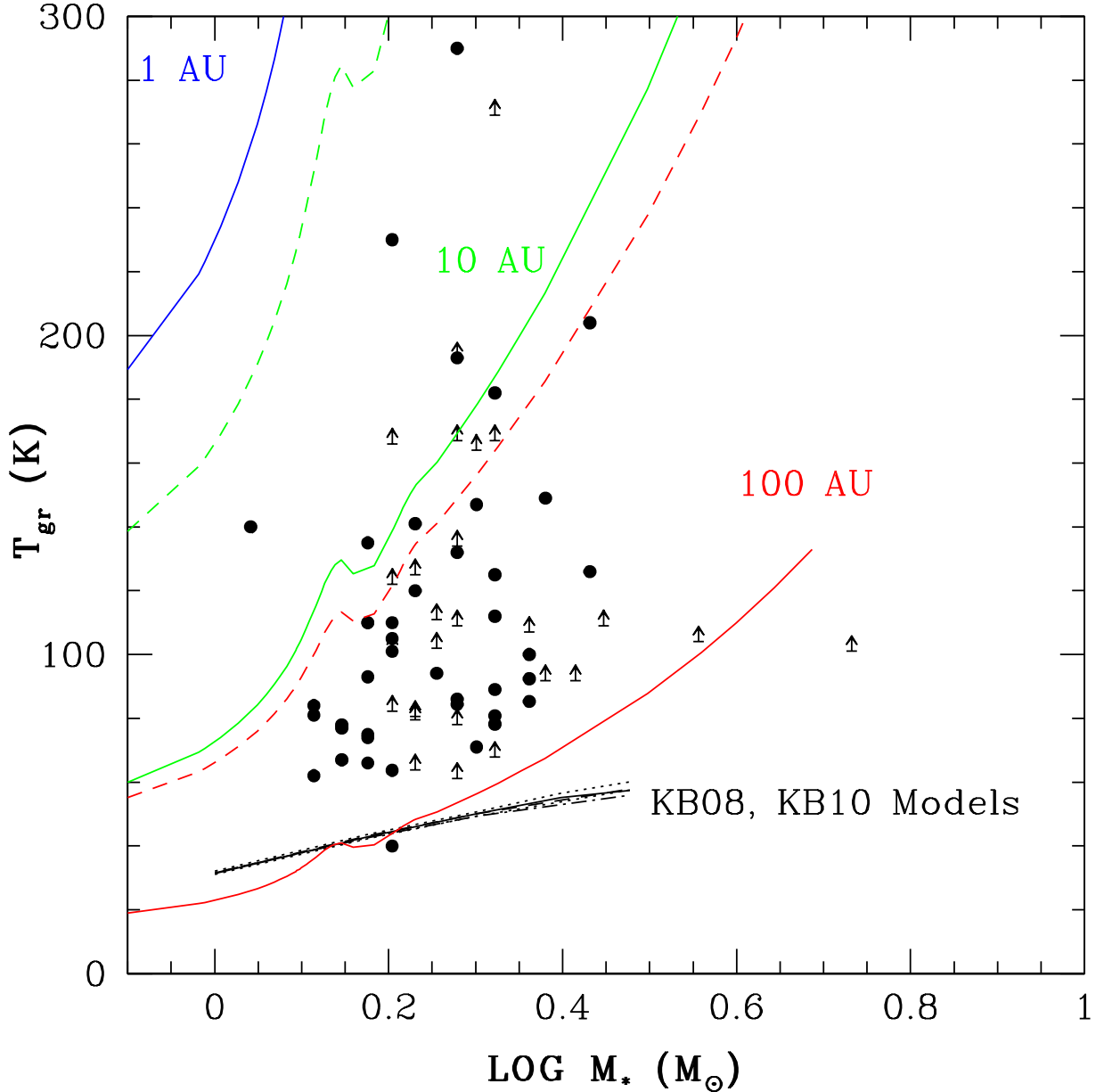


Fig. 10.— Grain temperatures (T_{gr}) of excess stars plotted as a function of stellar mass. The blue, green, and red solid lines show grain temperatures expected for black body grains at 1 AU, 10 AU, and 100 AU from the central star while the green and red dashed lines show grain temperatures expected for small grains ($2\pi a \ll \lambda$) at the same distances. The solid black line shows the grain temperatures predicted in the Kenyon & Bromley (2008) model for typical disks in which disk mass scales with stellar mass. The dashed lines show models for disks with masses that are a factor of three higher and lower. The dashed line and the dashed-dotted line show Kenyon & Bromley (2010) models for disks with weak planetesimals and an initial planetesimal surface density, $\Sigma \propto a^{-1}$ rather than $a^{-3/2}$. Be stars with infrared excesses have been removed from the sample.

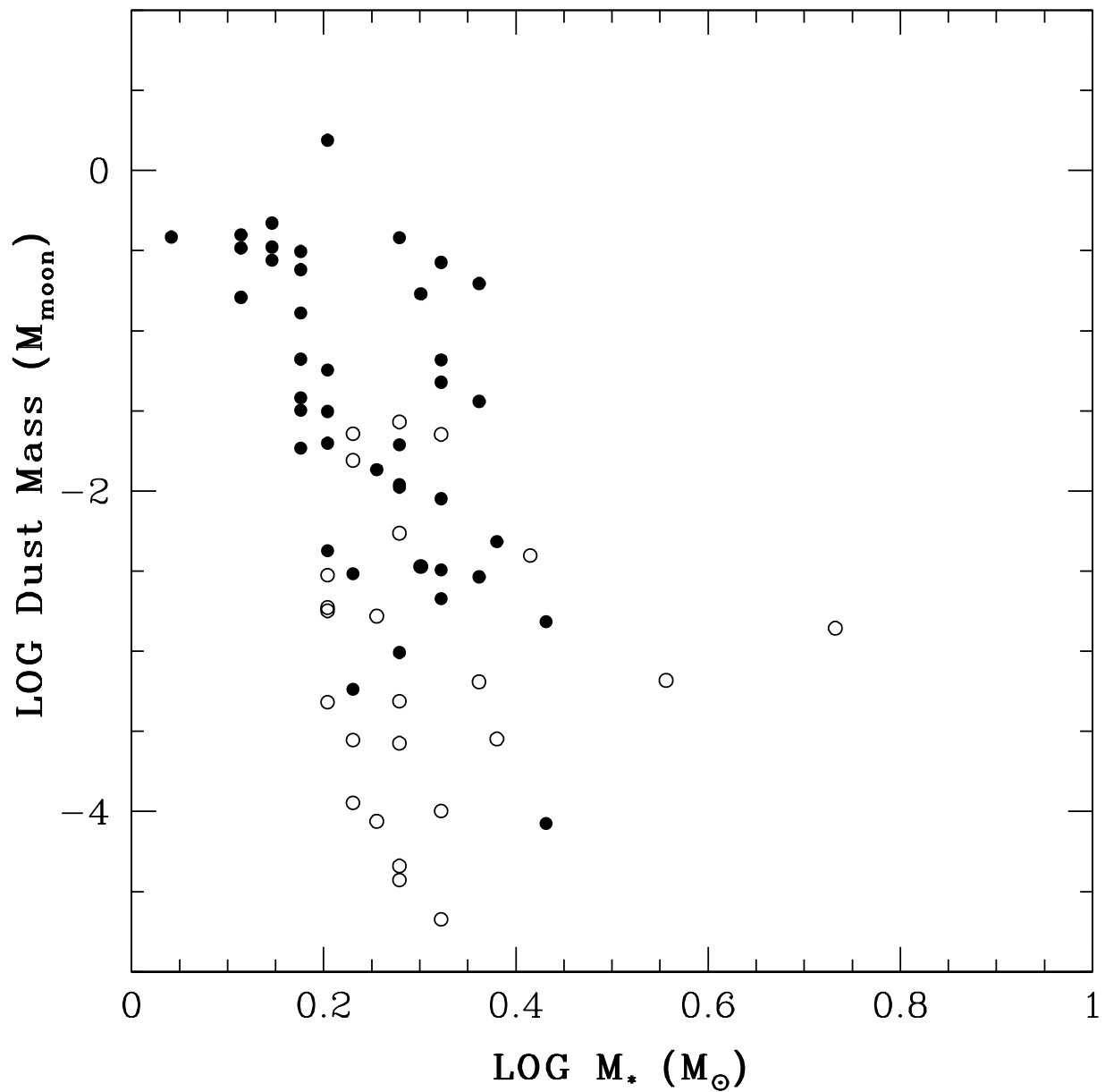


Fig. 11.— Estimated dust mass (M_d) of excess stars plotted as a function of stellar mass.

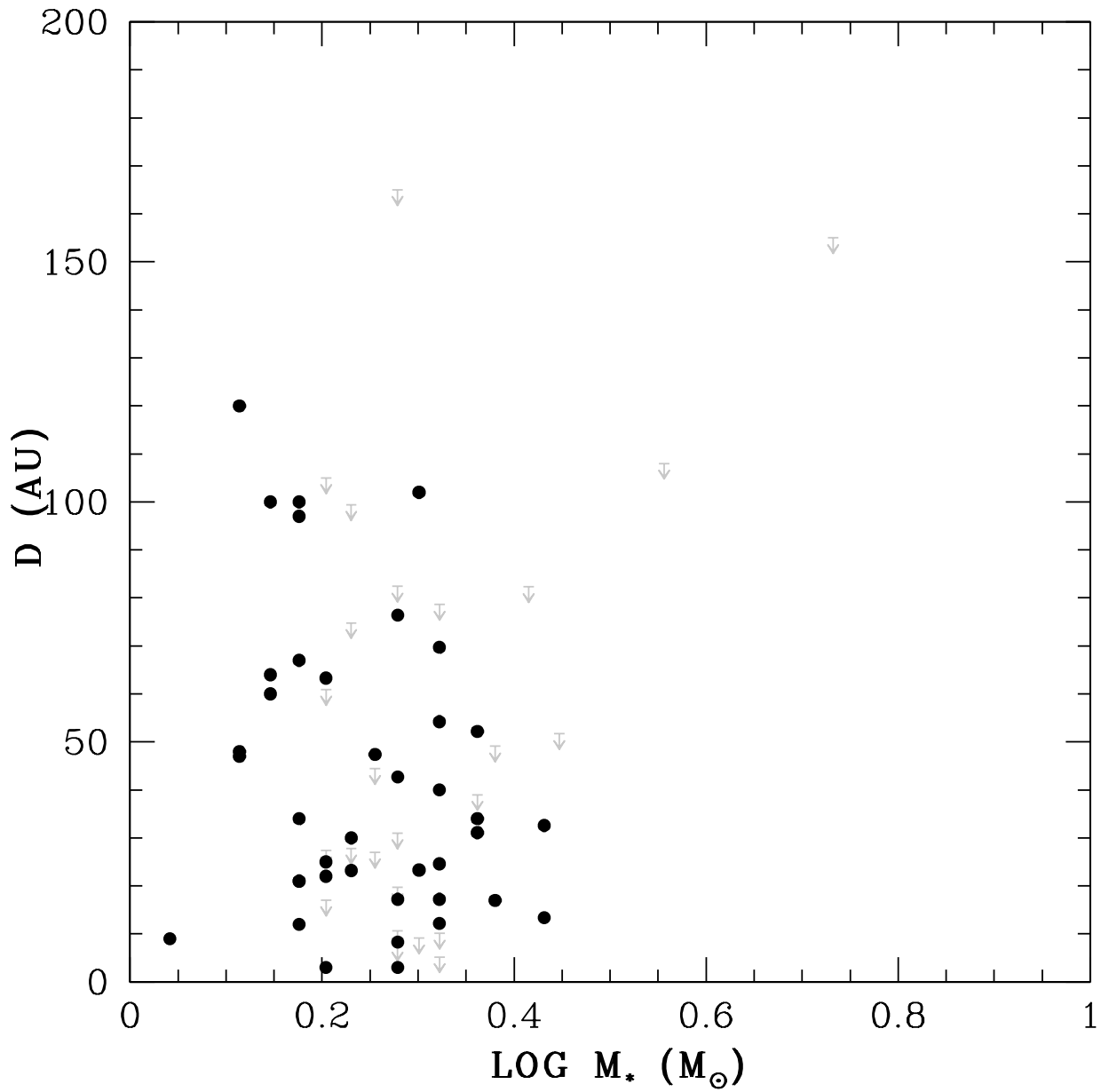


Fig. 12.— Estimated dust distance (D) of excess stars plotted as a function of stellar mass. Stars with infrared excess detected at both 24 and 70 μm are shown with solid circles while those that are only detected at 24 μm are shown with open circles.

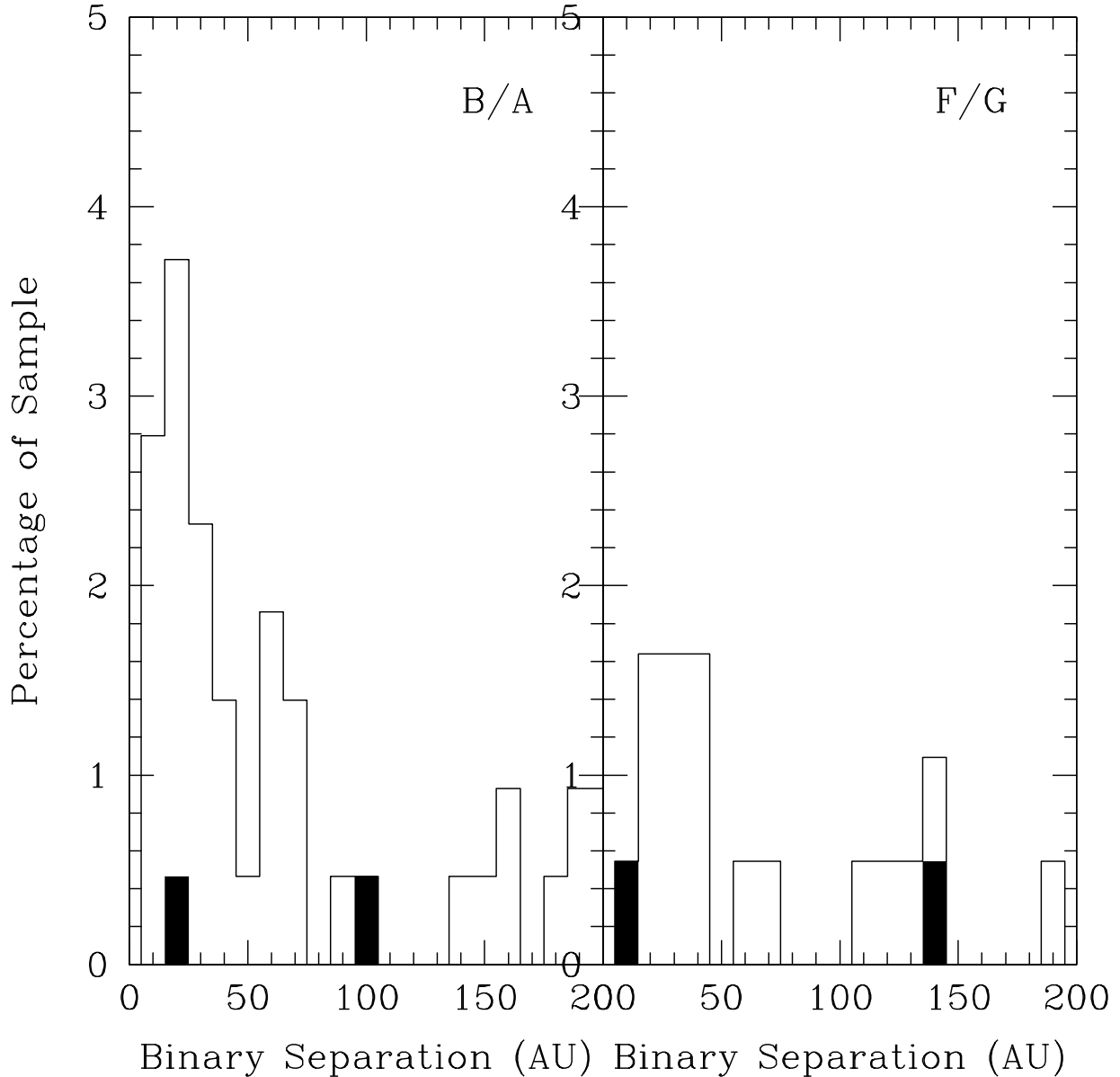


Fig. 13.— Histograms show the percentage of stars in (a) our B- and A-type ScoCen sample and (b) the Chen et al. (2011) F- and G-type ScoCen samples that possess stellar companions at distances 10 - 200 AU (solid line). Overlaid are histograms showing the percentage of binary systems with 24 μ m excesses (filled-in histogram).

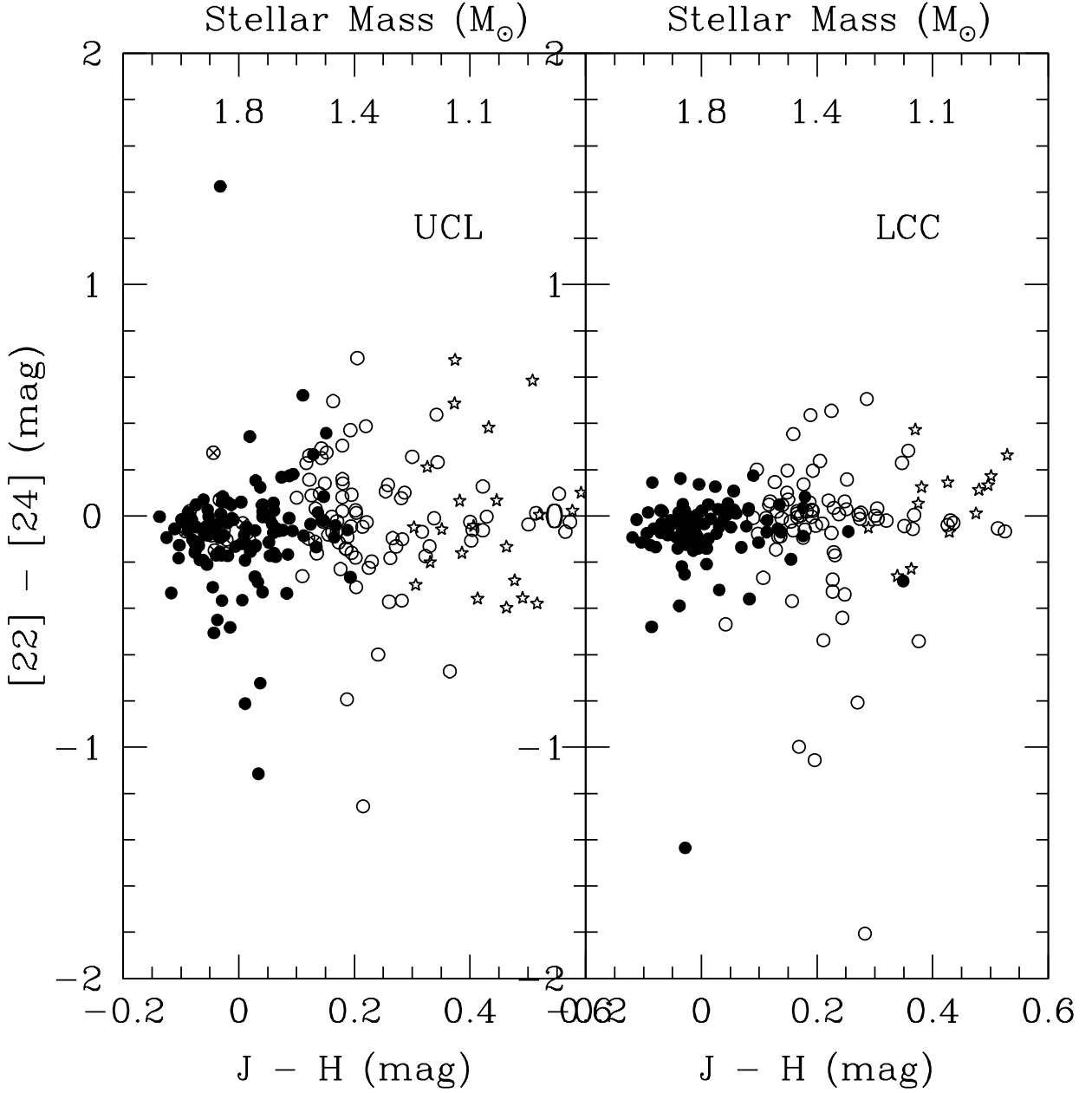


Fig. 14.— The WISE [22] - MIPS [24] color plotted as a function of the J - H color for the Upper Centaurus Lupus (UCL) and Lower Centaurus Crux (LCC) subgroups of Sco Cen. Our sample of 209 B- and A-type stars is shown as filled circles; open circles with crosses represent A-type stars from Su et al. (2006); F- and G-type stars from Chen et al. (2011) are shown as open circles; and the Carpenter et al. (2008) sample of F- and G-type stars is shown as open stars.

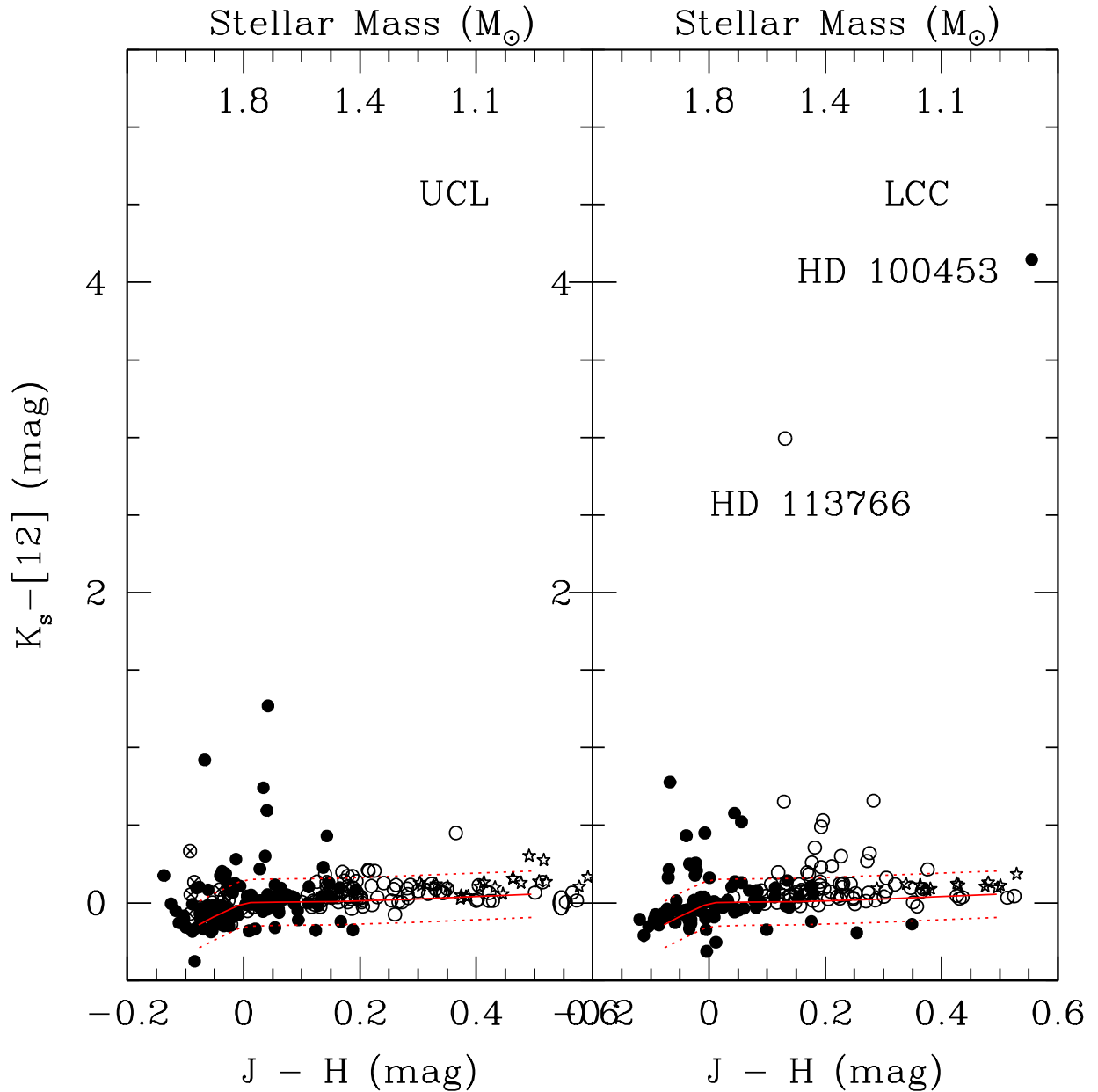


Fig. 15.— $K_s - [12]$ color plotted as a function of $J - H$ color for subgroups of Sco Cen. The symbols are as described in Figure 1. The dashed lines show the 3σ range in $K_s - [12]$ color (0.23 mag) around the main sequence.

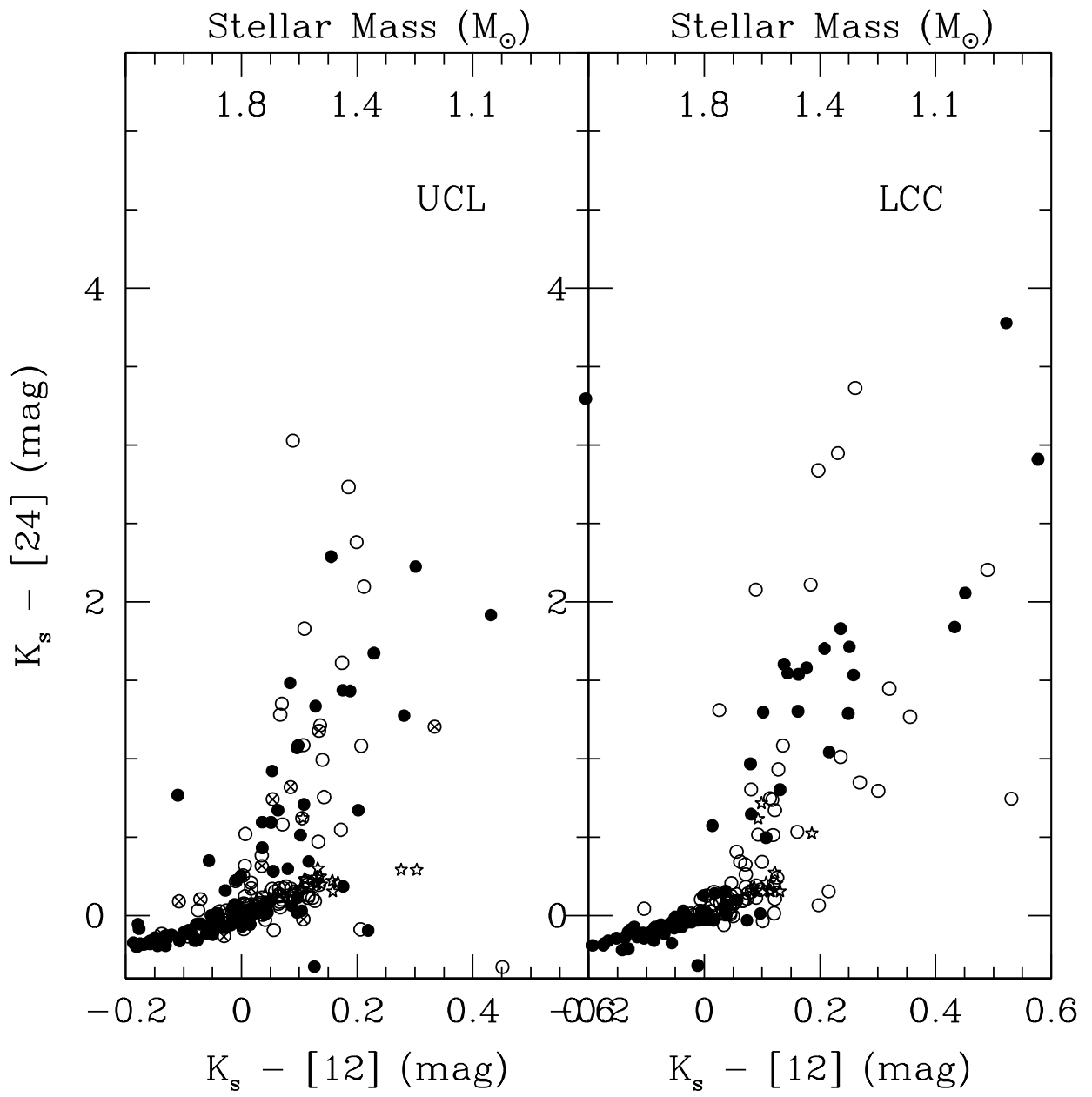


Fig. 16.— $K_s - [12]$ color plotted as a function of $K_s - [24]$ color for subgroups of Sco Cen. The symbols are as described in Figure 1.

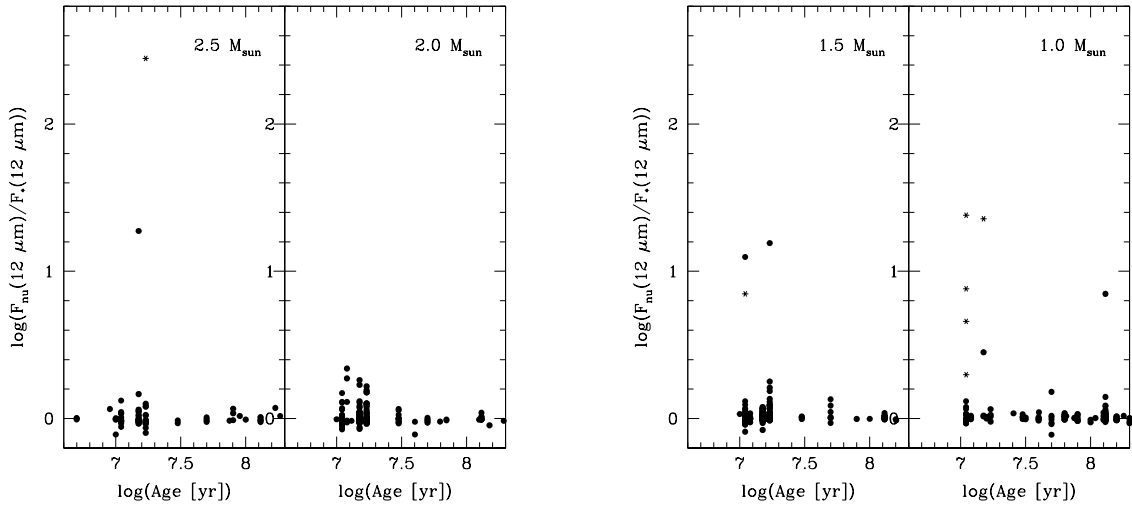


Fig. 17.— The $12 \mu\text{m}$ flux ratio ($F_{\nu}(12 \mu\text{m})/F_{*}(12 \mu\text{m})$) as a function of stellar age. The sample of $2.0\text{-}2.5 M_{\odot}$ stars is described in Table 4); the sample of $1.0\text{-}1.5 M_{\odot}$ stars is described in Chen et al. (2011). Objects with near-infrared (e.g., IRAC) and MIPS $24 \mu\text{m}$ excesses are plotted using asterisks; objects with only MIPS $24 \mu\text{m}$ excesses are plotted using solid circles.

Table 1. Stellar Properties

HIP	Name	Spectral Type	Distance (pc)	A_V (mag)	Subgroup	Separation (arcsec)	Notes
50083	HD 88981	A4mA6-F0 (8)	94.3 $^{+1.5}_{-1.5}$	0.149 \pm 0.047	LCC		
50520	HD 89715	A1V (2)	80.3 $^{+3.4}_{-3.1}$	0.006 \pm 0.018	LCC	2.1 (a,b,c)	VB
50847	HD 90264	B8V (8)	123.2 $^{+2.8}_{-2.7}$	0.026 \pm 0.017	LCC		SB
51991	HD 92315	A1Vp:Cr:Sr:Eu: (8)	215.1 $^{+30.0}_{-23.5}$	0.180 \pm 0.012	LCC		
52357	HD 92896	A3IV (8)	122.5 $^{+11.9}_{-9.9}$	0.349 \pm 0.019	LCC	0.53, 10.04 (a,b,c)	VB
53524	HD 95086	A8III (8)	90.4 $^{+3.5}_{-3.2}$	0.000 \pm 0.019	LCC	4.87 (b)	VB
53701	HD 95324	B8IV (8)	118.2 $^{+8.4}_{-7.3}$	0.044 \pm 0.017	LCC	3.88, 6.57 (a,b)	VB
54231	HD 96338	A0V (9)	117.9 $^{+7.3}_{-6.3}$	0.031 \pm 0.054	LCC		
55188	HD 98363	A2V (8)	123.6 $^{+8.1}_{-7.2}$	0.244 \pm 0.039	LCC		
55425	HD 98718	B5Vn (11)	109.6 $^{+4.2}_{-3.9}$	0.011 \pm 0.013	LCC	0.354 (e)	VB
55899	HD 99627	A0V (10)	136.8 $^{+12.0}_{-10.2}$	0.215 \pm 0.031	LCC	23 (a)	VB
56354	HD 100453	A9Ve (23)	121.5 $^{+10.4}_{-8.9}$	0.214 \pm 0.005	LCC		Herbig Ae
56379	HD 100546	B9Vne (8)	96.9 $^{+8.2}_{-3.9}$	0.194 \pm 0.017	LCC		Herbig Be
56543	HD 100786	A5V (9)	223.7 $^{+49.5}_{-34.3}$	0.000 \pm 0.061	LCC		
56561	HD 100841	B9.5IIn (4)	128.7 $^{+5.9}_{-5.4}$	0.015 \pm 0.039	LCC	0.734, 16.3 (a,e)	VB
56963	HD 101523	A3V (9)	116.6 $^{+11.3}_{-9.5}$	0.142 \pm 0.036	LCC		
56993	HD 101582	A0V (8)	183.8 $^{+21.5}_{-17.4}$	0.016 \pm 0.025	LCC	1.68 (b,c)	VB
57238	HD 102026	A1V (8)	182.1 $^{+34.8}_{-25.2}$	0.079 \pm 0.039	LCC		
57710	HD 102814	A3V (9)	117.1 $^{+15.0}_{-11.9}$	0.210 \pm 0.060	LCC		
57809	HD 102981	A0V (9)	135.1 $^{+9.2}_{-8.1}$	0.000 \pm 0.010	LCC		
57851	HD 103079	B4V (11)	111.1 $^{+6.1}_{-5.5}$	0.028 \pm 0.013	LCC	1.8 (a)	VB
58416	HD 104021	A7V (9)	112.1 $^{+9.5}_{-8.2}$	0.146 \pm 0.068	LCC	0.58 (b,c)	VB
58452	HD 104080	B8/9V (9)	121.8 $^{+5.7}_{-5.3}$	0.002 \pm 0.015	LCC		
58465	HD 104125	A2V (8)	100.9 $^{+5.4}_{-4.8}$	0.313 \pm 0.020	LCC		
58680	HD 104509	A4IV/V (9)	186.9 $^{+60.0}_{-36.5}$	0.326 \pm 0.032	LCC		
58720	HD 104600	B9V (8)	105.7 $^{+2.4}_{-2.3}$	0.024 \pm 0.004	LCC		
58859	HD 104839	B9.5V (9)	117.6 $^{+7.7}_{-6.8}$	0.000 \pm 0.025	LCC		
58884	HD 104878	A0IV (8)	106.5 $^{+4.6}_{-4.2}$	0.000 \pm 0.018	LCC	0.698 (a,e)	VB
59173	HD 105382	B2IIIne (11)	134.4 $^{+12.0}_{-10.2}$	0.043 \pm 0.009	LCC	268.6 (a)	VB, Be star
59282	HD 105613	A3V (8)	104.2 $^{+6.8}_{-6.0}$	0.192 \pm 0.027	LCC		
59397	HD 105857	A2V (8)	113.0 $^{+9.7}_{-8.3}$	0.132 \pm 0.002	LCC		
59413	HD 105874	A6V (9)	123.9 $^{+17.3}_{-13.5}$	0.199 \pm 0.027	LCC	3.18, 7.22 (a,b,c)	VB
59502	HD 106036	A2V (8)	100.7 $^{+4.1}_{-3.5}$	0.015 \pm 0.024	LCC	2.94, 9.05 (b,c)	VB
59505	HD 106048	A9V (8)	123.5 $^{+16.6}_{-13.1}$	0.266 \pm 0.038	LCC		
59724	HD 106473	A6III (9)	134.2 $^{+19.9}_{-15.3}$	0.292 \pm 0.032	LCC		
59747*	HD 106490	B2IV (11)	105.8 $^{+1.7}_{-1.7}$	0.000 \pm 0.008	LCC		
59898	HD 106797	A0V (8)	96.0 $^{+3.1}_{-2.9}$	0.022 \pm 0.019	LCC		
60009	HD 106983	B2.5V (11)	109.6 $^{+5.7}_{-5.2}$	0.014 \pm 0.025	LCC	33.8 (a)	VB
60084	HD 107143	A1V (9)	167.8 $^{+22.7}_{-17.9}$	0.211 \pm 0.020	LCC	0.46 (b,c)	VB
60183	HD 107301	B9V (8)	93.9 $^{+3.1}_{-2.9}$	0.067 \pm 0.008	LCC		
60320	HD 107566	A5IV-V (7)	101.1 $^{+3.6}_{-3.4}$	0.109 \pm 0.051	LCC	0.5, 32.4 (a)	VB
60379	HD 107696	B9V (11)	110.9 $^{+3.5}_{-3.5}$	0.017 \pm 0.008	LCC		
60459	HD 107821	A3V (8)	100.7 $^{+5.1}_{-4.6}$	0.182 \pm 0.008	LCC		
60561	HD 107947	A0V (8)	91.1 $^{+2.6}_{-2.5}$	0.000 \pm 0.025	LCC		

Table 1—Continued

HIP	Name	Spectral Type	Distance (pc)	A_V (mag)	Subgroup	Separation (arcsec)	Notes
60577	HD 108035	A8/9V (9)	104.2 $^{+10.9}_{-9.0}$	0.416 \pm 0.111	LCC	2.5 (a)	VB
60710	HD 108257	B3Vn (11)	137.4 $^{+4.7}_{-4.4}$	0.070 \pm 0.017	LCC	21.7 (a)	VB
60823*	HD 108483	B2V (11)	126.3 $^{+2.9}_{-2.8}$	0.065 \pm 0.025	LCC		
60851	HD 108501	A0V (8)	97.9 $^{+3.3}_{-3.1}$	0.047 \pm 0.012	LCC	2.01, 6.92 (b)	VB
61257	HD 109195	B9.5V (9)	135.7 $^{+10.3}_{-8.9}$	0.000 \pm 0.038	LCC	5.54 (b)	VB
61265	HD 109197	A2V (8)	148.1 $^{+16.9}_{-13.7}$	0.029 \pm 0.027	LCC	2.51, 3.43 (b,c)	VB
61585*	HD 109668	B2IV-V (11)	96.7 $^{+1.0}_{-1.0}$	0.000 \pm 0.013	LCC	4.853, 29.6 (a,e)	VB
61639	HD 109808	A1/2V (8)	111.0 $^{+9.9}_{-8.4}$	0.516 \pm 0.140	LCC	1.87, 4.21 (a,b,c)	VB
61684	HD 109832	A9V (8)	111.9 $^{+8.3}_{-7.3}$	0.261 \pm 0.061	LCC		
61782	HD 110058	A0V (9)	107.4 $^{+9.8}_{-8.3}$	0.436 \pm 0.026	LCC		
61796*	HD 110020	B8V (8)	114.3 $^{+3.9}_{-3.7}$	0.175 \pm 0.012	LCC	4.17, 9.89, 12.38 (b,c)	VB
62002	HD 110390	A1V (8)	101.9 $^{+7.6}_{-6.6}$	0.573 \pm 0.119	LCC	0.38, 5.33 (a,b,c)	VB
62026	HD 110461	B9V (8)	108.5 $^{+4.9}_{-4.5}$	0.141 \pm 0.017	LCC	0.23 (b,c)	VB
62058	HD 110506	B9Vn (17)	117.1 $^{+5.0}_{-4.6}$	0.000 \pm 0.019	LCC		
62179	HD 110698	A0IV/V (8)	111.2 $^{+8.1}_{-7.1}$	0.234 \pm 0.008	LCC	0.23, 4.47, 12.21 (a,b,c)	VB
62205	HD 110737	B9.5V (8)	180.5 $^{+35.5}_{-25.5}$	1.285 \pm 0.039	LCC	0.2 (a)	VB
62322	HD 110879	B2V (11)	104.7 $^{+4.7}_{-4.3}$	0.019 \pm 0.013	LCC	1.4 (a)	VB
62327	HD 110956	B3V (11)	117.9 $^{+3.1}_{-3.0}$	0.045 \pm 0.008	LCC	52.6 (a)	VB
62703	HD 111588	A5V (9)	101.8 $^{+7.3}_{-6.4}$	0.000 \pm 0.014	LCC		
63003*	HD 112092	B2IV-V (11)	127.1 $^{+2.7}_{-2.7}$	0.067 \pm 0.009	LCC	34.9 (a)	VB
63005	HD 112091	B5V(e) (11)	124.8 $^{+4.7}_{-4.4}$	0.200 \pm 0.017	LCC	34.9 (a)	VB, Be star
63007*	HD 112078	B4Vn (11)	117.6 $^{+3.0}_{-2.8}$	0.036 \pm 0.017	LCC		
63204*	HD 112381	B9.5Vp SiSr (20)	118.5 $^{+8.4}_{-7.4}$	0.000 \pm 0.036	LCC	0.15 (a,b,c)	VB
63210*	HD 112409	B8V (17)	113.0 $^{+3.6}_{-3.3}$	0.055 \pm 0.025	LCC		
63236	HD 112383	A2IV/V (8)	110.7 $^{+5.8}_{-5.3}$	0.000 \pm 0.048	LCC	7.56, 11.97 (b)	VB
63839	HD 113457	A0V (8)	99.4 $^{+4.4}_{-4.1}$	0.000 \pm 0.024	LCC	4.30, 5.99, 6.31 (b)	VB
63945	HD 113703	B5V (11)	119.6 $^{+3.7}_{-3.5}$	0.029 \pm 0.013	LCC	1.551, 11.4 (a,e)	VB
64004	HD 113791	B1.5V (11)	143.3 $^{+5.1}_{-4.8}$	0.061 \pm 0.005	LCC	25.1 (a)	SB, VB
64053	HD 113902	B8/9V (9)	100.1 $^{+3.3}_{-3.1}$	0.070 \pm 0.013	LCC		
64320*	HD 114365	B8Vp SiSr (20)	115.7 $^{+5.3}_{-4.9}$	0.000 \pm 0.013	LCC		
64425*	HD 114529	B8Vn (5)	116.1 $^{+12.7}_{-10.4}$	0.100 \pm 0.005	LCC	0.3, 1.7, 49 (a)	VB
64515	HD 114772	B9.5V (9)	112.2 $^{+9.7}_{-8.3}$	0.069 \pm 0.021	LCC	0.31 (a,b,c)	VB
64661	HD 114911	B8Vnn (5)	117.4 $^{+2.7}_{-2.6}$	0.022 \pm 0.013	LCC	60 (a)	SB, VB
64892	HD 115470	B9.5V (9)	125.3 $^{+8.1}_{-8.1}$	0.000 \pm 0.043	LCC		
64925	HD 115527	A0V (9)	131.6 $^{+8.9}_{-7.8}$	0.000 \pm 0.013	LCC		
64933	HD 115529	A0V (9)	186.9 $^{+26.3}_{-20.5}$	0.051 \pm 0.025	LCC		
65021	HD 115583	B9V (8)	149.5 $^{+10.5}_{-9.4}$	0.203 \pm 0.017	LCC		
65089	HD 115820	A7/8V (9)	96.5 $^{+7.9}_{-6.8}$	0.026 \pm 0.038	LCC		
65112	HD 115823	B6V (11)	125.3 $^{+5.9}_{-5.4}$	0.029 \pm 0.026	LCC		EB
65178	HD 115988	B9V (9)	123.9 $^{+9.4}_{-8.2}$	0.112 \pm 0.017	LCC		
65219	HD 116038	A3/4III/IV (9)	113.5 $^{+7.4}_{-6.6}$	0.294 \pm 0.033	LCC		
65271	HD 116087	B3V (11)	108.7 $^{+2.7}_{-2.5}$	0.062 \pm 0.017	LCC	0.164, 60 (a,e)	VB
65394	HD 116356	A1Vn: (8)	151.1 $^{+17.0}_{-13.9}$	0.000 \pm 0.029	LCC		
65426	HD 116434	A2V (9)	97.9 $^{+5.6}_{-5.0}$	0.038 \pm 0.024	LCC	0.1 (a)	VB

Table 1—Continued

HIP	Name	Spectral Type	Distance (pc)	A_V (mag)	Subgroup	Separation (arcsec)	Notes
65822	HD 117193	A1V (9)	136.1 $^{+9.9}_{-8.7}$	0.180 \pm 0.040	LCC	1.82 (b,c)	VB
65965	HD 117484	B9.5V (9)	147.3 $^{+16.4}_{-13.4}$	0.069 \pm 0.036	LCC	10.28 (b)	VB
66068	HD 117665	A1/2V (9)	147.9 $^{+11.1}_{-9.6}$	0.000 \pm 0.018	LCC		
66447	HD 118379	A3IV/V (9)	121.7 $^{+7.7}_{-6.8}$	0.184 \pm 0.061	UCL		
66454	HD 118354	B8V (9)	126.4 $^{+9.1}_{-7.9}$	0.000 \pm 0.017	LCC		
66566	HD 118588	A1V (9)	126.4 $^{+14.0}_{-11.5}$	0.097 \pm 0.039	LCC		
66651	HD 118697	B9.5V (8)	129.7 $^{+9.8}_{-8.5}$	0.181 \pm 0.039	LCC	7.58 (b)	VB
66908	HD 119221	A4V (9)	112.0 $^{+10.7}_{-9.0}$	0.091 \pm 0.022	UCL		
67036*	HD 119419	B9.5IVp SiSr (20)	119.0 $^{+6.9}_{-6.2}$	0.000 \pm 0.033	LCC		
67199	HD 119727	A1V (8)	104.9 $^{+5.3}_{-4.8}$	0.168 \pm 0.037	LCC		
67260	HD 119884	A0V (9)	110.9 $^{+9.2}_{-7.9}$	0.162 \pm 0.060	LCC	0.42, 1.23, 2.22 (a,b,c)	VB
67464*	HD 120307	B2IV (11)	133.9 $^{+3.1}_{-3.0}$	0.022 \pm 0.013	UCL		
67472	HD 120324	B2V:e (16)	155.0 $^{+3.9}_{-3.8}$	0.287 \pm 0.013	UCL	4.637, 48 (a,e)	VB, Be s
67919	HD 121040	A9V (8)	94.4 $^{+5.3}_{-4.7}$	0.131 \pm 0.041	LCC	0.69 (b,c)	VB
67973	HD 121190	B9V (9)	108.2 $^{+3.4}_{-3.2}$	0.035 \pm 0.025	UCL		
68080	HD 121336	A1Vn (19)	139.9 $^{+14.2}_{-11.8}$	0.082 \pm 0.026	UCL	1.92, 27.9 (a,b,c)	VB
68245*	HD 121743	B2IV (11)	161.0 $^{+4.5}_{-4.3}$	0.000 \pm 0.013	UCL		
68282*	HD 121790	B2IV-V (11)	131.1 $^{+2.8}_{-2.7}$	0.000 \pm 0.013	UCL		
68532	HD 122259	A3IV/V (10)	100.5 $^{+6.2}_{-5.5}$	0.343 \pm 0.067	UCL	3.05, 3.15 (b,c)	VB
68722	HD 122664	A7III/IV (10)	145.1 $^{+21.5}_{-16.6}$	0.076 \pm 0.016	UCL	22.2 (a)	VB
68781	HD 122705	A4V (22)	112.9 $^{+10.1}_{-8.6}$	0.000 \pm 0.029	UCL		
68862*	HD 122980	B2V (11)	156.5 $^{+5.3}_{-5.0}$	0.016 \pm 0.013	UCL		
68867	HD 122982	A0V (9)	175.1 $^{+19.4}_{-15.9}$	0.038 \pm 0.034	UCL	2.16 (b,c)	VB
68958	HD 123112	A0 SiCr (15)	182.5 $^{+17.9}_{-15.0}$	0.190 \pm 0.072	UCL		
69302	HD 123798	A8/9IV (9)	147.3 $^{+27.5}_{-20.0}$	0.218 \pm 0.024	UCL		
69605	HD 124469	A9V (10)	220.8 $^{+57.8}_{-37.9}$	0.124 \pm 0.030	UCL		
69618	HD 124367	B4Vne (11)	147.7 $^{+5.4}_{-5.1}$	0.409 \pm 0.048	UCL	33.9, 36 (a)	VB, Be s
69749	HD 124620	B9IV (8)	259.1 $^{+40.3}_{-30.8}$	0.881 \pm 0.017	UCL	1.5, 4.43, 5.57, 8.1, 8.79, 9.13, 30.2 (a,b,c)	VB
69845	HD 124961	B9V (9)	370.4 $^{+179.1}_{-91.0}$	0.207 \pm 0.029	UCL		
70149	HD 125541	A9V (9)	113.3 $^{+15.0}_{-11.8}$	0.146 \pm 0.048	UCL		
70300*	HD 125823	B2V (13)	140.3 $^{+3.2}_{-3.1}$	0.039 \pm 0.013	UCL		
70441	HD 126062	A1V (9)	110.4 $^{+9.1}_{-7.8}$	0.018 \pm 0.060	UCL		
70626	HD 126475	B9V (10)	147.3 $^{+9.7}_{-8.6}$	0.004 \pm 0.017	UCL		
70690	HD 126548	B9V (9)	206.6 $^{+36.1}_{-26.8}$	0.131 \pm 0.017	UCL		
70697	HD 126561	A0V (9)	126.7 $^{+9.7}_{-8.4}$	0.000 \pm 0.032	UCL		
70809	HD 126759	B9III: (24)	131.6 $^{+5.8}_{-5.3}$	0.000 \pm 0.008	UCL	4.97, 8.72 (b)	VB
70904*	HD 126859	A6V (8)	121.2 $^{+8.1}_{-7.1}$	0.182 \pm 0.019	UCL	6.08, 10.03 (b)	VB
70998	HD 127215	A1V (9)	141.2 $^{+13.6}_{-11.4}$	0.354 \pm 0.023	UCL	1.17 (b,c)	VB
71140	HD 127498	A7/8IV (9)	129.0 $^{+16.3}_{-13.0}$	0.105 \pm 0.024	UCL	0.2 (a)	VB
71271	HD 127750	A0V (9)	175.7 $^{+21.9}_{-17.5}$	0.040 \pm 0.056	UCL		
71321	HD 127879	A5V (22)	109.3 $^{+11.0}_{-9.2}$	0.291 \pm 0.025	UCL		
71498	HD 128155	A2V (8)	158.0 $^{+30.0}_{-21.7}$	0.455 \pm 0.034	UCL		
71536*	HD 128345	B5V (11)	96.9 $^{+1.5}_{-1.5}$	0.018 \pm 0.038	UCL		
71708	HD 128788	A5V (9)	150.6 $^{+28.6}_{-20.7}$	0.106 \pm 0.019	UCL		

Table 1—Continued

HIP	Name	Spectral Type	Distance (pc)	A_V (mag)	Subgroup	Separation (arcsec)	Notes
71724	HD 128819	B8/9V (9)	157.2 $^{+15.8}_{-13.1}$	0.059 \pm 0.023	UCL	8.66 (a,b,c)	VB
71727*	HD 128775	B8pSi (1)	208.8 $^{+29.3}_{-22.9}$	0.000 \pm 0.004	UCL	9.14 (a,b,c)	VB
71860*	HD 129056	B1.5III (11)	142.5 $^{+3.5}_{-3.4}$	0.094 \pm 0.009	UCL	27.6 (a)	VB
71865	HD 129116	B3V (11)	104.0 $^{+2.0}_{-1.9}$	0.043 \pm 0.009	UCL		
72140	HD 129732	A1IV/V (10)	208.8 $^{+29.3}_{-22.9}$	0.215 \pm 0.038	UCL	0.1 (a)	VB
72192	HD 129791	A0V (9)	148.4 $^{+23.3}_{-17.6}$	0.187 \pm 0.016	UCL	35.3 (a)	VB
72584	HD 130656	A2IV (10)	168.4 $^{+31.3}_{-22.8}$	0.278 \pm 0.044	UCL		
72630	HD 130731	A9IV/V (10)	215.1 $^{+67.4}_{-41.4}$	0.182 \pm 0.040	UCL		
72683	HD 130807	B5IV (11)	123.9 $^{+9.8}_{-8.4}$	0.038 \pm 0.013	UCL	0.1 (a,e)	VB
72800*	HD 131120	B7IIIp (11)	150.8 $^{+5.2}_{-4.8}$	0.085 \pm 0.013	UCL	1.046 (e)	VB
72940	HD 131399	A1V (10)	98.0 $^{+7.2}_{-6.3}$	0.276 \pm 0.070	UCL	3.16 (a,b,c)	VB
72984	HD 131461	A1V (19)	160.0 $^{+28.3}_{-20.9}$	0.101 \pm 0.045	UCL	4.71, 5.83 (a,b,c)	VB
73145	HD 131835	A2IV (10)	122.7 $^{+16.2}_{-12.8}$	0.187 \pm 0.084	UCL		
73147	HD 131777	A1V (19)	148.1 $^{+16.1}_{-13.2}$	0.130 \pm 0.016	UCL		
73266	HD 132094	B9V (10)	139.3 $^{+13.2}_{-10.4}$	0.074 \pm 0.017	UCL		
73334*	HD 132200	B2IV (11)	117.5 $^{+8.0}_{-7.0}$	0.023 \pm 0.013	UCL	0.128, 3.9 (a,d,e)	CPM
73393	HD 132302	A0V (9)	177.6 $^{+17.3}_{-14.5}$	0.000 \pm 0.017	UCL		
73559	HD 132763	A8/9III/IV (10)	128.0 $^{+6.0}_{-5.5}$	0.010 \pm 0.035	UCL		
73807	CD -46 9773	B5V+B5IV (11)	135.9 $^{+11.0}_{-9.4}$	0.044 \pm 0.005	UCL	1.4 (a)	VB
73913	HD 133574	A9/F0V (10)	145.6 $^{+26.0}_{-19.1}$	0.217 \pm 0.029	UCL		
73937*	HD 133652	B8:pSiCr (18)	121.4 $^{+8.0}_{-7.1}$	0.096 \pm 0.017	UCL	0.24 (a,b,c)	VB
73990	HD 133803	A9V (10)	124.8 $^{+14.6}_{-11.8}$	0.211 \pm 0.061	UCL		
74104*	HD 133954	A2/3III (9)	164.5 $^{+28.2}_{-21.0}$	0.251 \pm 0.056	UCL		
74117	HD 133955	B3V (11)	238.1 $^{+44.4}_{-32.3}$	0.032 \pm 0.009	UCL	0.2 (a)	VB
74449	HD 134687	B3IV (11)	154.6 $^{+5.2}_{-4.9}$	0.012 \pm 0.009	UCL	SB	
74479	HD 134837	B8V (10)	120.8 $^{+5.8}_{-5.3}$	0.074 \pm 0.017	UCL	4.65 (b,c)	VB
74657	HD 135174	B9IV (9)	210.1 $^{+47.6}_{-32.8}$	0.194 \pm 0.017	UCL	13.9 (a)	VB
74797	HD 135619	A2IV (10)	199.2 $^{+97.5}_{-49.3}$	0.284 \pm 0.055	UCL	18.2 (a)	VB
74950	HD 135876	B7V+B9V (14)	167.8 $^{+8.9}_{-8.0}$	0.038 \pm 0.021	UCL		EB
74985	HD 136013	A0V (19)	164.5 $^{+18.3}_{-15.0}$	0.239 \pm 0.018	UCL	6.37 (b)	VB
75056	HD 136164	A2V (10)	142.2 $^{+17.8}_{-14.2}$	0.321 \pm 0.005	UCL	5.19 (b,c)	VB
75141*	HD 136298	B1.5IV (11)	271.0 $^{+46.5}_{-34.6}$	0.031 \pm 0.021	UCL		
75264	HD 136504	B2IV-V (11)	157.0 $^{+19.4}_{-15.5}$	0.013 \pm 0.013	UCL	0.279, 0.6, 26.5 (a,e)	SB, VB
75304	HD 136664	B4V (11)	159.2 $^{+5.2}_{-4.9}$	0.052 \pm 0.013	UCL		
75509	HD 137119	A2V (10)	107.2 $^{+6.7}_{-6.7}$	0.067 \pm 0.037	UCL		
75647	HD 137432	B4Vp (11)	131.2 $^{+6.4}_{-6.4}$	0.019 \pm 0.013	UCL	20, 30 (a,d)	SB, VB
75957	HD 137957	A0V (19)	221.7 $^{+7.8}_{-28.3}$	0.212 \pm 0.023	UCL	5.56, 9.21 (b)	VB
76001	HD 138138	A2/3V (10)	102.8 $^{+7.8}_{-6.8}$	0.249 \pm 0.053	UCL		
76048	HD 138221	B7V (12)	128.9 $^{+7.2}_{-6.5}$	0.656 \pm 0.013	UCL		
76297	HD 138690	B2IV (11)	129.0 $^{+8.9}_{-7.8}$	0.015 \pm 0.013	UCL	0.59, 2.3 (d)	SB, CPM
76371	HD 138769	B3V+B6V (2)	131.2 $^{+7.8}_{-7.0}$	0.000 \pm 0.005	UCL	2.2 (a)	VB, Be star
76600	HD 139365	B2.5V (11)	112.5 $^{+2.6}_{-2.5}$	0.022 \pm 0.015	UCL		SB
76945	HD 140008	B5V (11)	111.5 $^{+3.5}_{-3.3}$	0.016 \pm 0.009	UCL	0.2, 0.507 (a,d,e)	SB, VB
77086	HD 140285	B9V (2)	143.9 $^{+14.6}_{-12.1}$	0.193 \pm 0.017	UCL	3.7 (a)	VB

Table 1—Continued

HIP	Name	Spectral Type	Distance (pc)	A_V (mag)	Subgroup	Separation (arcsec)	Notes
77150	HD 140475	A2V (10)	124.2 $^{+12.4}_{-10.3}$	0.218 \pm 0.094	UCL	0.2 (a)	VB
77286*	HD 140784	B7Vn (11)	117.9 $^{+4.0}_{-3.8}$	0.000 \pm 0.013	UCL	0.1 (a)	VB
77295	HD 140757	A2IV/V (10)	171.8 $^{+29.0}_{-21.7}$	0.152 \pm 0.025	UCL	4.63 (b)	VB
77315	HD 140817	A0V (10)	147.3 $^{+21.9}_{-16.9}$	0.105 \pm 0.017	UCL	0.68, 37.7 (a,b)	VB
77317	HD 140840	B9/A0V (10)	125.8 $^{+11.8}_{-9.9}$	0.000 \pm 0.067	UCL	32.8 (a,b)	VB
77388	HD 140958	A6V (10)	138.9 $^{+17.6}_{-14.0}$	0.211 \pm 0.048	UCL		
77523	HD 141327	B9V (10)	195.3 $^{+27.9}_{-21.7}$	0.139 \pm 0.017	UCL		
77968	HD 142256	B8V (9)	176.7 $^{+17.1}_{-14.3}$	0.302 \pm 0.019	UCL	6.43, 6.54 (b)	VB
78150	HD 142546	A7V(M) (9)	102.0 $^{+7.8}_{-6.8}$	0.094 \pm 0.035	UCL		
78324	HD 143022	B9.5V (9)	167.2 $^{+30.8}_{-22.5}$	0.761 \pm 0.097	UCL		
78384	HD 143118	B2.5IV (11)	135.5 $^{+3.4}_{-3.2}$	0.015 \pm 0.005	UCL	15, 115 (a,d)	CPM
78533*	HD 143473	B8Vp SiSr (20)	116.1 $^{+10.1}_{-8.6}$	0.549 \pm 0.013	UCL	6.09 (b)	VB
78541	HD 143488	A0V (10)	124.2 $^{+10.4}_{-8.9}$	0.000 \pm 0.022	UCL		
78641	HD 143675	A5IV/V (10)	113.4 $^{+9.9}_{-8.4}$	0.049 \pm 0.063	UCL		
78655	HD 143699	B6IV (11)	122.5 $^{+4.7}_{-4.3}$	0.036 \pm 0.010	UCL		
78754	HD 143927	B8/9V (10)	133.9 $^{+13.6}_{-11.3}$	0.337 \pm 0.048	UCL		
78756*	HD 143939	B9III (3)	144.7 $^{+16.1}_{-13.1}$	0.000 \pm 0.017	UCL	8.63 (a,b,c)	VB
78853	HD 144118	A5V (10)	129.0 $^{+22.3}_{-16.5}$	0.361 \pm 0.079	UCL	1.99, 7.12 (a,b,c)	VB
78918	HD 144294	B2.5Vn (11)	127.1 $^{+8.1}_{-7.2}$	0.053 \pm 0.038	UCL		
79044	HD 144591	B9V (10)	102.7 $^{+10.8}_{-8.9}$	0.000 \pm 0.041	UCL	5.02 (b)	VB
79400	HD 145357	A5V (9)	146.8 $^{+27.4}_{-19.9}$	0.342 \pm 0.013	UCL	5 (a)	VB
79631	HD 145880	B9.5V (10)	127.9 $^{+10.8}_{-9.3}$	0.324 \pm 0.155	UCL	2.94, 8.85 (b,c)	VB
80142*	HD 147001	B7V (9)	137.2 $^{+9.9}_{-8.6}$	0.166 \pm 0.013	UCL	5.88, 8.54, 9.32 (b,c)	VB
80208	HD 147152	B6IV (11)	141.8 $^{+6.7}_{-6.2}$	0.250 \pm 0.025	UCL		
80390	HD 147628	B8V (10)	129.0 $^{+4.3}_{-4.0}$	0.018 \pm 0.018	UCL	0.1 (a)	VB
80425	HD 147809	A1V (4)	151.5 $^{+40.1}_{-26.2}$	1.521 \pm 0.172	US		Herbig Ae
80591	HD 148055	A5V (10)	112.6 $^{+12.4}_{-10.2}$	0.118 \pm 0.020	UCL		
80897	HD 148657	A0V (10)	165.6 $^{+38.9}_{-26.5}$	0.864 \pm 0.024	UCL		
81316	HD 149425	B9V (9)	180.8 $^{+19.6}_{-16.1}$	0.557 \pm 0.052	UCL		
81472*	HD 149711	B2.5IV (11)	192.3 $^{+33.4}_{-24.8}$	0.457 \pm 0.004	UCL	4.52, 5.21, 16.3 (a,b)	VB
81751	HD 150287	A9V (9)	136.4 $^{+33.1}_{-22.3}$	0.561 \pm 0.029	UCL	6.12, 8.91 (b)	VB
81914	HD 150591	B6/7V (9)	167.2 $^{+8.8}_{-8.0}$	0.248 \pm 0.013	UCL	5.15, 6.18, 9.11, 95.7 (a,b)	VB
81949	HD 150645	A3V (9)	147.1 $^{+27.5}_{-20.0}$	0.446 \pm 0.045	UCL	5.27, 6.26 (b,c)	VB
81972	HD 150742	B3V (11)	163.7 $^{+8.7}_{-7.9}$	0.227 \pm 0.009	UCL	2.02, 2.79, 5.04, 7.02, 7.92 (a,b,c)	VB
82154	HD 151109	B8V (21)	222.7 $^{+37.0}_{-27.8}$	0.074 \pm 0.017	UCL	8.39 (b)	VB
82430	HD 151726	B9V (10)	120.9 $^{+9.5}_{-8.2}$	0.114 \pm 0.023	UCL	4.59, 5.98, 6.08 (b)	VB
82545*	HD 151985	B2IV (11)	145.3 $^{+2.6}_{-2.5}$	0.064 \pm 0.013	UCL		
82560	HD 151966	A0V (9)	155.8 $^{+5.5}_{-12.9}$	0.469 \pm 0.045	UCL	3.94, 4.73, 6.20 (b)	VB
83457*	HD 153805	A9V (10)	151.7 $^{+26.2}_{-19.5}$	0.237 \pm 0.015	UCL	0.4 (a)	VB
83693	HD 154310	A2IV (9)	142.2 $^{+9.5}_{-8.4}$	0.100 \pm 0.044	UCL	5.82, 12.69 (a,b,c)	VB

Note. — Upper Centaurus Lupus (UCL), Lower Centaurus Crux (LCC)

Note. — Common Proper Motion Binary (CPM), Eclipsing Binary (EB), Spectroscopic Binary (SB), Visual Binary (VB)

References. — (1) Buscombe & Kennedy (1965); (2) Corbally (1984); (3) Gahm et al. (1983); (4) Garrison (1967); (5) Garrison & Gray

(1994); (6) Gray & Garrison (1987); (7) Gray & Garrison (1989); (8) Houk & Cowley (1975); (9) Houk (1978); (10) Houk (1982); (11) Hiltner et al. (1969); (12) Hube (1970); (13) Jaschek et al. (1968); (14) Jordi et al. (1997); (15) Levato et al. (1996); (16) Morgan et al. (1978); (17) Morris (1961); (18) Osawa (1965); (19) Paunzen et al. (2001); (20) Pecaut 2012, private communication; (21) Schild et al. (1971); (22) Upgren et al. (1972); (23) Vieira et al. (2003); (24) Wood (1977)

References. — (a) Dommangé & Nys (2002); (b) Kouwenhoven et al. (2005); (c) Kouwenhoven et al. (2007); (d) Levato et al. (1987); (e) Shatsky & Tokovinin (2002)

Table 2. MIPS 24 μm and 70 μm Fluxes (Not Color-Corrected)

HIP	Name	AOR	Measured $F_\nu(24 \mu\text{m})$	Measured $\sigma_{F_{24}}^\dagger$	Predicted $F_\nu(24 \mu\text{m})$	χ_{24}	Measured $F_\nu(70 \mu\text{m})$	Measured $\sigma_{F_{70}}^\dagger$	Predicted $F_\nu(70 \mu\text{m})$	χ_{70}
	ID	(mJy)	(mJy)	(mJy)	(mJy)		(mJy)	(mJy)		
50083	HD088981	22767616	99.5	0.1	100.1	-0.2	<23.9	...	10.9	...
50520 [†]	HD089715	22767872	37.0	0.1	42.7	-3.8	<16.8	...	4.6	...
50847	HD090264	22768128	44.2	0.2	47.9	-2.2	<22.6	...	5.1	...
51991	HD092315	22768384	4.5	0.1	4.5	0.1	<14.6	...	0.5	...
52357 [†]	HD092896	22768640	14.2	0.2	14.6	-0.7	<13.2	...	1.6	...
53524 [†]	HD095086	16106496	45.6	0.1	13.7	31.1	654.6	5.4	1.5	14.7
53701 [†]	HD095324	22768896	16.7	12.7	20.8	-0.3	<826.3	...	2.2	...
54231	HD096338	22769152	14.4	0.1	13.8	1.3	<5.5	...	1.5	...
55188	HD098363	22769408	104.2	0.3	7.2	44.9	97.8	31.4	0.8	3.0
55425	HD098718	22769664	123.3	0.2	119.6	0.9	<27.7	...	12.8	...
55899	HD099627	22769920	10.1	0.1	10.6	-1.1	<9.0	...	1.2	...
56354 [†]	HD100453	22770176	59.0	1.7	41.9	7.1	13390.0	24.2	4.6	14.9
56379	HD100546	22770432	47.6	...	15430.0	24.2	5.2	14.9
56543 [†]	HD100786	22770688	5.5	0.2	5.5	-0.4	<2.3	...	0.6	...
56561 [†]	HD100841	22770944	406.9	0.8	414.1	-0.5	<125.1	...	45.0	...
56963 [†]	HD101523	22771456	7.7	0.1	7.5	0.6	<4.5	...	0.8	...
56993 [†]	HD101582	22771712	7.7	0.1	7.9	-0.4	<14.2	...	0.9	...
57238 [†]	HD102026	22771968	3.6	0.1	3.3	1.6	<22.3	...	0.4	...
57710 [†]	HD102814	22772480	5.6	0.1	5.8	-0.8	<10.2	...	0.6	...
57809 [†]	HD102981	22772736	26.8	0.1	15.4	15.6	78.8	4.3	1.7	11.3
57851 [†]	HD103079	22772992	54.2	0.2	51.7	1.3	<44.9	...	5.5	...
58416	HD104021	22773760	14.0	0.1	14.4	-0.7	<6.4	...	1.6	...
58452	HD104080	22774016	16.7	0.1	16.5	0.3	<10.7	...	1.8	...
58465	HD104125	22774272	22.4	0.1	22.2	0.2	<15.8	...	2.4	...
58680	HD104509	22774528	3.0	0.1	3.2	-1.1	<6.2	...	0.3	...
58720	HD104600	22774784	108.8	0.1	24.7	35.9	98.5	4.0	2.7	12.4
58859	HD104839	22775040	16.0	0.1	16.5	-1.0	<8.5	...	1.8	...
58884	HD104878	22775296	48.0	0.1	51.4	-1.9	<0.6	...	5.6	...
59173	HD105382	22775808	73.6	0.5	70.2	1.3	<28.4	...	7.5	...
59282	HD105613	22776064	23.9	0.2	11.5	20.1	<20.7	...	1.3	...
59397	HD105857	22776320	37.0	0.1	11.1	30.9	<14.5	...	1.2	...
59413 [†]	HD105874	22776576	10.2	0.1	10.2	0.0	<6.5	...	1.1	...
59502	HD106036	22776832	92.9	0.8	13.8	37.7	<254.1	...	1.5	...
59505 [†]	HD106048	22777088	6.5	0.1	6.1	1.6	<12.0	...	0.7	...
59724	HD106473	22777344	33.9	0.1	7.9	34.9	34.6	4.0	0.9	7.3
59747	HD106490	22777600	245.6	0.5	224.3	2.5	<59.8	...	24.1	...
59898	HD106797	22778368	138.3	0.2	27.9	37.4	<14.0	...	3.0	...
60009	HD106983	22778624	96.3	0.5	94.7	0.4	<83.9	...	10.2	...
60084	HD107143	22778880	7.8	0.1	6.8	3.2	<15.9	...	0.7	...
60183	HD107301	22779136	95.3	0.2	21.3	36.0	57.9	10.8	2.3	4.8
60320	HD107566	22779392	102.3	0.1	108.7	-1.7	<46.3	...	11.9	...
60379	HD107696	22779648	35.0	0.2	36.4	-1.1	<28.7	...	3.9	...
60459	HD107821	22779904	11.0	0.3	11.3	-0.6	<45.2	...	1.2	...

Table 2—Continued

HIP	Name	AOR	Measured	Measured	Predicted	Measured	Measured	Predicted		
	ID	(mJy)	$F_\nu(24 \mu\text{m})$ (mJy)	$\sigma_{F_{24}}^\dagger$ (mJy)	$F_\nu(24 \mu\text{m})$ (mJy)	χ_{24} (mJy)	$F_\nu(70 \mu\text{m})$ (mJy)	$\sigma_{F_{70}}^\dagger$ (mJy)	$F_\nu(70 \mu\text{m})$ (mJy)	χ_{70}
60561	HD107947	22780160	42.2	0.1	15.8	26.6	32.5	4.1	1.7	6.6
60577 [†]	HD108035	22780672	16.2	0.1	10.6	11.6	<18.5	...	1.2	...
60710	HD108257	16107264	51.0	0.4	50.5	0.3	<54.7	...	5.4	...
60823	HD108483	22780928	100.0	0.2	98.1	0.5	<10.1	...	10.6	...
60851 [†]	HD108501	22781184	29.1	0.3	29.0	0.0	<34.2	...	3.2	...
61257	HD109195	22782464	15.9	0.2	15.6	0.4	<18.1	...	1.7	...
61265	HD109197	22782720	7.7	0.1	7.7	0.0	<12.0	...	0.8	...
61585	HD109668	22782976	290.6	2.5	298.8	-0.7	<21.2	...	32.2	...
61639 [†]	HD109808	22783232	23.7	0.2	24.0	-0.3	<28.6	...	2.6	...
61684	HD109832	22783488	39.1	0.2	9.6	34.2	69.0	5.0	1.1	9.9
61782 [†]	HD110058	16170752	215.4	0.1	6.8	47.4	337.1	5.8	0.7	14.4
61796	HD110020	22783744	18.9	0.2	19.4	-0.7	<26.9	...	2.1	...
62002 [†]	HD110390	22784000	17.4	0.2	18.9	-2.1	<18.7	...	2.1	...
62026	HD110461	22784256	32.5	0.2	27.3	4.9	<43.4	...	3.0	...
62058	HD110506	22785024	21.8	0.2	22.7	-1.1	<51.8	...	2.5	...
62179 [†]	HD110698	22785280	19.9	0.2	20.0	-0.2	<29.4	...	2.2	...
62205 [†]	HD110737	22785536	8.4	0.2	9.3	-2.4	<10.6	...	1.0	...
62322 [†]	HD110879	22785792	221.6	1.2	212.4	1.2	<47.7	...	22.9	...
62327 [†]	HD110956	22786048	55.6	0.9	59.6	-1.7	<112.4	...	6.4	...
62703	HD111588	22786816	50.2	0.2	51.0	-0.4	<115.4	...	5.6	...
63003	HD112092	22787072	93.0	0.4	93.8	-0.2	<27.3	...	10.1	...
63005	HD112091	22787328	326.8	0.5	47.9	40.8	144.8	10.9	5.1	9.5
63007	HD112078	22787584	61.9	0.2	64.8	-1.3	<11.5	...	6.9	...
63204 [†]	HD112381	22788352	26.5	0.2	25.2	1.3	<6.5	...	2.7	...
63210	HD112409	22788608	45.2	0.2	48.5	-1.9	<29.9	...	5.2	...
63236	HD112383	22788864	51.2	0.1	15.4	31.1	<7.9	...	1.7	...
63839	HD113457	22789376	86.1	0.3	15.4	38.4	<38.5	...	1.7	...
63945	HD113703	4790016	62.0	0.1	60.7	0.6	<25.8	...	6.5	...
64004	HD113791	4790272	72.8	0.2	71.9	0.3	<37.5	...	7.8	...
64053	HD113902	22790144	66.4	0.2	34.5	18.6	17.0	6.5	3.7	2.0
64320	HD114365	22790912	20.5	0.2	21.0	-0.7	<25.4	...	2.3	...
64425 [†]	HD114529	22791424	84.9	0.4	87.0	-0.7	<110.2	...	9.4	...
64515	HD114772	22791680	28.0	0.1	29.0	-1.0	<13.2	...	3.2	...
64661	HD114911	22791936	64.2	0.2	66.5	-1.0	<23.0	...	7.2	...
64892 [†]	HD115470	22792448	12.3	0.2	12.8	-0.9	<15.8	...	1.4	...
64925	HD115527	22792704	11.7	0.1	12.4	-1.6	<4.4	...	1.4	...
64933	HD115529	22792960	26.2	0.2	25.7	0.4	<19.6	...	2.8	...
65021	HD115583	22793216	8.8	0.2	9.0	-0.6	<6.4	...	1.0	...
65089	HD115820	22793472	20.2	0.1	8.3	23.8	<14.7	...	0.9	...
65112	HD115823	22793728	30.0	0.2	30.7	-0.6	<16.9	...	3.3	...
65178	HD115988	22794240	13.6	0.2	14.6	-2.0	<9.2	...	1.6	...
65219	HD116038	22794496	16.8	0.1	17.5	-1.0	<9.8	...	1.9	...
65271 [†]	HD116087	22794752	70.1	0.8	70.3	-0.1	<120.4	...	7.5	...

Table 2—Continued

HIP	Name	AOR	Measured	Measured	Predicted		Measured	Measured	Predicted	
	ID	(mJy)	$F_\nu(24 \mu\text{m})$ (mJy)	$\sigma_{F_{24}}^\dagger$ (mJy)	$F_\nu(24 \mu\text{m})$ (mJy)	χ_{24}	$F_\nu(70 \mu\text{m})$ (mJy)	$\sigma_{F_{70}}^\dagger$ (mJy)	$F_\nu(70 \mu\text{m})$ (mJy)	χ_{70}
65394 [†]	HD116356	22795008	8.4	0.2	8.4	-0.2	<25.7	...	0.9	...
65426	HD116434	22795264	15.8	0.1	13.9	3.5	<11.4	...	1.5	...
65822	HD117193	22795776	14.8	0.1	15.2	-0.7	<8.4	...	1.7	...
65965 [†]	HD117484	22796032	37.9	0.2	6.8	38.2	73.6	4.1	0.7	11.4
66068	HD117665	22796288	43.5	0.2	10.4	34.7	16.1	4.2	1.1	3.4
66447	HD118379	22727936	22.6	0.2	9.7	22.6	39.8	14.8	1.1	2.6
66454	HD118354	22796544	22.0	0.1	23.0	-1.2	<19.6	...	2.5	...
66566 [†]	HD118588	22796800	40.0	0.2	8.3	36.6	<37.3	...	0.9	...
66651 [†]	HD118697	22797056	7.9	0.2	8.2	-0.7	<13.6	...	0.9	...
66908	HD119221	22728192	12.8	0.2	13.0	-0.4	<9.4	...	1.4	...
67036	HD119419	22797568	13.9	0.1	14.1	-0.4	<7.0	...	1.5	...
67199	HD119727	22797824	23.6	0.2	24.2	-0.8	<12.2	...	2.6	...
67260	HD119884	22798336	14.4	0.2	14.8	-0.7	<15.5	...	1.6	...
67464	HD120307	22728448	142.3	0.4	118.0	5.3	<10.5	...	12.7	...
67472	HD120324	22728704	1474.0	0.2	155.1	43.4	314.7	4.7	16.7	13.7
67919	HD121040	22798592	18.5	0.2	18.5	0.0	<21.4	...	2.0	...
67973	HD121190	22728960	40.2	0.1	30.5	7.8	<1.5	...	3.3	...
68080 [†]	HD121336	22729216	52.1	0.2	29.8	15.9	20.4	5.8	3.2	2.9
68245	HD121743	22729472	102.4	0.2	96.1	1.8	11.2	4.3	10.4	0.2
68282	HD121790	22729728	98.7	0.2	98.5	0.1	11.6	3.9	10.6	0.2
68532 [†]	HD122259	22729984	12.4	0.2	12.3	0.1	<5.6	...	1.3	...
68722	HD122664	22730240	5.9	0.1	5.8	0.4	<24.8	...	0.6	...
68781	HD122705	22730496	15.4	0.1	8.2	17.8	<10.2	...	0.9	...
68862	HD122980	22730752	64.3	0.2	64.7	-0.1	<28.7	...	7.0	...
68867 [†]	HD122982	22731008	9.3	0.2	9.6	-0.9	<13.3	...	1.0	...
68958 [†]	HD123112	22731264	14.6	0.2	14.3	0.5	<51.3	...	1.6	...
69302 [†]	HD123798	22731520	6.4	0.1	6.0	1.6	<18.5	...	0.7	...
69605 [†]	HD124469	22731776	7.1	0.1	4.8	10.5	<8.5	...	0.5	...
69618	HD124367	22732032	731.1	0.3	80.8	43.0	234.7	12.0	8.7	11.4
69749	HD124620	22732288	19.2	0.2	17.1	3.0	<32.8	...	1.9	...
69845 [†]	HD124961	22732544	5.6	0.1	5.4	0.6	<14.0	...	0.6	...
70149	HD125541	22732800	14.0	0.1	4.1	30.6	<14.3	...	0.5	...
70300	HD125823	22733056	65.2	0.2	65.7	-0.2	<25.8	...	7.1	...
70441 [†]	HD126062	22733312	22.5	0.1	8.3	27.0	158.3	4.7	0.9	13.5
70626	HD126475	22733568	15.8	0.1	15.4	0.6	<17.3	...	1.7	...
70690 [†]	HD126548	22733824	5.6	0.1	5.8	-1.0	<8.7	...	0.6	...
70697 [†]	HD126561	22734080	9.3	0.2	9.2	0.3	<12.5	...	1.0	...
70809	HD126759	22734336	15.6	0.2	16.0	-0.6	<17.6	...	1.7	...
70904 [†]	HD126859	22734592	20.7	0.2	20.7	0.0	<18.9	...	2.3	...
70998	HD127215	22734848	10.2	0.2	11.1	-2.1	<11.3	...	1.2	...
71140 [†]	HD127498	22735104	10.4	0.2	10.3	0.1	<10.7	...	1.1	...
71271 [†]	HD127750	22735360	18.7	0.1	6.7	27.2	70.1	4.9	0.7	10.2
71321	HD127879	22735616	10.2	0.2	10.1	0.2	<14.0	...	1.1	...

Table 2—Continued

Table 2—Continued

HIP	Name	AOR	Measured	Measured	Predicted		Measured	Measured	Predicted	
	ID	(mJy)	$F_{\nu}(24 \mu\text{m})$ (mJy)	$\sigma_{F_{24}}^{\ddagger}$ (mJy)	$F_{\nu}(24 \mu\text{m})$ (mJy)	χ_{24}	$F_{\nu}(70 \mu\text{m})$ (mJy)	$\sigma_{F_{70}}^{\ddagger}$ (mJy)	$F_{\nu}(70 \mu\text{m})$ (mJy)	χ_{70}
76371 [†]	HD138769	22746624	58.2	0.2	56.5	0.8	<16.8	...	6.1	...
76600	HD139365	22746880	137.4	0.2	139.3	-0.4	<41.4	...	15.0	...
76945	HD140008	22747136	57.4	0.2	58.3	-0.4	<20.2	...	6.2	...
77086 [†]	HD140285	22747392	21.8	0.2	28.0	-6.5	<27.5	...	3.0	...
77150	HD140475	22747648	11.4	0.2	8.7	6.9	<24.2	...	1.0	...
77286	HD140784	22747904	28.5	0.2	28.1	0.4	<17.9	...	3.0	...
77295 [†]	HD140757	22748160	6.8	0.1	6.4	1.6	<7.3	...	0.7	...
77315	HD140817	22766848	57.5	0.2	15.2	33.3	22.9	7.1	1.7	2.9
77317 [†]	HD140840	22748416	32.0	0.1	7.8	34.4	79.0	6.2	0.9	9.5
77388	HD140958	22748672	8.0	0.1	8.0	0.2	<22.2	...	0.9	...
77523	HD141327	22748928	14.9	0.1	7.6	18.9	<14.7	...	0.8	...
77968 [†]	HD142256	22749184	10.7	0.2	11.0	-0.6	<23.6	...	1.2	...
78150 [†]	HD142546	22749440	9.8	0.4	9.3	0.9	<65.3	...	1.0	...
78324	HD143022	22749696	7.3	0.1	7.6	-0.9	<23.2	...	0.8	...
78384	HD143118	22749952	140.5	0.2	141.3	-0.2	<29.2	...	15.3	...
78533	HD143473	22750208	16.2	0.2	11.4	9.4	<11.9	...	1.2	...
78641	HD143675	22750464	49.9	0.1	6.4	41.9	37.7	5.5	0.7	6.1
78655	HD143699	22750720	47.3	0.2	49.3	-1.2	<17.7	...	5.3	...
78754 [†]	HD143927	22750976	10.7	0.2	11.3	-1.4	<9.7	...	1.2	...
78756	HD143939	22751232	15.9	0.2	9.5	13.6	<11.9	...	1.0	...
78853 [†]	HD144118	22751488	9.8	0.2	10.5	-1.6	<21.9	...	1.1	...
78918	HD144294	22751744	79.8	0.2	81.6	-0.6	<11.3	...	8.8	...
79044	HD144591	22752000	11.0	0.2	11.8	-1.7	<35.5	...	1.3	...
79400 [†]	HD145357	22752256	15.3	0.1	7.7	18.7	<71.1	...	0.8	...
79631 [†]	HD145880	22752512	90.0	0.2	15.4	39.2	338.3	9.4	1.7	13.7
80142 [†]	HD147001	22752768	15.3	0.5	15.3	0.0	<86.6	...	1.6	...
80208 [†]	HD147152	22753024	47.3	5.9	46.1	0.2	<10941.0	...	4.9	...
80390	HD147628	22753280	33.9	0.2	35.7	-1.3	<107.6	...	3.8	...
80425 [†]	HD147809	16107520	43.3	10.0	12.4	3.1	82.1	28.0	1.4	2.8
80591	HD148055	22753536	6.9	0.1	5.3	6.2	<47.7	...	0.6	...
80897 [†]	HD148657	22753792	35.0	0.2	5.9	37.7	<596.3	...	0.6	...
81316 [†]	HD149425	22754304	15.4	0.5	15.0	0.6	<28.3	...	1.6	...
81472 [†]	HD149711	22754560	27.4	0.4	27.3	0.1	<37.3	...	2.9	...
81751 [†]	HD150287	22754816	3.5	0.2	3.4	0.1	<31.5	...	0.4	...
81914 [†]	HD150591	22755072	20.2	1.2	19.8	0.2	<117.6	...	2.1	...
81949 [†]	HD150645	22755328	8.3	1.7	8.7	-0.2	<87.0	...	1.0	...
81972	HD150742	22755584	61.3	0.3	29.3	20.5	<36.0	...	3.1	...
82154	HD151109	22755840	41.1	0.8	10.4	25.8	<68.0	...	1.1	...
82430 [†]	HD151726	22756096	8.3	0.4	8.6	-0.7	<102.3	...	0.9	...
82545	HD151985	22756352	130.9	0.3	113.9	3.9	<45.8	...	12.3	...
82560 [†]	HD151966	22756608	15.7	1.4	17.2	-1.0	<80.6	...	1.9	...
83457 [†]	HD153805	22756864	17.6	0.9	18.6	-1.0	<273.9	...	2.0	...
83693 [†]	HD154310	22757120	38.0	0.6	38.1	0.0	<47.6	...	4.1	...

Table 2—Continued

HIP	Name	AOR	Measured $F_\nu(24 \mu\text{m})$ (mJy)	Measured σ_{F24}^\dagger (mJy)	Predicted $F_\nu(24 \mu\text{m})$ (mJy)	χ_{24}	Measured $F_\nu(70 \mu\text{m})$ (mJy)	Measured σ_{F70}^\dagger (mJy)	Predicted $F_\nu(70 \mu\text{m})$ (mJy)	χ_{70}
-----	------	-----	--	---	---	-------------	--	---	---	-------------

[†]Source suffers some contamination at 24 μm .

$\ddagger\sigma_{F24}$ and σ_{F70} are the statistical uncertainties in the 24 and 70 μm photometry. The total uncertainty can be calculated by adding the systematic, repeatability, and calibration uncertainties in quadrature (see Section 2.1).

Table 3. Single Temperature Black Body Model Parameters

HIP	Name	T_{eff} (K)	L_* (L_\odot)	M_* (M_\odot)	t_{age} (Myr)	T_{gr} (K)	L_{IR}/L_*	a_{min} (μm)	D (AU)	M_{dust} (M_{moon})	M_{PB} (M_{moon})
Lower Centaurus Crux											
53524	HD 95086	7500	$7.2^{+0.6}_{-0.5}$	1.6	17	63.7	1.4×10^{-3}	0.8	270	1.5	>1
55188	HD 98363	8770	$11.4^{+1.7}_{-1.5}$	1.9	17	132	7.1×10^{-4}	2.6	17.2	0.011	>1
56354	HD 100453	7500	$10.5^{+1.9}_{-1.6}$	1.6	17	40	3.9×10^{-2}	1.4	829	700	>52
57809	HD 102981	9550	$38.2^{+7.4}_{-6.2}$	2.1	17	78.2	8.4×10^{-5}	7.9	69.7	0.066	>0.4
58720	HD 104600	11614	$68.7^{+7.7}_{-6.9}$	2.7	17	126	7.7×10^{-5}	8.7	32.6	0.0015	>0.7
59282	HD 105613	8551	$11.6^{+1.6}_{-1.4}$	1.8	17	>111	4.4×10^{-5}	2.6	<27.0	0.26	>0.06
59397	HD 105857	8770	$14.0^{+2.5}_{-2.1}$	1.9	17	>167	9.0×10^{-5}	2.8	<10.6	0.33	>0.2
59502	HD 106036	8770	$13.8^{+1.4}_{-1.3}$	1.9	17	>109	2.2×10^{-4}	2.8	<31.0	0.25	>0.4
59724	HD 106473	7998	$10.7^{+3.2}_{-2.4}$	1.7	17	120	2.6×10^{-4}	1.6	30	0.00058	>0.3
59898	HD 106797	9550	$32.9^{+5.0}_{-4.3}$	2.1	17	>269	1.2×10^{-4}	7.8	<5.2	0.25	0.5
60183	HD 107301	10765	$36.5^{+2.5}_{-2.4}$	2.4	17	149	9.3×10^{-5}	8.1	17	0.0048	>0.4
60561	HD 107947	9550	$17.5^{+2.6}_{-2.3}$	2.1	17	125	7.0×10^{-5}	7.3	17.2	0.0021	>0.2
60577	HD 108035	7464	$6.5^{+1.6}_{-1.3}$	1.6	17	>101	3.6×10^{-5}	0.8	<60.9	0.26	>0.03
61684	HD 109832	7447	$7.2^{+1.2}_{-1.0}$	1.6	17	101	3.9×10^{-4}	0.8	63.3	0.020	>0.4
61782	HD 110058	9500	$10.2^{+2.4}_{-1.9}$	2.1	17	112	1.5×10^{-3}	2.8	24.6	0.048	>2
63236	HD 112383	8770	$20^{+2.5}_{-2.2}$	1.9	17	>193	8.4×10^{-5}	6.9	<7.6	0.33	>0.2
63839	HD 113457	9550	$20.3^{+3.3}_{-2.9}$	2.1	17	>167	1.3×10^{-4}	7.4	<10.1	0.26	>0.3
64053	HD 113902	11695	$77.6^{+5.6}_{-5.2}$	2.7	17	204	2.4×10^{-5}	8.7	13.4	0.000084	>0.2
65089	HD 115820	7656	$4.9^{+0.8}_{-0.7}$	1.7	17	>125	8.7×10^{-5}	0.8	<27.8	0.23	>0.05
65965	HD 117484	10209	$23.6^{+7.2}_{-5.5}$	2.3	17	100	2.2×10^{-4}	7.7	31.1	0.036	>0.7
66068	HD 117665	8974	$24.4^{+3.9}_{-3.4}$	1.9	17	193	1.7×10^{-4}	7.4	8.3	0.00098	>0.5
66566	HD 118588	9204	$14.9^{+3.5}_{-2.8}$	2	17	>164	1.3×10^{-4}	6.3	<9.1	0.41	>0.2
Upper Centaurus Lupus											
66447	HD 118379	8551	$13.3^{+1.9}_{-1.7}$	1.8	15	94.1	1.3×10^{-4}	2.7	47.4	0.014	>0.2
67973	HD 121190	11967	$95.7^{+14.2}_{-12.4}$	2.8	15	>109	4.5×10^{-6}	8.8	<51.7	0.28	>0.05
68080	HD 121336	9204	$64.9^{+13.8}_{-11.4}$	2	15	147	3.5×10^{-5}	8	23.3	0.0034	>0.3
68781	HD 122705	8279	$8.9^{+1.6}_{-1.4}$	1.8	15	>102	3.9×10^{-5}	1.6	<44.4	0.30	>0.04
69605	HD 124469	7447	$14.1^{+7.3}_{-4.8}$	1.6	15	>82.2	3.0×10^{-5}	1.7	<105	1.1	>0.05
70149	HD 125541	7447	$3.2^{+0.9}_{-0.7}$	1.6	15	>122	1.5×10^{-4}	0.6	<27.4	0.32	>0.05
70441	HD 126062	9204	$11.4^{+2.1}_{-1.8}$	2	15	71	3.4×10^{-4}	2.8	102	0.17	>0.4
71271	HD 127750	9550	$26.9^{+8.0}_{-6.2}$	2.1	15	80.8	1.9×10^{-4}	7.6	54.2	0.009	>0.6
71498	HD 128155	8770	$9.4^{+3.6}_{-2.6}$	1.9	15	>61.2	8.1×10^{-6}	2.5	<165	0.51	>0.008
71708	HD 128788	8072	$9.6^{+3.6}_{-2.6}$	1.7	15	>79.6	1.9×10^{-5}	1.6	<99.4	0.51	>0.02
72584	HD 130656	8770	$17.9^{+6.7}_{-4.9}$	1.9	15	86	8.3×10^{-5}	6.2	42.7	0.019	>0.2
73145	HD 131835	8770	$17.9^{+3.0}_{-2.3}$	1.9	15	84.4	1.4×10^{-3}	2.6	76.4	0.38	>3
73990	HD 133803	7447	$8.1^{+2.0}_{-1.6}$	1.6	15	>166	2.3×10^{-4}	0.8	<17.0	0.41	>0.2
74950	HD 135876	13900	$343.6^{+37.5}_{-33.8}$	3.6	15	>104	2.1×10^{-6}	9	<108	0.68	>0.08
75509	HD 137119	8770	$9.0^{+1.4}_{-1.2}$	1.9	15	>134	8.7×10^{-5}	1.7	<19.7	0.29	>0.09
77150	HD 140475	8770	$12.8^{+2.9}_{-2.4}$	1.9	15	>78.0	1.2×10^{-5}	2.7	<82.4	0.34	>0.02

Table 3—Continued

HIP	Name	T_{eff} (K)	L_* (L_\odot)	M_* (M_\odot)	t_{age} (Myr)	T_{gr} (K)	L_{IR}/L_*	a_{min} (μm)	D (AU)	M_{dust} (M_{moon})	M_{PB} (M_{moon})
77315	HD 140817	9550	$41.5^{+13.8}_{-10.4}$	2.1	15	182	1.2×10^{-4}	7.9	12.2	0.0032	>0.6
77317	HD 140840	10209	$19.5^{+5.6}_{-4.4}$	2.3	15	92.4	1.8×10^{-4}	7.6	34	0.0029	>0.4
77523	HD 141327	10304	$48.3^{+13.9}_{-10.8}$	2.3	15	>107	2.2×10^{-5}	8.2	<39.0	0.92	>0.1
78533	HD 143473	13000	$43.1^{+9.4}_{-7.7}$	8.6	15	>80.3	1.5×10^{-4}	0.8	<61	0.30	>0.03
78641	HD 143675	8072	$6.4^{+1.2}_{-1.0}$	1.7	15	141	4.6×10^{-4}	0.8	23.2	0.003	>0.3
78756	HD 143939	10593	$39.6^{+8.9}_{-7.3}$	2.4	15	>91.8	1.3×10^{-5}	8.1	<49.1	0.49	>0.06
79400	HD 145357	8072	$12.9^{+4.8}_{-3.5}$	1.7	15	>80.6	4.9×10^{-5}	2.6	<74.8	0.48	>0.07
79631	HD 145880	10209	$32.1^{+10.1}_{-7.7}$	2.3	15	85.3	4.4×10^{-4}	7.9	52.2	0.20	>2
80591	HD 148055	8072	$5.2^{+1.2}_{-1.0}$	1.7	15	>63.8	1.5×10^{-5}	0.8	<230	0.26	>0.009
80897	HD 148657	9550	$21.3^{+10.5}_{-7.0}$	2.1	15	>67.8	1.4×10^{-4}	7.5	<78.6	0.58	>0.3
81972	HD 150742	17298	$623.7^{+69.7}_{-62.7}$	5.4	15	>101	5.3×10^{-6}	8.9	<155	0.64	>0.4
82154	HD 151109	11298	$116.9^{+22.1}_{-18.6}$	2.6	15	>91.8	5.0×10^{-5}	8.8	<82.3	1.2	>0.6

Table 4. Spitzer Intermediate-Age Disk Surveys

Region	Age (Myr)	Avg Distance (pc)	Selection Criteria	2.0 M_{\odot}		2.5 M_{\odot}		Photometry Reference
				N_{stars}	Range	N_{stars}	Range	
Upper Sco	10	~146	SpT	24	A0-A9	16	B9-B9.5	1
β Pic MG	12	\lesssim 60	SpT	5	A0-A7	1	B9-B9.5	4
UCL	15	~142	SpT	6	A0-A7	3	B9-B9.5	6
			SpT	44	A0-A7	16	B9-B9.5	8
LCC	17	~118	SpT	46	A0-A7	15	B9-B9.5	8
Tuc-Hor	30	\lesssim 30	SpT	12	A0-A7	2	B9-B9.5	7
Argus	40	\lesssim 150	SpT	5	A0-A7	...	B9-B9.5	7
IC 2391	50	~150	SpT	5	A0-A7	...	B9-B9.5	5
AB Dor	130	\lesssim 30	SpT	2	A0-A7	2	B9-B9.5	7
Pleiades	130	~130	SpT ^a	8	A1-A7	2	B9-A0	2
			SpT	2	A1-A7	1	B9-A0	6
Field	5-300	\leq 300	SpT	6	A0-F1	22	B9-A6	6
			SpT	8	A0-F1	1	B9-A6	3

References. — (1) Carpenter et al. (2009); (2) Gorlova et al. (2006); (3) Plavchan et al. (2009); (4) Rebull et al. (2008); (5) Siegler et al. (2007); (6) Su et al. (2006); (7) Zuckerman et al. (2011); (8) this work

^aPhotosphere estimates made based on *Spitzer* IRAC photometry published in Stauffer et al. (2005).

Table 5. Observations of 2 - 2.5 M_{\odot} Stars in US

HIP	SpT	$F_{\nu}(24 \mu\text{m})/F_{*}(24 \mu\text{m})$	Type	Notes
2.5 M_{\odot} Stars				
76701	B9V	0.98±0.07	No Excess (1)	
76633	B9V	1.30±0.07	No Excess (1)	
78530	B9V	1.07±0.07	No Excess (1)	
78549	B9.5V	1.03±0.07	No Excess (1)	
78809	B9V	1.02±0.07	No Excess (1)	
78956	B9.5V	1.55±0.07	Debris (1)	
78968	B9V	1.84±0.07	Debris (1)	
79124	A0V	1.06±0.07	No Excess (1)	
79410	B9V	3.77±0.07	Debris (1)	
79439	B9V	1.99±0.07	Debris (1)	
79771	B9V	0.97±0.07	No Excess (1)	
79860	A0V	1.03±0.07	No Excess (1)	
79878	A0V	3.23±0.07	Debris (1)	
79897	B9V	1.11±0.07	No Excess (1)	
80324	A0V+A0V	1.03±0.07	No Excess (1)	
81624	A1Ve	400± 20	Protoplanetary (4)	Herbig Ae (5)
2.0 M_{\odot} Stars				
76310	A0V	17.17±0.07	Debris (1)	
77960	A4IV/V	1.02±0.07	No Excess (1)	
78099	A0V	1.31±0.07	No Excess (1)	
78494	A2mA7-F2	0.94±0.07	No Excess (1)	
78847	A0V	1.00±0.07	No Excess (1)	
78977	F7V	1.35±0.04	Debris (2)	
78996	A9V	3.71±0.07	Debris (1)	
79083	F3V	1.03±0.07	No Excess (1)	
79156	A0V	2.83±0.07	Debris (1)	
79250	A3III/IV	1.29±0.07	No Excess (1)	
79366	A3V	0.99±0.07	No Excess (1)	
79476	A5Ve	3.9±0.2	Protoplanetary (4)	Herbig Ae (5)
79606	F6	0.96±0.07	No Excess (1)	
80024	B9II/III	3.36±0.07	Debris (1)	
80059	A7III/IV	0.99±0.07	No Excess (1)	
80130	A9V	1.04±0.07	No Excess (1)	
80311	A0V	0.86±0.07	No Excess (1)	
80425	A1V	4.98±0.04	Protoplanetary (3)	
80586	F5V	1.03±0.04	No Excess (2)	
82319	F3V	1.00±0.07	No Excess (1)	

References. — (1) Carpenter et al. (2009); (2) Chen et al. (2011); (3) this work; (4) Oudmaijer et al. (1992); (5) Vieira et al. (2003)

Table 6. Observations of 2 - 2.5 M_{\odot} Stars in UCL

HIP	SpT	$F_{\nu}(24 \mu\text{m})/F_{*}(24 \mu\text{m})$	Type	Notes
2.5 M_{\odot} Stars				
69113	B9V	0.96±0.05	No Excess (2)	
69749	B9IV	1.12±0.04	No Excess (3)	
69845	B9V	1.03±0.04	No Excess (3)	
70690	B9V	0.96±0.04	No Excess (3)	
71724	B8/9V	0.95±0.04	No Excess (3)	
73266	B9V	0.90±0.04	No Excess (3)	
75151	B9IVSi(SrCr)	1.01±0.17	No Excess (2)	
75210	B8/9V	2.97±0.07	Debris (2)	
75915	B9.5V	1.14±0.33	No Excess (2)	
77086	B9V+kA3hA7VmA5	0.78±0.04	No Excess (3)	
77317	B9/A0V	4.10±0.04	Debris (3)	
77523	B9V	1.97±0.04	Debris (3)	
78324	B9.5V	0.96±0.04	No Excess (3)	
78754	B8/9V	0.94±0.04	No Excess (3)	
78756	B9III	1.68±0.04	Debris (3)	
79044	B9V	0.93±0.04	No Excess (3)	
79631	B9.5V	5.86±0.04	Debris (3)	
81316	B9V	1.03±0.04	No Excess (3)	
82154	B8V	3.96±0.08	Debris (3)	
82430	B9V	0.96±0.06	No Excess (3)	
2.0 M_{\odot} Stars				
66447	A3IV/V	2.32±0.06	Debris (3)	
66722	A0V	0.96±0.04	No Excess (2)	
66908	A4V	0.99±0.04	No Excess (3)	
68080	A1Vn	1.75±0.05	Debris (3)	
68532	A3IV/V	1.01±0.04	No Excess (3)	
68781	A4V	1.88±0.05	Debris (3)	
68867	A0V	0.97±0.04	No Excess (3)	
70441	A1V	2.73±0.06	Debris (3)	
70697	A0V	1.01±0.04	No Excess (3)	
70918	A0/1V	0.93±0.04	No Excess (2)	
70998	A1V	0.92±0.04	No Excess (3)	
71023	F0V	1.34±0.04	Debris (1)	
71271	A0V	2.77±0.06	Debris (3)	
71498	A2V	1.22±0.04	Debris (3)	
71767	F3V	1.09±0.04	No Excess (1)	
72140	A1IV/V	0.90±0.04	No Excess (3)	
72192	A0V	0.97±0.04	No Excess (3)	
72584	A2IV	1.71±0.05	Debris (3)	
72627	A2V	0.93±0.04	No Excess (2)	

Table 6—Continued

HIP	SpT	$F_\nu(24 \mu\text{m})/F_*(24 \mu\text{m})$	Type	Notes
72940	A1V	1.01±0.04	No Excess (3)	
72984	A1V	0.92±0.04	No Excess (3)	
73145	A2IV	20.70±0.42	Debris (3)	
73147	A1V	1.06±0.04	No Excess (3)	
73393	A0V	1.04±0.04	No Excess (3)	
73666	F3IV	1.13±0.04	No Excess (1)	
73742	F8V	1.02±0.04	No Excess (1)	
74104	A2/3III	1.01±0.04	No Excess (3)	
74772	F3V	1.11±0.05	No Excess (1)	
74797	A2IV	1.02±0.04	No Excess (3)	
74985	A0V	0.99±0.04	No Excess (3)	
75056	A2V	0.93±0.04	No Excess (3)	
75077	A1V	1.29±0.04	Debris (2)	
75476	A1V	1.18±0.04	Debris (2)	
75491	F3V	3.44±0.04	Debris (1)	
75509	A2V	3.26±0.08	Debris (3)	
75933	F3V	1.04±0.04	No Excess (1)	
75957	A0V	1.07±0.04	No Excess (3)	
76001	A2/3V	0.94±0.04	No Excess (3)	
76501	F2V	1.11±0.04	No Excess (1)	
77150	A2V	1.31±0.04	Debris (3)	
77295	A2IV/V	1.07±0.04	No Excess (3)	
77315	A0V	3.79±0.08	Debris (3)	
77502	F3V	1.17±0.04	No Excess (1)	
78684	G9.5IV	1.11±0.04	No Excess (1)	
80663	F1V	0.91±0.21	No Excess (1)	
80897	A0V	5.91±0.13	Debris (3)	
81949	A3V	0.96±0.20	No Excess (3)	
82560	A0V	0.91±0.09	No Excess (3)	
82569	F3V	1.01±0.08	No Excess (1)	
83693	A2IV	1.00±0.04	No Excess (3)	

References. — (1) Chen et al. (2011); (2) Su et al. (2006); (3) this work

Table 7. Observations of $2 - 2.5 M_{\odot}$ Stars in LCC

HIP	SpT	$F_{\nu}(24 \mu\text{m})/F_{*}(24 \mu\text{m})$	Type	Notes
2.5 M_{\odot} Stars				
56379	B9Vne	5105±150	Protoplanetary (2)	Herbig Be (4)
58452	B8/9V	1.01±0.04	No Excess (3)	
58720	B9V	4.40±0.04	Debris (3)	
60183	B9V	4.47±0.04	Debris (3)	
61796	B8V	0.97±0.04	No Excess (3)	
62058	B9Vn	0.96±0.04	No Excess (3)	
65021	B9V	0.98±0.04	No Excess (3)	
65178	B9V	0.93±0.04	No Excess (3)	
65965	B9.5V	5.56±0.04	Debris (3)	
66651	B9.5V	0.97±0.04	No Excess (3)	
2.0 M_{\odot} Stars				
50083	A4mA6-F0	0.99±0.04	No Excess (3)	
50520	A1V	0.87±0.03	No Excess (3)	
51991	A1Vp:Cr:Sr:Eu:	1.01±0.04	No Excess (3)	
52357	A3IV	0.97±0.04	No Excess (3)	
54231	A0V	1.05±0.04	No Excess (3)	
55188	A2V	14.41±0.30	Debris (3)	
55899	A0V	0.96±0.04	No Excess (3)	
56561	B9.5IIIn	0.98±0.04	No Excess (3)	
56673	F5IV	1.34±0.04	Debris (1)	
56963	A3V	1.02±0.04	No Excess (3)	
56993	A0V	0.98±0.04	No Excess (3)	
57238	A1V	1.08±0.05	No Excess (3)	
57595	F5V	0.99±0.04	No Excess (1)	
57710	A3V	0.97±0.04	No Excess (3)	
57809	A0V	1.73±0.05	Debris (3)	
58146	F2IV/V	1.09±0.04	No Excess (1)	
58465	A2V	1.01±0.04	No Excess (3)	
58680	A4IV/V	0.95±0.04	No Excess (3)	
58884	A0IV	0.93±0.04	No Excess (3)	
59282	A3V	2.08±0.05	Debris (3)	
59397	A2V	3.32±0.08	Debris (3)	
59502	A2V	6.73±0.15	Debris (3)	
59898	A0V	4.95±0.11	Debris (3)	
60084	A1V	1.14±0.04	No Excess (3)	
60459	A3V	0.97±0.04	No Excess (3)	
60561	A0V	2.68±0.06	Debris (3)	
60851	A0V	1.00±0.04	No Excess (3)	
61265	A2V	1.00±0.04	No Excess (3)	
61639	A1/2V	0.99±0.04	No Excess (3)	

Table 7—Continued

HIP	SpT	$F_\nu(24 \mu\text{m})/F_*(24 \mu\text{m})$	Type	Notes
61782	A0V	31.68±0.65	Debris (3)	
62002	A1V	0.92±0.04	No Excess (3)	
62179	A0IV/V	0.99±0.04	No Excess (3)	
62431	F0	1.01±0.04	No Excess (1)	
62677	F0/2V:	1.12±0.04	No Excess (1)	
63236	A2IV/V	3.32±0.07	Debris (3)	
63527	F0/2V	1.01±0.04	No Excess (1)	
63839	A0V	5.58±0.12	Debris (3)	
63975	F3/5V	80.01±0.04	Debris (1)	
64925	A0V	0.94±0.04	No Excess (3)	
64933	A0V	1.02±0.04	No Excess (3)	
65219	A3/4III/IV	0.96±0.04	No Excess (3)	
65394	A1Vn:	0.99±0.04	No Excess (3)	
65426	A2V	1.14±0.04	No Excess (3)	
65822	A1V	0.97±0.04	No Excess (3)	
66068	A1/2V	4.17±0.09	Debris (3)	
66566	A1V	4.84±0.10	Debris (3)	
67199	A1V	0.97±0.04	No Excess (3)	
67230	F5V	3.31±0.08	Debris (1)	
67260	A0V	0.97±0.04	No Excess (3)	

References. — (1) Chen et al. (2011); (2) Oudmaijer et al. (1992); (3) this work; (4) Vieira et al. (2003)

Table 8. $F_\nu(24 \mu\text{m})/F_*(24 \mu\text{m})$ Statistics for ScoCen Evolutionary Sample

Group	Age (Myr)	Mean	Std Dev	3rd Q	Median	1st Q	RS Z	RS Prob
2.5 M _⊙ Stars - All								
US	10	30	100	1.03	1.11	1.99	0 (-1.6)	1 (0.06)
UCL	15	1.7	1.4	0.95	1.03	1.97	1.6 (0)	0.06 (1)
LCC	17	500	1600	0.97	1.01	4.47	0.8 (0.9)	0.2 (0.2)
2.5 M _⊙ Stars - Primordial Removed								
US	10	1.5	0.9	1.03	1.07	1.84	0 (-1.3)	1 (0.1)
UCL	15	1.7	1.4	0.95	1.03	1.97	1.3 (0)	0.1 (1)
LCC	17	2.2	1.9	0.97	0.98	4.47	1.1 (0.5)	0.1 (0.3)
2.0 M _⊙ Stars - All								
US	10	22	86	1.00	1.04	3.36	0 (0.9)	1 (0.2)
UCL	15	1.8	2.9	0.97	1.06	1.31	-0.9 (0)	0.2 (1)
LCC	17	4	12	0.97	1.01	2.68	0.9 (0.2)	0.2 (0.4)
2.0 M _⊙ Stars - Primordial Removed								
US	10	2.3	3.8	0.99	1.03	1.35	0 (0.3)	1 (0.4)
UCL	15	1.8	2.9	0.97	1.06	1.31	-0.3 (0)	0.4 (1)
LCC	17	4	12	0.97	1.01	1.34	0.4 (0.2)	0.4 (0.4)

Note. — Statistics comparing the populations of US, UCL, and LCC. We calculate the mean $F_\nu(24 \mu\text{m})/F_*(24 \mu\text{m})$ for each subgroup (including and excluding "primordial disks"), the standard deviation (σ), the 1st quartile, the median, the 3rd quartile, and the Wilcoxon rank sum probability and Z parameter. For the Wilcoxon rank sum test parameters, the first (second) entry in the rank sum test statistics compares each population to US (UCL). A positive Z parameter means that the sample has a larger median value than US (first entry) and UCL (second entry). A low rank sum probability means that the median $F_\nu(24 \mu\text{m})/F_*(24 \mu\text{m})$ of the populations are very different.